Assessment of chlorophyll fluorescence yields at canopy level by active and passive methods. Application to water stress detection

Hildo Loayza Loza

▶ **To cite this version:**

Hildo Loayza Loza. Assessment of chlorophyll fluorescence yields at canopy level by active and passive methods. Application to water stress detection. Meteorology. Sorbonne Université, 2022. English. NNT : 2022SORUS465 . tel-04028411

HAL Id: tel-04028411
https://theses.hal.science/tel-04028411

Submitted on 14 Mar 2023

HAL is a multi-disciplinary open access archive for the deposit and dissemination of scientific research documents, whether they are published or not. The documents may come from teaching and research institutions in France or abroad, or from public or private research centers.

L'archive ouverte pluridisciplinaire **HAL**, est destinée au dépôt et à la diffusion de documents scientifiques de niveau recherche, publiés ou non, émanant des établissements d'enseignement et de recherche français ou étrangers, des laboratoires publics ou privés.

Sorbonne Université

Ecole doctorale 129 – Sciences de l'environnement

Laboratoire de Météorologie Dynamique / Equipe Atmosphère Biosphère Climat Télédétection

Suivi expérimental du rendement de fluorescence des couverts végétaux par des techniques actives et passives. Application à la détection du stress hydrique.

Par Hildo Loayza Loza

Thèse de doctorat de Surfaces Continentales

Dirigée par Yves Goulas et Ismaël Moya

Présentée et soutenue publiquement le 12 décembre 2022

Devant un jury composé de:

M.	Jaume FLEXAS	Rapporteur
M.	Jean Philippe GASTELLU-ETCHEGORRY	Rapporteur
Mme.	Fabienne MAIGNAN	Examinatrice
M.	Hervé LE TREUT	Examinateur
M.	Fermín MORALES	Examinateur
Mme	Valérie LE DANTEC	Examinatrice

Sorbonne Université

Ecole doctorale 129 – Sciences de l'environnement

Laboratoire de Météorologie Dynamique / Equipe Atmosphère Biosphère Climat

Télédétection

Assessment of chlorophyll fluorescence yields at canopy level by active and passive methods. Application to water stress detection.

Presented by Hildo Loayza Loza

Doctoral Thesis in Continental Surfaces

Supervised per Yves Goulas and Ismaël Moya

Presented and defended in public on December 12th 2022

In front of a jury composed by:

M.	Jaume FLEXAS	Rapporteur
M.	Jean Philippe GASTELLU-ETCHEGORRY	Rapporteur
Mme.	Fabienne MAIGNAN	Examinatrice
M.	Hervé LE TREUT	Examinateur
M.	Fermín MORALES	Examinateur
Mme	Valérie LE DANTEC	Examinatrice

I dedicate this work:

To my Adriano and Marita, my strength y motivation.

To Maximo and Yola, my dear parents.

To Gaby and Javier, my brothers.

ACKNOWLEDGMENTS

I am very grateful to Ismael Moya, co-director of my thesis. For his role of advisor, partner and friend. For transmitting his experience and knowledge, for the talks and discussions, for sharing his time with me. Ismael is and will always be a guide in my personal, professional and scientific life.

I am very grateful to Yves Goulas, director of my thesis. For his support, experience, guidance and encouragement. Fundamental in the final stage of execution of my PhD project, where the workload and personal overwhelmed me. Yves, thank you for supporting me and giving me the confidence to reach the goal.

I thank Roberto Quiroz, my former boss in the International Potato Center (CIP), who gave me the opportunity and support to start my doctoral studies. For trusting in my abilities and always encouraging me to keep going.

I thank Raymundo Gutierrez, my partner and friend, for the advice, discussions and guidance.

I thank Luis Silva, my co-worker at CIP. For his support and his excellent performance while I was in France focused on my PhD project.

I thank the colleagues whom I met during the execution of my project. To Abderrahmane Ounis for his guidance and experience, to María de los LLanos López, Jordi Bach and Camill Rhoul, for their empathy, charisma and camaraderie.

I thank the International Potato Center (CIP) and its leaders for giving me the opportunity to work and study. To the Laboratoire de Météorologie Dynamique (LMD) for allowing me to develop in their laboratories, and financial support to enroll me as PhD student.

Hildo Loayza

Table of contents

ABBREVIATIONS

NDVI	Normalized Difference Vegetation Index
NIR	Near Infra-Red
R	Red
PAR	Photosynthetic Active Radiation
GPP	Gross Primary Production
PRI	Photosynthetic Reflectance Index
ρ531	Reflectance at 531 nm
ρ570	Reflectance at 570 nm
ChlF	Chlorophyll Fluorescence
LED	Light Emitting Diode
PAM	Pulse Amplitude Modulation
Fo	Minimum Dark Adapted Fluorescence yield
Fs	Stationary Fluorescence yield
Fm	Maximum Dark-Adapted Fluorescence yield
Fm’	Maximum Steady State Fluorescence yield
LIDAR	Laser Induced Detection And Ranging
UV	Ultra-violet
LIF	Laser or Led Induced Fluorescence
SIF	Sun induced fluorescence
PVC	Poly Vinyl Chloride
TTL	Transistor-Transistor Logic
DAQ	Data Acquisition
ADC	Analog to Digital Conversion
Rc	Reflected light
Tdiode	Detector Temperature
Tled	Light Emitting Diodes Temperature
Tair	Air Temperature measured by a thermistor outside Ledflex
SNR	Signal to Noise Ratio
PPFD	Photosynthetic Photon Flux Density
FWHM	Full Width at Half-Maximum
SIF	Solar-induced fluorescence
ASFY	Apparent Spectral Fluorescence Yield
F760	Fluorescence fluxes at 760 nm
FY760	Fluorescence Yield at 760 nm
ASFY760	Apparent spectral fluorescence yield at 760 mn
F687	Fluorescence fluxes at 687 nm
FY687	Fluorescence Yield at 687 nm
ASFY687	Apparent spectral fluorescence yield at 687 mn
IDE	Environment Development Software
DAQ	Data Acquisition

SSR	Sum of squared residuals
SEM	Standard error of the mean
O_2-A	Oxygen A absorption band
O_2-B	Oxygen B absorption band
PS I	Photosystem I
PS II	Photosystem II
NQP	Non-Photochemical Quenching
D760	The atmospheric oxygen band depth at 760 nm
F_yield	Apparent fluorescence yield at 760 nm
Fmin	Minimum of stationary fluorescence at around solar noon

CHAPTER 1

1.1 General Introduction

Optical methods are currently considered a promising tool to monitor plant status as they can be applied remotely for monitoring large areas in a relatively short time.

The methods based in reflectance such as Normalized Difference Vegetation Index (NDVI) = (NIR-R) / (NIR + R), is one the most utilized due to its relation with the foliage biomass, leaf area index and the percentage of vegetation cover (Jordan, 1969) Despite its popularity, NDVI and related indexes only detects water stress when the chlorophyll content is affected causing irreversible damage. Another index, based on reflectivity, is the Photochemical Reflectance Index (PRI) = (R531-R570) / (R531+R570)). Works such as those by Peguero-Pina et al., 2008 have shown that the PRI correlates with the non-photochemical quenching (NPQ) and it is an indicator of stomatal closure by water scarcity. However, at canopy level, the PRI is affected by several structure parameters including pigment content, geometry of foliage, leaf angle and viewing angle of the detector.

Compared to other remote sensing methods - such as visible or near infrared reflectance - the chlorophyll fluorescence (ChlF) is a signal directly related to the photosynthetic process, because absorbed energy in the form of excited state of chlorophyll molecules can drive three competing process which are photochemical conversion, thermal dissipation and fluorescence. Therefore, it is a valuable signal to assess the physiological status of plants at distance. However, much of our knowledge about the relationship between fluorescence and the physiological status of plants come from leaf level studies carried out under laboratory conditions. Under our current knowledge, the physiological significance of ChlF at canopy level and under natural conditions is still a major subject of research and a source of uncertainties in the interpretation of Sun Induced Fluorescence (SIF) (Porcar-Castell et al., 2014). At canopy level, this physiological link between fluorescence and photosynthesis may be blurred by structural vegetation changes and geometrical effects linked to interactions between sunlight and the three-dimensional structure of the canopy (Dechant et al., 2020). In this sense, an active measurement would provide a more direct way to monitor ChlF yield, but there is currently no simple active fluorometer that can work at canopy level to monitor changes in florescence yield.

This doctoral project aims at resolving this bottleneck in the interpretation of SIF and investigates the properties of ChlF yield at canopy level in relation with the physiological status of different crops. These questions introduce the following objectives of my thesis:

1 - To develop an instrument for the direct measurement of chlorophyll fluorescence (ChlF) yields at canopy level and assess the diurnal time course of the stationary fluorescence level under unstressed and stressed conditions. (Chapter 2, published in Photosynthesis research journal, Moya et al., 2019)

2 - To study the relationship between ChlF yields measured with an active instrument and SIF on a potato crop. Propose methods to recover a proxy of ChlF yield from SIF measurements at 687 nm and 760 nm. (Chapter 3, published in Photosynthesis Research journal, Loayza et al., 2022)

3 - To detect water stress using proximal remote sensing of chlorophyll fluorescence at field level and investigate the possibilities of water stress detection by airborne SIF measurements. (Chapter 4, published in Photosynthesis Research journal, Moya et al., 2023).

1.2 Photosynthesis and chlorophyll fluorescence

Photosynthesis takes place in a specialized organelle, the chloroplast (see Fig. 1. 1). It is delimited by a double envelope, composed of an outer membrane, permeable to low molecular weight metabolites, and an inner membrane delimiting an intra-chloroplast matrix, the stroma. Inside the chloroplasts are lipid bilayers, the lamellae, which form a network of closed vesicles, the thylakoids, and define two immediately non-communicating phases, the stromatic space and the intrathylakoid space, or lumen. In places, the lamellae stick together to form stacks of discs, the grana, which remain in a relationship of continuity with the non-joined lamellae. These membranes contain the photosynthetic pigments that absorb light energy, and the proteins needed to convert this energy into chemical energy.

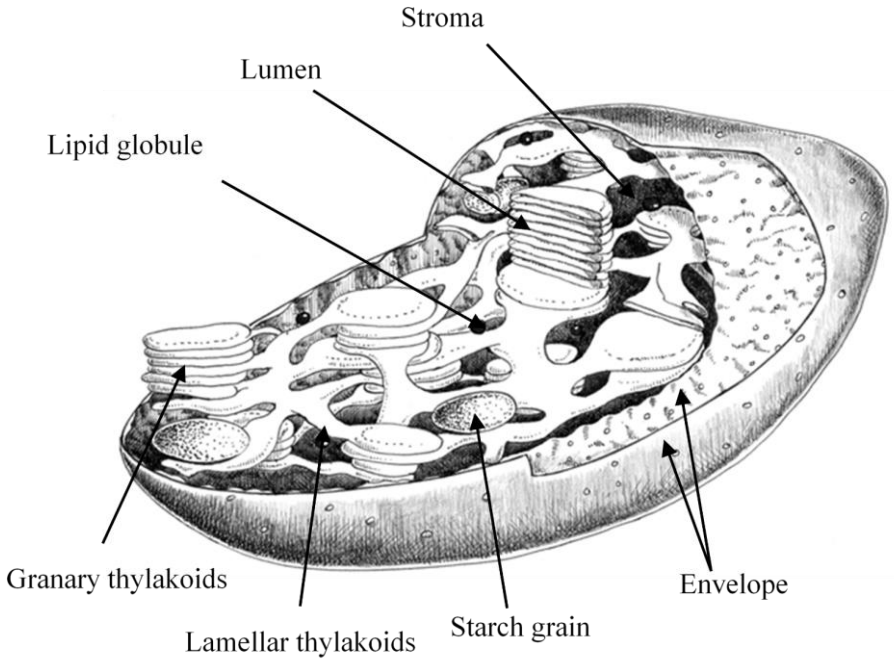

Fig. 1. 1. Diagram of a chloroplast of a plant cell (extracted and adapted of Louis, 2004).

1.2.1 Electron transport chain

The photosynthetic apparatus is organized into several subunits located along the thylakoid membranes and linked by transporters, soluble molecules in the membrane or in the lumen (Fig. 1. 2). These subunits are photosystems I and II (PS I and PS II), cytochrome *b6/f* and ATP synthase. The majority of the PS II are found in the granary piles while the majority of the PS I are found in the lamellae.

The first steps of photosynthesis take place at the level of photosystem II. This is made up of a reaction center and collecting antennas or LHCII (Light Harvesting Complex). The antennae are made up of protein-pigment complexes, the pigments being chlorophylls a and b and carotenoids. They contain between 200 and 300 molecules of Chl *a*. Their role is to absorb light energy, which is then transferred to the reaction center, by a mechanism involving dipole-dipole couplings. This contains a pair of Chl *a* molecules, called P_{680}, surrounded by two proteins D1 and D2, two pheophytins a, a strongly bound plastoquinone, Q_A and a more weakly bound plastoquinone, Q_B. The D1 protein has a redox-active tyrosine. Excitation of P_{680} induces

charge separation, an electron being transferred from P_{680} to pheophytin *a* and then to plastoquinone Q_A. The P+ oxidant created by the charge separation is reduced by an electron donated by tyrosine, which is then reduced by an electron from water. On the acceptor side of the photosystem, the electron is then transferred from Q_A to Q_B in a slower reaction. After receiving two electrons, Q_B binds two protons from the lumen and dissociates to join the pool of plastoquinones located in the membrane. The chain of membrane transporters continues with cytochrome *b6/f* and a plastocyanin, a soluble protein from the lumen, which is the donor of PS I.

The PS I also consists of a reaction center (P_{700}) and an antenna (LHCI). It carries out a charge separation by using the energy absorbed at the level of the antennas and transferred to the reaction center. The electron is then transferred to ferredoxin which allows the reduction of NADP+ to NADPH by ferredoxin-NADP reductase. The electron transfer between the transporters of the photosynthetic chain takes place in the direction of the redox potential, except at the level of the PS I and PS II where the light energy makes it possible to carry out energy jumps.

Electron transfer generates a transmembrane proton gradient with passage of protons from the stroma to the lumen. The energy contained in this gradient is used by ATP synthase for the synthesis of ATP from ADP and inorganic phosphate. The chemical energy produced during the photosynthetic transfer of electrons then allows the synthesis of carbohydrates from CO_2.

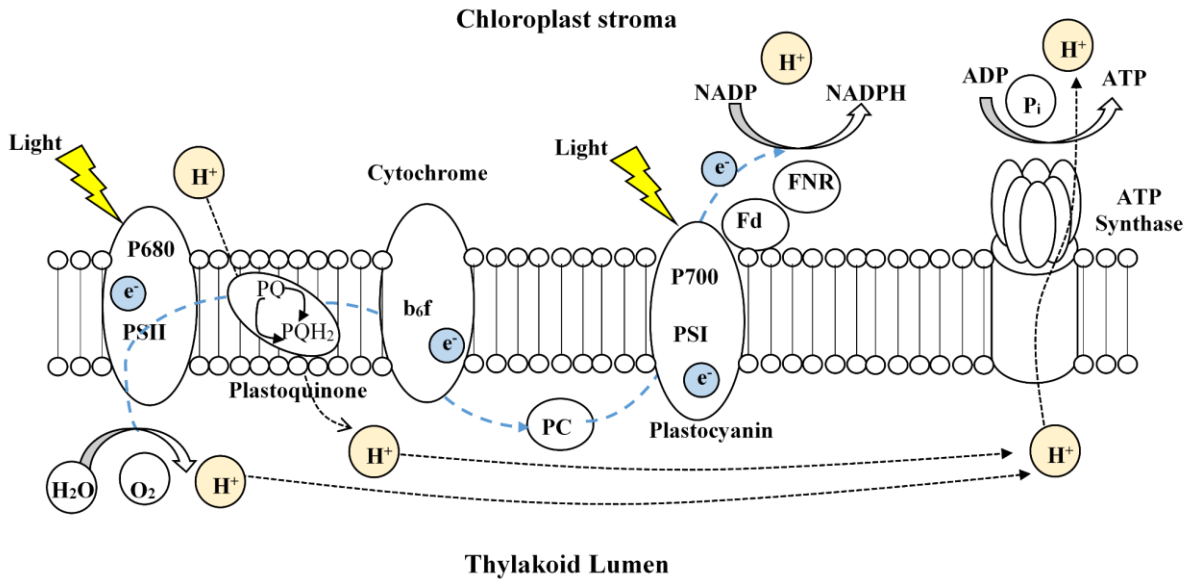

Fig. 1. 2 Diagram of photosynthetic electron transport in higher plants pathway. Adapted of Sarvikas, 2010.

1.2.2 Photosynthesis regulation mechanisms

When the light absorbed by plants exceeds that used by the photosynthetic pathway, mechanisms are set in motion that help reduce and avoid the possible damage caused by an excess of absorbed energy. These photoprotective mechanisms can be mechanical, such as the movement of leaves and chloroplasts to decrease light interception.

They can also be biochemical, through the accumulation of photoprotective substances on the foliar surface or the accumulation in the leaf of other photoprotective compounds such as pigments (anthocyanins) and antioxidant molecules (tocopherols, vitamin B6, etc.). At the level of the thylakoid membranes, in the PS II antennae, the excess of absorbed light can be dissipated through the thermal pathway. The mechanisms that dissipate excess energy in the form of heat belong to the so-called non-photochemical quenching (NPQ) (Bilger & Björkman, 1990; Horton et al., 1994; Krause & Jahns, 2004; Krause & Weis, 1991; Osmond, 1994). The NPQ, associated with the processes of thermal dissipation within the leaf, is mainly made up of three components that are part of the photo-protection mechanisms of the photosynthetic apparatus against an excess of absorbed light: energy-dependent quenching (qE), photoinhibitory quenching (qI) and quenching of transition state (qT).

The majority component of NPQ depends on pH. It is therefore called energy quenching (qE). It appears in a few minutes and relaxes in 1 or 2 minutes in the dark. Membrane energization activates several mechanisms, including the conversion of violaxanthin to zeaxanthin (xanthophyll cycle) and a conformational change in LHCII. These structural modifications result in an increase in the dissipation of energy by thermal means. Energization of the membrane activates another mechanism, photoinhibition (qI), which relaxes after a much longer time than qE.

Photoinhibition occurs under all light intensities, and even in plants that are not stressed, but in these cases, the rate of PS II repair related to the rate of synthesis of certain proteins (D1) is higher than the rate of photodamage of PS II (Tyystjärvi & Aro, 1996). The photoinhibitory mechanisms are still not completely clear, although they have been associated with several processes. For example, qI has been associated with an accumulation of inactive or photoinhibited reaction centers due to an inhibition in the rate of PS II repair, which is in turn related to the inhibition of PS II protein synthesis (particularly protein D1). The net photoinhibition rate is the result of the balance between PS II's photodamage rate and its repair rate. The life of reaction centers is shorter in strong light, this phenomenon being accentuated under stress. The synthesis of new proteins being quite slow, this can lead to a decrease in photosynthesis.

Another mechanism exists in low light (Baker, 2008). A part of the LHCII is mobile and can detach from the PS II and migrate in the membrane towards the PS I. This migration is called change of state (qT) (Allen, 1992; Wollman, 2001). The mobility of LHCIIs depends on their state of phosphorylation, controlled by a kinase. Its activity depends on the level of oxide-reduction of the electron transfer chain. This “state 1-state 2” state transition allows a redistribution of the excitation energy between the two photosystems. It has the effect of reducing the absorption of energy by the PS II. This phenomenon tends to disappear for stronger lights when qE increases.

In addition to the aforementioned photoprotective processes, another of the regulatory mechanisms of photosynthesis is photorespiration. It is an alternative process to the Calvin cycle in which the Rubisco enzyme is also involved, where O_2 is consumed, CO_2 is released and energy is dissipated.

1.2.3 Chlorophyll fluorescence emission

When a photon of light is intercepted by the plant cover, it is absorbed by the photosynthetic pigments located in the chloroplasts of the leaves, mainly. This energy absorption causes the excitation of the antenna pigments and the target chlorophyll P680 and P700, in the PS II and PS I respectively. The chlorophyll fluorescence of the leaves is emitted by the chl *a* molecules of the antennae of the photosystems. It is a process of radiative deactivation of molecules excited by the absorption of a photon, in competition with the photochemical conversion of energy and with dissipation by thermal means. From the fluorescence point of view, photosynthesis therefore represents photochemical quenching (qP) and thermal dissipation non-photochemical quenching (NPQ). Another remarkable property of chlorophyll fluorescence in vivo is its variable yield. It depends in fact on photosynthetic activity and active regulatory mechanisms. More specifically, the fluorescence yield of PS II is variable while that of PS I is constant.

At room temperature, a small fraction of the absorbed light energy is re-emitted as fluorescence. The chlorophyll fluorescence spectral emission spans approximately 650 – 800 nm. In intact leaves, the chlorophyll *a* fluorescence emission spectrum is characterized by a major peak around 685 – 690 nm (F685) attributable to PS II and a broad shoulder in the far-red from 730 to 740 nm (F740), due to both PS II and PS I (Govindje, 1995), see Fig. 1. 3.

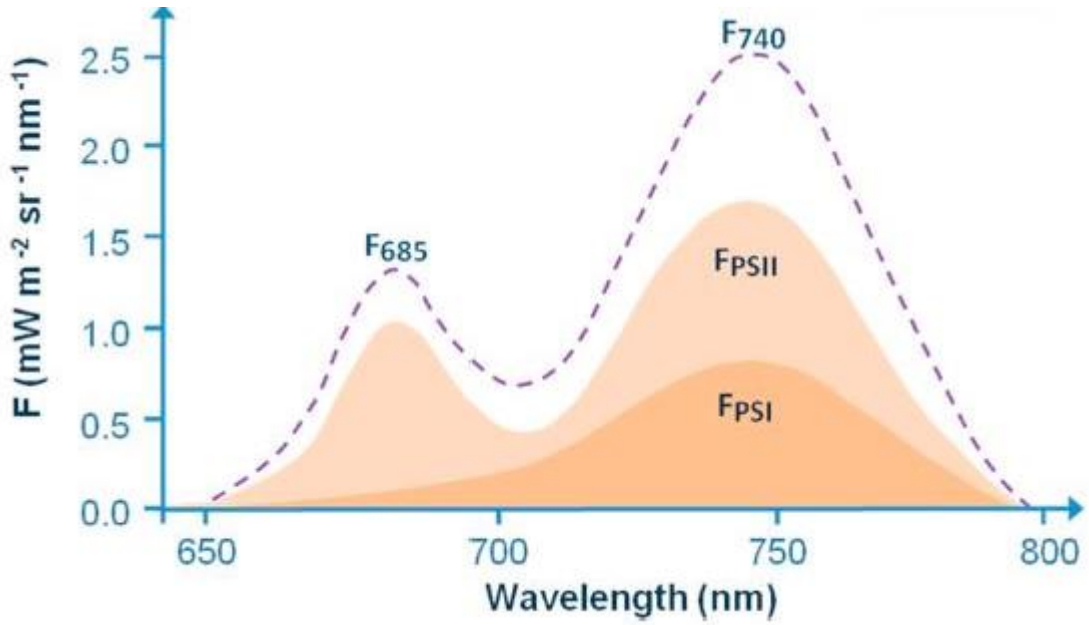

Fig. 1. 3 PS II contributes to both red and far-red emissions. Whilst PS I mainly to the far-red region. In healthy green leaves the red peak typically is lower than the far-red one, due to greater reabsorption of red fluorescence by chlorophyll. Figure derived from Mohammed et al., (2019).

1.2.4 Fluorescence lifetime

For a molecule isolated in liquid or gaseous phase, the decrease in the concentration of chlorophyll molecules in excited state ([Chl*]) is given by the following differential equation (Moya, 1979):

$$\frac{d[Chl^*]}{dt} = -(kf + knr + kp)[Chl^*]$$

With kf the deactivation constant by fluorescence, knr, the deactivation constant by non-radiative pathway and kp the deactivation constant by photochemistry.

Integrating this differential equation gives:

$$[Chl^*] = [Chl^*]_0 e^{-t/\tau}$$

Where the half-life of the excited state of chlorophyll (Chl*) can be expressed as:

$$t_{mean} = \frac{\int_0^\infty t[Chl^*]dt}{\int_0^\infty [Chl^*]dt} = \tau$$

With: $\tau = (kf + knr + kp)^{-1}$

These relations make it possible to express the quantum yield of fluorescence, ϕ_f, defined by the ratio of the number of photons emitted by fluorescence to the number of photons absorbed, using the rate constants of the different mechanisms involved:

$$\phi_f = \frac{Number\ of\ emitted\ photons}{Number\ of\ absorbed\ photons} = \frac{kf}{(kf + knr + kp)}$$

By setting τ_0 the lifetime of the excited state if fluorescence was the only de-excitation phenomenon, i.e. $\tau_0 = kf^{-1}$, ϕ_f can be expressed only as a function of the lifetimes τ and τ_0.

$$\phi_f = \frac{\tau}{\tau_0}$$

Therefore, the chlorophyll fluorescence yield could be expressed as a function of lifetime. Although these relationships have been considered for isolated pigment solutions, this same relationship between ϕ_f and τ has been found in leaves where chlorophyll is bound to highly organized protein complexes, leading to the "Lake model" whereby the organization of the photosynthetic units form a continuous network that allows the excitation energy to be carried to other photosynthetic units.

1.3 Chlorophyll fluorescence remote sensing

The efficiency of the fluorescence emission in vivo is very low (less than 1 - 2% of absorbed energy). Nevertheless, chlorophyll fluorescence is widely used in the laboratory as it is a specific emission of green plants. In addition, chlorophyll is probably one of the rare constituents of the biosphere to fluoresce in the red and far-red parts of the spectrum. Remote sensing of ChlF relies on two major class of methods: active methods, which were historically first developed, use an artificial light source for fluorescence excitation, and passive methods, which detect ChlF induced by solar light.

1.3.1 Active methods

In active methods, a modulated and/or spectrally selected source of light excites the chlorophyll molecules that fluoresce between 650 and 800 nm. Most of active systems in remote sensing make use of pulsed light (lasers, laser diodes, LEDs) in the microsecond, nanosecond or even picosecond time range together with a synchronized detection necessary to measure it under day light conditions. As an example, the PAM (Pulse Amplitude Modulation) fluorimeter (Heinz Walz, Effeltrich, Germany), based on the pioneering work of Schreiber (Schreiber, 1986), has been the basis of a huge development of fluorescence measurements at the leaf level. A large number of publications refers to this family of instruments. Measurements can be done on the dark-adapted state (Fo) or under ambient light (Fs). Changes in Fs with PAR are related to changes of so called “fluorescence quenchings”, either photochemical or non-photochemical, building the link between fluorescence and photosynthetic performance (Baker, 2008; Maxwell & Johnson, 2000; Schreiber, 1986). Moreover, using saturating pulses, the maximum fluorescence level of the dark adapted state (Fm) or under natural light (Fm') can be measured, from which the photosystem II photochemical yield can be calculated according to Genty et al., (1989). Notwithstanding, due to limitations of the light source for saturating pulses, measurements can only be performed on a reduced target area ($\approx$ 1 cm^2). During the last two decades, many efforts have been made to be less invasive and to perform measurements at several meters of distance using, for instance, a laser-diode at $\approx$ 635 nm which can be more easily focused than LEDs by virtue of its higher radiance (Evain et al., 2004; Flexas et al., 2000; López González, 2015). It was then possible to monitor Fs on a fixed leaf continuously during several days or weeks, with a time resolution of a few seconds, and to follow the onset and demise of stresses (for a review, see Moya & Cerovic, 2004). Nevertheless, the illuminated area was still of the same order than the original PAM fluorometer, and to obtain an information at plant or canopy levels a greater number of individual leaves had to be sampled.

Specific LIDARs (light detection and ranging) were developed for vegetation fluorosensing using green (532 nm) or UV (355 nm, 337 nm) lasers and even with dual lasers (355 and 532 nm) (Andersson et al., 1994; Cecchi et al., 1994; Cerovic et al., 1996; Chekalyuk & Gorbunov, 1994; Goulas et al., 1997; Guenther et al., 1991; Hoge et al., 1983; Ounis et al., 2001; Rosema et al., 1998). Thanks to the high directional radiance and high peak power of pulsed lasers, laser-induced-fluorescence (LIF) measurements were possible up to distances of several hundred of meters. However, measurements in saturating conditions were severely limited by the high continuous power required to saturate Fm over an area of $\approx$1 m^2 or more

when working on canopies. Eye-safety restrictions are 10 times more restricting when using excitation wavelengths above 400 nm. This is the main reason why most of remote sensing fluorescence applications under field conditions are based on the measurement of Fs. Even if these variations are lower than those of Fm, it can be up to 100% of the minimum stationary value (Cerovic et al., 1996). Although most of these works were intended to demonstrate the possibility to detect chlorophyll fluorescence at a distance, they were implemented in indoors or under protected conditions and without studying any particular stress. An interesting exception was the work of Rosema et al., (1998) which established a fluorescence signature for drought on poplar plants. In this particular experiment, the samples were placed inside a green-house and chlorophyll fluorescence was analyzed by means of a laser set-up (Laser Environmental Active Fluorosensor, LEAF-NL). The Nd:YAG laser of the LEAF-NL instrument provided a 10 mJ per 10 ns duration pulse at 532 nm forming a spot hitting the plants of ≈ 60 cm of diameter. Continuous measurements during several days allowed Rosema et al., (1998) to evidence a strong Fs quenching (Fs < Fo) at noon under drought conditions that partially reverses during the night.

Despite these historical developments on remote sensing of ChlF with active methods, and although active ChlF measurements provide a direct assessment of fluorescence quenching, as stated above, there is currently no simple active fluorimeter that can acquire fluorescence on a target large enough for canopy studies.

1.3.2 Passive methods

Recently, new passive methods for quantifying ChlF at canopy level attracted a large audience. Their development was motivated by the possibility to monitor ChlF from spaceborne platforms, giving access to study at larger scales compared to active methods. In this goal, the natural radiation of the sun is used as an excitation source to provide the so called solar-induced fluorescence (SIF). Passive methods are based on the existence of dark bands in the solar spectrum - the so-called Fraunhofer lines - which are well superimposed with the chlorophyll fluorescence emission spectrum (Moya et al., 1998). The basic principle of these methods is well illustrated by the Fraunhofer Line Discrimination Principle (FLD), which was historically the first method to be proposed for SIF detection. In short, the FLD compares the depth of the line in the solar irradiance spectrum to the depth of the line in the radiance spectrum of plants, which is affected by fluorescence emission. (Plascyk & Gabriel, 1975) were the first to develop an airborne instrument (FLD II) principally used to detect fluorescence of rhodamine dye in water for marine studies. In a second step, the method was exploited for measuring steady-state SIF from plants, using the Hα line at 656.28 nm (Hemphill et al., 1975; Plascyk, 1975).

A new option for measuring SIF was later developed by (Moya et al., 1998) using the oxygen absorption bands. Compared to solar absorption lines, oxygen absorption bands have the advantage of being relatively broad, deep, and well superimposed with the two characteristic peaks of the fluorescence emission spectrum at 685 and 740 nm (Moya et al., 2004), see Fig. 1. 4. Several works using narrow interferential filters allowed (Louis et al., 2005) to measure fluorescence at distances up to 50 m. Moya et al., (2006) quantified the fluorescence emission of fields at both 687 and 760, from an airborne platform with a filter based home-made

instrument and emphasized the strong effect of the tridimensional structure of the vegetation on the F687/F760 fluorescence ratio. The clear decrease of the F687/F760 fluorescence ratio on going from a planophile field (e.g., sugar beet) to an erectophile one (e.g., wheat) was later analyzed on ground by Fournier et al., (2012) using a spectrograph-based instrument which confirmed these results.

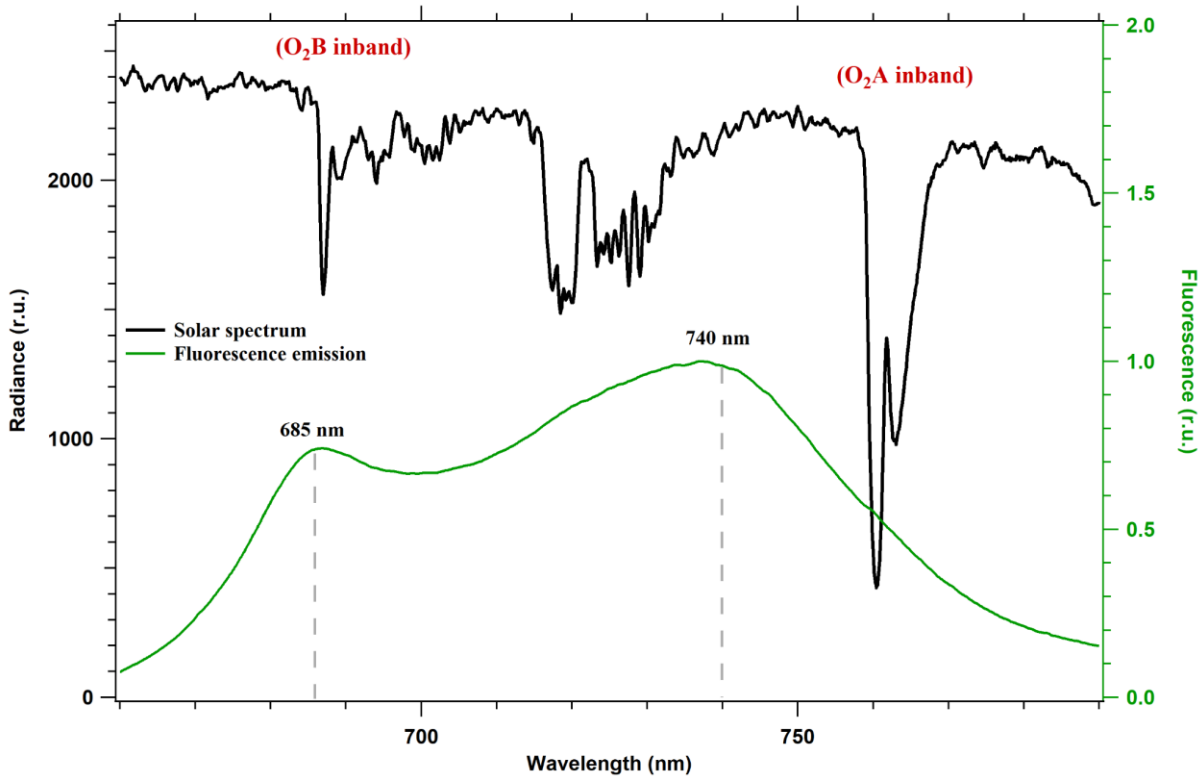

Fig. 1. 4. In black the solar spectrum at sea level and in green the fluorescence emission spectrum of a pea leaf excited with natural light. The position of atmospheric oxygen bands A and B are highlighted in red.

Thanks to the recent availability of compact, high-resolution spectrometers, a great number of SIF measurements have been conducted using the atmospheric oxygen absorption bands. Different setups were used from leaf to canopy level (Y.-B. Cheng et al., 2013; Cogliati et al., 2015; Damm et al., 2010; Daumard et al., 2010, 2012; Fournier et al., 2012; Meroni et al., 2009; Meroni & Colombo, 2006; Rossini et al., 2010) or from an airborne platform (Damm et al., 2015; Rascher et al., 2015; Zarco-Tejada et al., 2009). In most of the cases, passive instruments based on spectrometers used an optical fiber with a numerical aperture of 0.22 (acceptance angle of 25°) which means a target size of about 1 m at a distance of 4 meters. This makes the method well adapted to work at canopy level and obviously under full sunlight conditions.

1.3.3 Diurnal cycles of passive fluorescence measurements

Significant progress has been made in our knowledge of solar-induced chlorophyll fluorescence (SIF) diurnal cycles at the canopy level. For instance, Louis et al., (2005); Goulas et al., (2017); Du et al., (2019), with different instruments, presented diurnal cycles of SIF at O_2-B and O_2-A on pines of the boreal forest, wheat, or maize fields, respectively, showing

different patterns along the day. Other works also reported fluorescence flux diurnal cycles within the two bands (Daumard et al., 2010; Xu et al., 2021) but the resolution of the data presented is relatively low.

PS II predominantly produces the fluorescence flux retrieved in the O_2-B band, while the O_2-A band has fluorescence contributions from PS II and PS I ((Boardman et al., 1966; Govindje, 1995). As a consequence, their kinetics are expected to be different. To study the diurnal kinetics of fluorescence retrieved from O_2 bands, we built a new version of Spectroflex, first described by Fournier et al., (2012). It is a spectrometer-based passive instrument to continuously recover chlorophyll fluorescence emissions within O_2-A and O_2-B bands from potato crops. The main improvements were (i) the enlargement of the spectral bandwidth in the green region from 630-820 nm to 510-818 nm, (ii) a better resolution of the ADC converter (16 bits vs 14 bits), and (iii) a new software for measurements of SIF along the day.

We chose the potato crop due to its importance as a food security crop, as indicated by the Food and Agriculture Organization of the United Nations (FAO), due to its widely adaptive range, excellent yield potential, and high nutritional value (Devaux et al., 2014). In addition, to our knowledge, there are only a few studies of SIF measurements on potato crops at the canopy level, except for recent studies performed by Xu et al., (2021).

1.3.4 Diurnal cycle of passive and active measures of ChlF

Combined LIF and SIF measurements at the foliage scale are scarce, and we found just one such study. Louis et al., (2005) measured scot pines with both methods. They presented the first approximation of passive fluorescence measurements using the Passive Multi-wavelength Fluorescence Detector (PMFD), described by Evain et al., (2001), together with the active fluorescence measurements using the micro-LIDAR FIPAM (Flexas et al., 2000). The comparisons showed a discrepancy at solar noon, and the authors attributed it to differences in the structure of the targets measured by both instruments. For example, FIPAM saturates and measures fluorescence at 2 m covering an area of 3x20 mm. In comparison, PMFD covers a full tree at 40 m.

The study presented by Louis et al., (2005) was a first attempt to compare LIF and SIF measurements at canopy level. SIF measurements are easily scalable, while LIF-based methods are limited by the fluorescence excitation source. In short, Louis et al., (2005) did not have the appropriate active instrument to measure fluorescence yields at canopy level.

In this thesis work, we are going to study comparative measurements of ChlF diurnal cycles performed by both methods. As a first step, we will develop a new active instrument to measure fluorescence yields continuously and at foliage level (Chapter 2). And next, we will investigate diurnal cycle comparisons of SIF and LIF fluorescence measurements (Chapter 3)

CHAPTER 2

Fluorescence measurements at canopy level.

In this chapter is described one of the two field instruments developed in the frame of this project. It is Ledflex, a new active fluorescence instrument designed to perform measurement of ChlF yield at canopy level in the objective of water stress detection. Whilst the passive fluorescence instrument is described in detail in Chapter 3.

Ledflex is a robust instrument able to measure fluorescence yield in outdoor conditions during several days and under different weather conditions. This instrument was conceived by Ismael Moya, co-advisor of my thesis, and my main contributions were: 1) to develop the software that allows it works continuously. To acquire synchronized signals with the turning on of source of light and detection fluorescence system. To acquire asynchronously measurements as air temperature and incident PAR, 2) to perform Ledflex tests in laboratory and open field, and 3) to perform calibrations and tuning of different instrument parts: the optics, the source of light and the fluorescence detection system. Two Ledflex were implemented for my thesis work. One of them was used in controlled water stress experiments with crops planted on pots (menthe and pea) in the facilities of Site Instrumental de Recherche par Télédétection Atmosphérique (SIRTA) placed in Palaiseau – France, and with fescue meadow in Barrax – Spain. Whilst the second Ledflex was underwent to a field experiment with potato crops in Lima- Peru.

Ledflex was presented in a paper published in Photosynthesis Research journal (Moya et al., 2019). In this paper, we gave a deep description of Ledflex and presented a simple methodology to detect water stress in peas and menthe crops using stationary fluorescence (Fs) values retrieved from diurnal cycles of Fs.

2.1 Article: Canopy chlorophyll fluorescence applied to stress detection using an easy-to-build micro-LIDAR

Ismael Moya[1], **Hildo Loayza**[2], Maria Llanos López[3], Roberto Quiroz[4], Abderrahmane Ounis[1], Yves Goulas[1]

2.1.1 Abstract

Ledflex is a micro-LIDAR dedicated to the measurement of vegetation fluorescence. The light source consists of 4 blue Light-Emitting Diodes (LED) to illuminate part of the canopy in order to average the spatial variability of small crops. The fluorescence emitted in response to a 5-µs width pulse is separated from the ambient light through a synchronized detection. Both the reflectance and the fluorescence of the target are acquired simultaneously in exactly the same field of view, as well as the photosynthetic active radiation and air temperature. The footprint is about 1 m^2 at a distance of 8 m. By increasing the number of LEDs longer ranges can be reached. The micro-LIDAR has been successfully applied under full sunlight conditions to establish the signature of water stress on pea (*Pisum sativum*) canopy. Under well-watered conditions the diurnal cycle presents an M shape with a minimum (Fmin) at noon which is Fmin

> Fo. After several days withholding watering, Fs decreases and Fmin < Fo. The same patterns were observed on mint (*Menta spicata*) and sweet potatoes (*Ipomoea batatas*) canopies. Active fluorescence measurements with Ledflex produced robust fluorescence yield data as a result of the constancy of the excitation intensity and its geometry fixity. Passive methods based on Sun-Induced chlorophyll Fluorescence (SIF) that uses high-resolution spectrometers generate only flux data and are dependent on both the 3D structure of vegetation and variable irradiance conditions along the day. Parallel measurements with Ledflex should greatly improve the interpretation of SIF changes.

Keywords: µ-LIDAR LIF SIF Stress detection Ledflex

Abbreviations

NDVI	Normalized Difference Vegetation Index
NIR	Near Infra-Red
R	Red
PAR	Photosynthetic Active Radiation
GPP	Gross Primary Production
PRI	Photosynthetic Reflectance Index
$\rho 531$	Reflectance at 531 nm
$\rho 570$	Reflectance at 570 nm
ChlF	Chlorophyll Fluorescence
LED	Light Emitting Diode
PAM	Pulse Amplitude Modulation
Fo	Minimum Dark Adapted Fluorescence yield
Fs	Stationary Fluorescence yield
Fm	Maximum Dark-Adapted Fluorescence yield
Fm’	Maximum Steady State Fluorescence yield
LIDAR	Laser Induced Detection And Ranging
UV	Ultra-violet
LIF	Laser or Led Induced Fluorescence
SIF	Sun induced fluorescence
PVC	Poly Vinyl Chloride
TTL	Transistor-Transistor Logic
DAQ	Data Acquisition
ADC	Analog to Digital Conversion
Rc	Reflected light
Tdiode	Detector Temperature
Tled	Light Emitting Diodes Temperature
Tair	Air Temperature
SNR	Signal to Noise Ratio
PPFD	Photosynthetic Photon Flux Density
FWHM	Full Width at Half-Maximum

2.1.2 Introduction

Photosynthesis is the process by which plants absorb H_2O from the soil and CO_2 from the atmosphere to generate sugars and release O_2. Light collected by photosynthetic pigments (mainly chlorophylls and carotenoids) is the source of energy. To assess plant development and growth at medium scale (e.g., canopy to parcel), it is necessary to monitor the photosynthetic activity at a comparable scale. Chlorophyll absorption exhibits a strong transition in the near infrared reflectance spectrum. This spectral change has been used for a long time to determine the amount of vegetation. For instance, the normalized difference vegetation index (NDVI): NDVI = (NIR−R)/(NIR + R), which compares the vegetation reflectance in the near infrared (NIR) and red (R) parts of the spectrum is widely used in remote sensing. (Sellers, 1987) was the first to show a link between NDVI, absorbed, and incident photosynthetically active radiation (PAR) as

NDVI ≈ (absorbed PAR/incident PAR)

Using remotely sensed NDVI as a proxy for the fraction of absorbed PAR, gross primary production (GPP) can be estimated as GPP = α × NDVI × PAR, where α is a conversion efficiency empirically determined in the field for each vegetation type (see Moya & Flexas, 2012 for a review). However, NDVI fails to detect dynamic variations of photosynthesis rates, like those occurring during the day or under certain stress (Running & Nemani, 1988).

Another proposed reflectance index is the photochemical reflectance index (PRI): PRI = (ρ531−ρ570)/(ρ531+ρ570), where ρ531 and ρ570 are the vegetation reflectance at 531 and 570 nm. This index uses two spectral bands in the green and yellow parts of the reflectance spectrum to track reflectance changes near 531 nm associated with the deepoxidation of the violaxanthin pigment into zeaxanthin that takes place under excess light conditions (Gamon et al., 1992). Evain et al., (2004) showed that PRI correlates better with non-photochemical quenching, related to dissipation of energy excess, than with photochemical quenching (e.g., photosynthesis activity), and is a good indicator for stomata closure upon water shortage. Indeed, PRI has been considered as a potential indicator of water stress (Goerner et al., 2009; Peguero-Pina et al., 2008; Suárez et al., 2008, 2009) or light use efficiency (Y. Cheng et al., 2006; Drolet et al., 2008) and it is also influenced by seasonal changes in pigment contents and canopy structure (Gamon et al., 2004). Besides these first employed reflectance signals, chlorophyll fluorescence is another parameter that increasingly interests scientists.

Chlorophyll fluorescence (ChlF) can be regarded as a small “leak” occurring during energy transfer in light-harvesting antennae. It is a natural emission between 650 and 800 nm (with two maxima in the red and far-red part of the spectrum) which emanates from the two photosynthetic systems. As fluorescence emission competes with photochemical conversion and thermal deactivation, in vivo chlorophyll fluorescence is variable and its variations mirror photochemical changes. Plant fluorescence is then subject to changes according to environmental constraints: light, temperature, water, and nutrient supply, among others. Although small (less than 1% of absorbed radiation) vegetation fluorescence is an attractive proxy for remote assessment of photosynthesis. Chlorophyll fluorescence can be measured using active or passive methods.

2.1.2.1 Active methods

In active methods, a modulated and/or spectrally selected source of light excites the chlorophyll molecules that fluoresce between 650 and 800 nm. Most of active systems in remote sensing make use of pulsed light (lasers, laser diodes, LEDs) in the microsecond or even picosecond time range together with a synchronized detection necessary to measure it under day light conditions. As an example, the PAM (Pulse Amplitude Modulation) fluorimeter (Heinz Walz, Effeltrich, Germany), based on the pioneering work of Schreiber (Schreiber, 1986), has been the basis of a huge development of fluorescence measurements at the leaf level. A large number of publications refer to this family of instruments. Measurements can be done on the dark-adapted state (Fo) or under ambient light (Fs). Changes in Fs with PAR are related to the photosynthetic performance (Baker, 2008; Maxwell & Johnson, 2000; Schreiber, 1998). Moreover, using saturating pulses, the maximum fluorescence level in the dark (Fm) or under natural light (Fm') can be measured, from which the photosystem II photochemical yield can be calculated according to Genty et al., (1989). Notwithstanding, due to limitations of the light source for saturating pulses, measurements can only be performed on a reduced target area (≈ 1 cm^2). During the last two decades, many efforts have been made to be less invasive and to perform measurements at several meters of distance using, for instance, a laser diode at ≈ 635 nm which can be more easily focused than LEDs by virtue of its higher radiance (Evain et al., 2004; Flexas et al., 2000; López González, 2015). It was then possible to monitor Fs on a fixed leaf continuously during several days or weeks, with a time resolution of a few seconds, and to follow the onset and demise of stresses (Moya & Cerovic, 2004). Nevertheless, the illuminated area was still of the same order than the original PAM fluorometer, and to obtain an information at plant or canopy level, a greater number of individual leaves had to be sampled.

Specific LIDARs (Light Detection And Ranging) were developed for vegetation fluorosensing using green (532 nm) or UV (355 nm, 337 nm) lasers and even with dual lasers (355 and 532 nm) (Andersson et al., 1994; Cecchi et al., 1994; Cerovic et al., 1996; Chekalyuk & Gorbunov, 1994; Goulas et al., 1997; Guenther et al., 1991; Hoge et al., 1983; Ounis et al., 2001; Rosema et al., 1998). Laser-induced-fluorescence (LIF) measurements were severely limited by the high power required to saturate Fm over an area of ≈ 1 m^2 or more when working on canopies. To overcome these limitations, the laser-induced fluorescence transient (LIFT) method proposed to use fast repetition rate (FRR) of sub-saturating light pulses to retrieve an extrapolated Fm value from the analysis of the observed induction kinetics (Ananyev et al., 2005). On the other hand, eye-safety restrictions are 10 times more restricting when using excitation wavelengths above 400 nm. Most of remote-sensing fluorescence applications under field conditions are based on the measurement of FS. Even if these variations are lower than those of Fm, it can be up to 100% of the stationary value (Cerovic et al., 1996). Although most of these works were intended to demonstrate the possibility to detect chlorophyll fluorescence at a distance, they were implemented in indoors or under protected conditions and without studying any particular stress. An interesting exception was the work of Rosema et al., (1998) which established a fluorescence signature for drought on poplar plants. In this particular experiment, the samples were placed inside a greenhouse and chlorophyll fluorescence was analyzed by means of a laser set-up (Laser Environmental Active Fluorosensor, LEAF-NL). The Nd:YAG laser of the LEAF-NL instrument provided a 10-mJ per 10 ns duration pulse at 532 nm forming a spot hitting the plants of ≈ 60 cm of diameter. Continuous measurements during several days

allowed Rosema et al., (1998) to evidence a strong Fs quenching (Fs < Fo) at noon under drought conditions that partially reverses during the night.

2.1.2.2 Passive methods

Recently, new passive methods for quantifying ChlF at canopy level attracted a large audience. They are based on the existence of dark bands in the solar spectrum - the so-called Fraunhofer lines - which are well superimposed with the chlorophyll fluorescence emission spectrum (Moya et al., 1998) and often measured using the Fraunhofer Line Discrimination Principle (FLD). In short, the FLD compares the depth of the line in the solar irradiance spectrum to the depth of the line in the radiance spectrum of plants. (Plascyk & Gabriel, 1975) were the first to develop an airborne instrument (FLD II) principally used to detect fluorescence of rhodamine dye in water. In a second step, the method was envisaged for measuring steady-state sun-induced fluorescence (SIF) from plants, using the Hα line at 656.28 nm (Plascyk, 1975). A new option for measuring SIF was later developed by Moya et al., (1998) using the oxygen absorption bands. Compared to solar absorption lines, oxygen absorption bands have the advantage of being relatively broad, deep, and well superimposed with the two characteristic peaks of the fluorescence emission spectrum at 685 and 740 nm (Moya & Cerovic, 2004). Several works using narrow interferential filters allowed Louis et al., (2005) to measure fluorescence at distances up to 50 m. Moya et al., (2006) quantified the fluorescence emission of fields at both 687 and 760, from an airborne platform with a filter-based home-made instrument and emphasized the strong effect of the tridimensional structure of the vegetation on the F687/F760 fluorescence ratio. The clear decrease of the F687/F760 fluorescence ratio on going from a planophile field (e.g., sugar beet) to an erectophile one (e.g., wheat) was later analyzed on ground by Fournier et al., (2012) using a spectrograph-based instrument which confirmed these results.

Thanks to the recent availability of compact, high-resolution spectrometers, a great number of SIF measurements have been conducted using the atmospheric oxygen absorption bands. Different setups were used from leaf to canopy level (Y.-B. Cheng et al., 2013; Cogliati et al., 2015; Damm et al., 2010; Daumard et al., 2010, 2012; Fournier et al., 2012; Meroni et al., 2009; Meroni & Colombo, 2006; Rossini et al., 2010) or from an airborne platform (Damm et al., 2015; Rascher et al., 2015; Zarco-Tejada et al., 2009). In most of the cases, passive instruments based on spectrometers used an optical fiber with a numerical aperture of 0.22 (acceptance angle of 25°) which means a target size of about 1 m at a distance of 4 meters. This makes the method well adapted to work at canopy level and obviously under full sunlight conditions. However, SIF may show variations linked to the angular distribution of incident light, depending on canopy architecture (Fournier et al., 2012; Goulas et al., 2017), impeding the interpretation of SIF in terms of fluorescence quenching and physiological acclimation of plants. On the other hand, although active ChlF measurements provide a direct assessment of fluorescence quenching, as stated above, there is no simple active fluorimeter that can acquire fluorescence on a target large enough for canopy studies.

The aim of this paper is to describe an easy-to-built instrument, named Ledflex, that measures ChlF at canopy level requiring only a few skills in mechanics and electronics that are usually available in most of plant-physiology laboratories, and to evaluate its potential in plant stress detection. Our work aimed to:

– Design, build, and test a prototype of an active fluorometer, capable of performing measurements at several meters from the target, with a spot size large enough to integrate its spatial heterogeneity; and
– Record continuously the stationary ChlF (Fs) under outdoor conditions and full solar illumination, in order to obtain a plant status fluorescence signature. The possibility to obtain the fluorescence signature of a moderate (reversible) water stress, before pre-visual signs appeared, is discussed.

2.1.3 Materials and methods

2.1.3.1 Description of the Ledflex micro-LIDAR

We developed a micro-LIDAR (μLIDAR) system to monitor chlorophyll fluorescence from vegetation, an instrument composed of three main parts: (i) a light source, (ii) an optical telescope, and (iii) a detection system (Fig. 2. 1). It was designed to work day and night under all weather conditions. All the detection parts were housed into a "drainage" pipe (polyvinyl chloride (PVC) tube of 160 mm diameter). The light source was contained within the 50 mm of diameter PVC pipe and connected to the detection pipe by a flexible 25 mm of diameter PVC pipe. The light source and telescope were fixed on two independent mounts and were mechanically adjustable, depending on the working distance.

The excitation light source

Nowadays, there are many LEDs that fit our needs to induce ChlF provided that its wavelength emission is below 650 nm. We choose LED470L emitting at 470 ± 5 nm, with a full width at half-maximum (FWHM) of 22 nm (Thorlabs, Maisons- Laffitte, France) for the following reasons:
– Spectral purity (no emission in the red or infrared parts of the spectrum).
– Maximum continuous optical power 170 mW (at 350 mA).
– High-peak current > 3A at a frequency of 100 Hz for a pulse duration of 5 μs. The optical peak power should be > 1 W.
– Low power supply voltage (3.8 V).

Fig. 2. 1 The Ledflex micro-LIDAR. The smaller tube contains the excitation source and the driver electronics. The larger tube contains the detection optics, the detector and its amplifier, the acquisition board and the computer.

Pulsed light is a pre-requisite to disentangle the weak fluorescence emission from the continuous daylight background. We chose to detect pulses of ≈ 5 µs of duration as it fitted well the time constant of our detection system (see below). As a result we pushed the current up to 3A without damage. We estimated the rise time of natural daylight variations (changes in illumination due to clouds) at a few seconds. Using pulses repetition rate of about 100 Hz and an averaging of the elementary measurements to a final frequency of ≈ 0.5 Hz to improve the signal-to-noise ratio, we were able to follow these daylight variations. Four LED470L LEDs were mounted in series in our instrument to obtain enough signal to measure at a distance up to ≈ 10 m, depending on the target (see below). In our experiments, the illuminated area was about 50 cm × 50 cm at a distance of 4 m. Even in the dark, the blue light of Ledflex was found to be not disturbing at this distance i.e., it did not drive any change in fluorescence and photosynthesis.

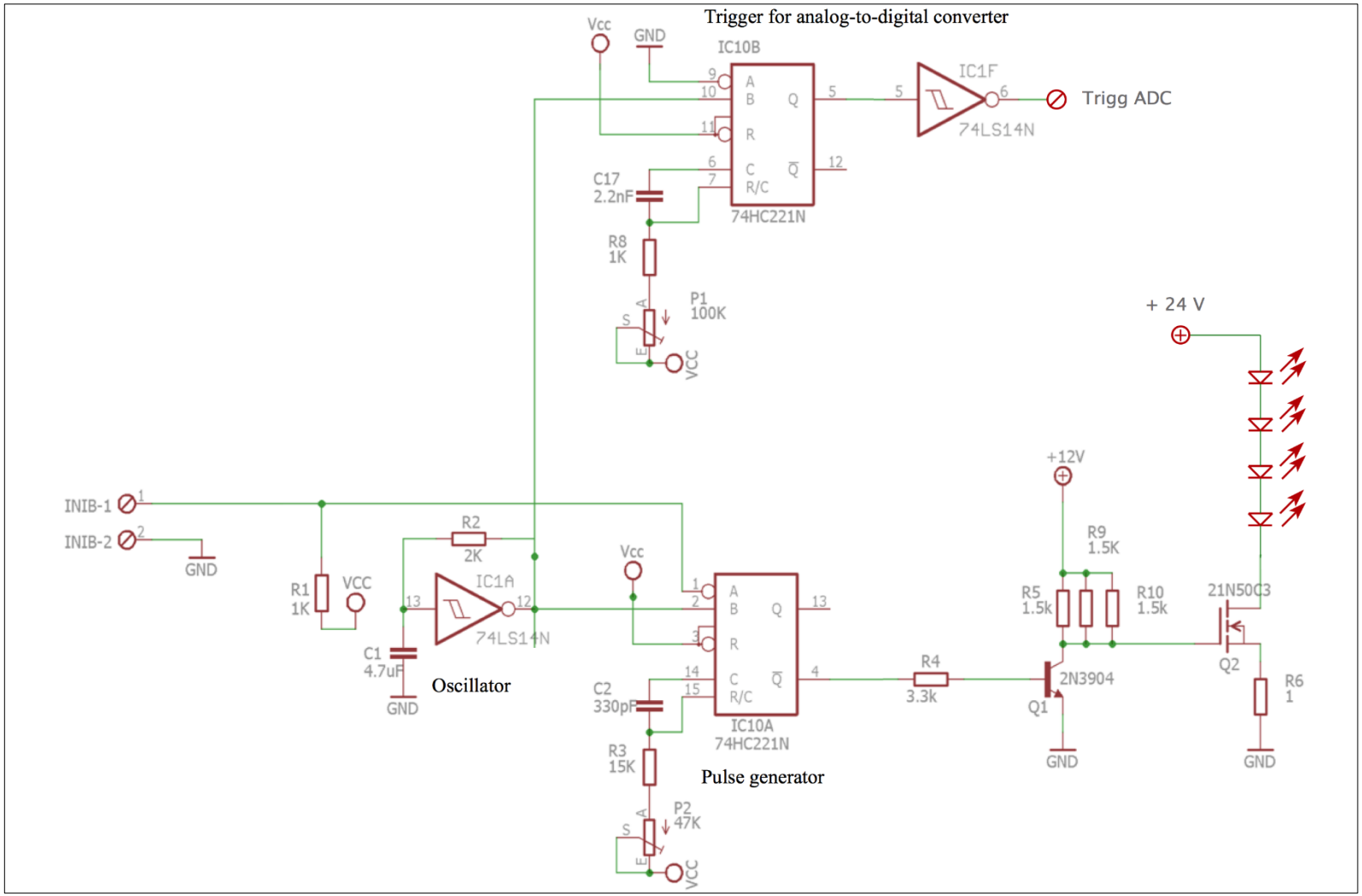

Fig. 2. 2 Scheme of the light source electronics

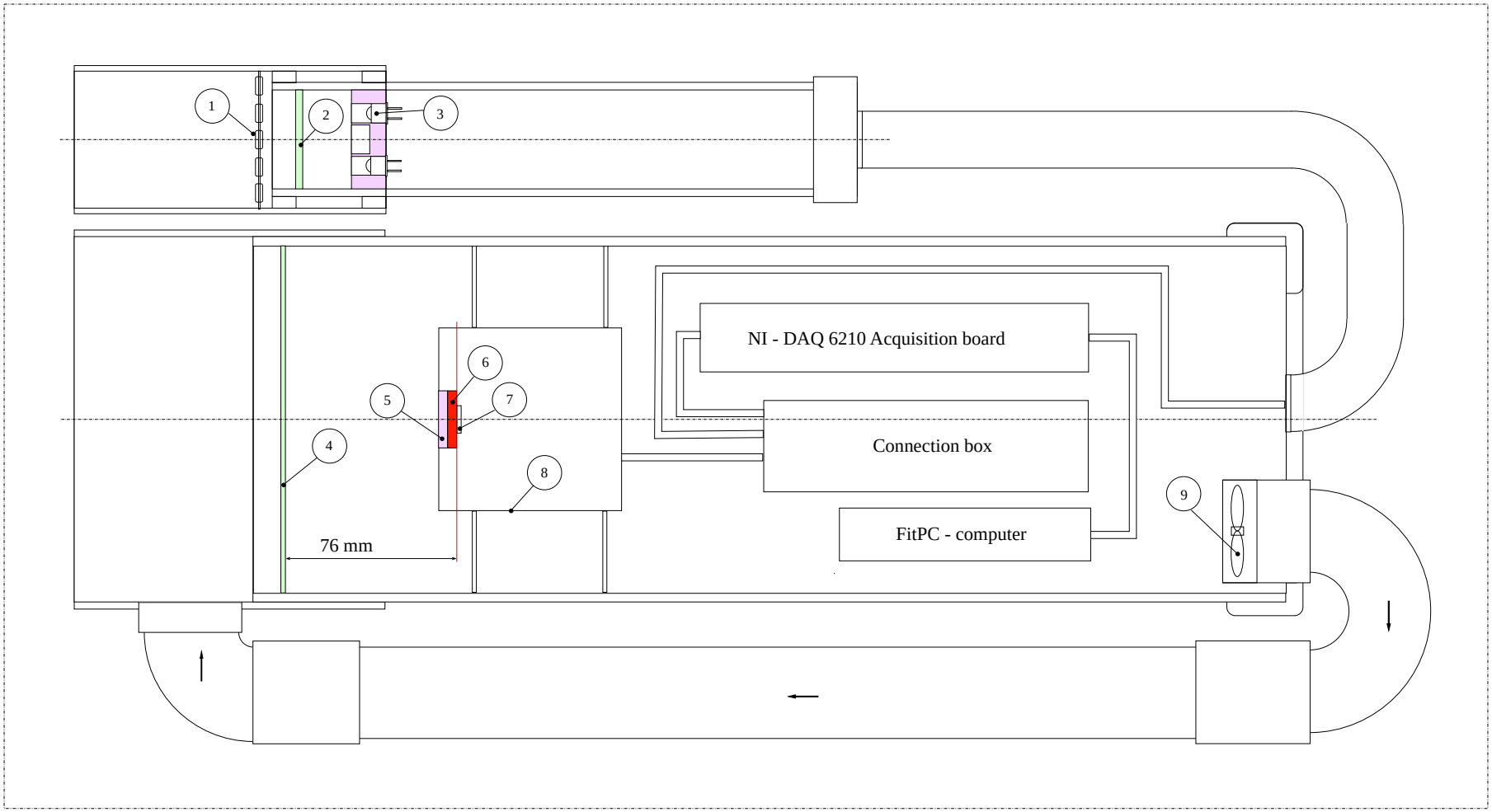

Fig. 2. 3 Schematic view of Ledflex. 1. Heating resistors, 2. Glass window, 3. Excitation LEDs, 4. Fresnel lens, 5. Low-pass filter (λ <800 nm), 6. High-pass filter (λ >660 nm). 7. 10mm x10mm Photodiode, 8. Detector housing, 9. Fan.

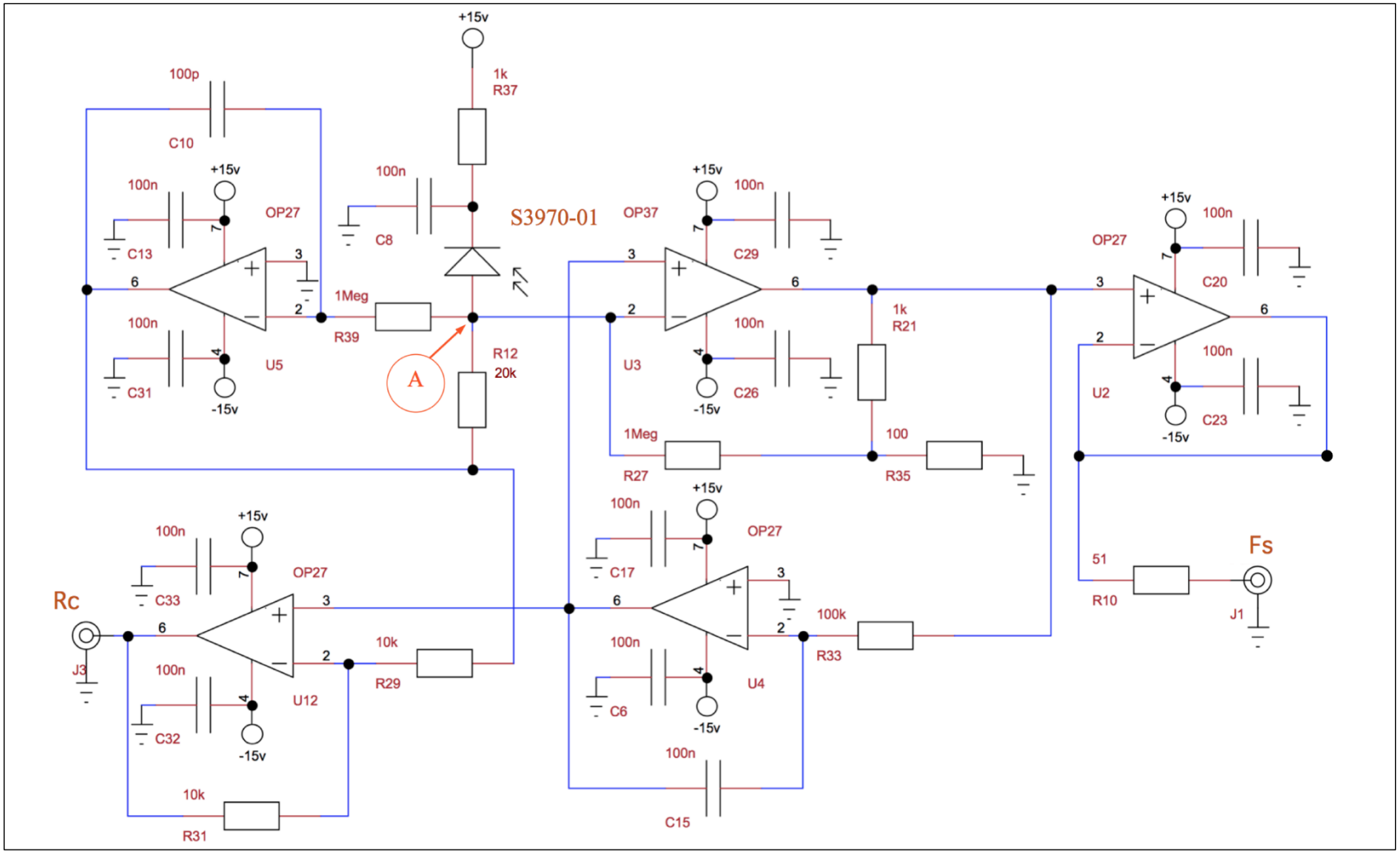

Fig. 2. 4 Electronics scheme for the detector.

The scheme for the electronic circuitry that drives light source is given in Fig. 2. 2. The time base frequency was produced by a Schmitt-trigger inverter (IC1A; 1/6 74LS14 N, Texas Instruments, Dallas USA) inserted in a feedback loop including a RC (Resistor Capacity, with R = 2 kΩ and C = 4.7 μF, RC = 9.4 ms) cell to generate a square wave of approximately 100 Hz. The Schmitt-trigger output was fed to a first monostable (IC10A; 1/2 74HC221 N, Mouser electronics, USA) that defines an adjustable pulse duration of about ≈ 5 μs. The output of the first monostable was amplified by a transistor 2N3904 (Farnell, France) to generate a signal of ≈ 12 V, which in turn fed a 21N50C3 MOSFET (Infineon, Germany) that drove the current for powering the diodes. Four identical LEDs were mounted in series and required 24 V. To synchronize the LED emission and the detection, we generated a TTL signal that triggered an analog to digital conversion card (USB-6210, National Instruments, USA). This was achieved by a second monostable (IC10B, 1/2 74HC221 N) synchronous with the first one followed by a second Schmitt-trigger inverter (IC1F; 1/6 74LS14 N). For practical reasons, the whole instrument was powered by a unique source of voltage (12 V). The total power consummation of the whole instrument was < 1.3 A/12 V which can be easily powered by a solar panel. We generated 24 V using a DC–DC converter (12 V-24 V XPPOWER, USA) (not shown). A second DC–DC converter generated ± 5 V and ± 15 V using a DC/DC 12/5, ± 15 V (XP-POWER, USA) whose voltages were required to generate TTL signals and to power the OP27/37 amplifiers of the detection system. By adjusting the voltage of the MOSFET, we determined the current (3 A for each diode).

The Optics

The fluorescence of the target was collected by a 152-mm diameter Fresnel lens (Edmund Optics, France) with a focal length of 76 mm and focused on a PIN photodiode (Hamamatsu S3590-01) after passing through a high-pass filter (Schott RG665, Edmund Optics, UK). In addition a low-pass filter (λ < 800 nm, Edmund Optics, UK) reduced the spectral range to the useful zone (650–800 nm) where chlorophyll fluorescence was emitted.

To limit water condensation on the optical parts often occurring in the early morning, a heating system was added. Hot air produced by the computer and electronic components was extracted from the head by a small fan and directed by a PVC pipe to the outside face of the Fresnel lens (Fig. 2. 3). This cooling of the electronics worked permanently and warmed the Fresnel lens on the outside. It was also necessary to warm the window in front of the LEDs. For this, we used a set of 5 11 Ω (0.5 W) resistors mounted in series and forming a ring through which the LEDs' light crossed. The ring was placed outside, against the window protecting the LEDs in the sunshade. Powered by 12 V, they maintained the window at +10 °C above ambient temperature.

The fluorescence detection system

The fluorescence detection was designed to detect the fluorescence pulses generated by the LEDs' excitation and at the same time be insensitive to ambient light. The light sensor was a PIN photodiode (S3970-01Hamamatsu, France) of 10 x10 mm that detected light in the range 300-1100 nm with a peak at 920 nm. It was reverse biased at 15 V. To detect the pulsed fluorescence, a circuit originally developed in the lab by M. Bergher (Fig. 2. 4) used basically two amplifiers: a fast one (OP37, U3) and a slower one (OP27, U4 Analogue device, France)

mounted as low-pass filter (cutoff frequency 1.6 kHz) in a feedback loop. As a result, the output of the slower amplifier corresponded to the averaged signal while the faster one only output the fluorescence pulses. A third OP27, (U5) was mounted as a low-pass filter (cutoff frequency 1.6 kHz) and maintained the potential of the photodiode cathode (point A, Fig. 2. 4) near zero. Thanks to a fourth OP27, (U12), the amplitude of the low frequency (f<1.6 kHz) signal was formed by the algebraic difference between the outputs of the U4 and U5 amplifiers (low-pass filters) whose responses were in phase opposition. The low frequency signal detected by the photodiode mainly consisted of the backscattered sunlight coming from the exact target place, seen in the spectral bandwidth of the fluorescence signal and the viewing direction of the sensor. Finally, a fifth OP27, (U2) was mounted as a follower to isolate the pulsed output from perturbations produced by the measuring devices. This detection system, used in our lab for more than 20 years, was the heart of our fluorimeter as it allows to measure under full sunlight conditions.

A USB M Series 6210 multifunction DAQ board (National Instruments, USA) was used to collect and digitize fluorescence signals and other environmental parameters. A small computer FITLET-IA10-BB (D2M, France) powered with 12 V and placed inside the main drainage pipe controlled the acquisition card and the data transfer between the card and the computer memory (see Fig. 2. 3). The computer was programmed using HT BASIC 10 (TransEra Corporation, Orem, Utah, USA) for historical reasons but several other alternatives like C or Labview (National Instruments) exist. The computer was controlled over the internet to perform unattended measurements.

The 6210 board was configured with 8 differential channels. It had a single channel maximum rate of 250 KHz and an analog to digital conversion (ADC) resolution of 16 bits. One channel was devoted to the pulsed fluorescence measurement (OP27 U2, Fs). In order to be locked with the LED pulses, the output of the Schmitt-trigger IC1F (Trigg ADC, Fig. 2. 2) was used to trigger the 6210 board to measure Fs at the peak value of the signal pulse. Here, a correct delay had to be adjusted. We used an oscilloscope to visualize both the TTL signal Trigg ADC and the Fs pulses. Then the instruction for measuring Fs at the peak was defined using steps of 50 ns. As the width of the Fs pulse was about several µs, this adjustment was not delicate. The other channels were operated in internal triggering mode and included measurements of the OP27 U12 output (Rc, Fig. 2. 4), the Photosynthetic Active Radiation (PAR), detector temperature (Tdiode), LEDs temperature (Tled) and ambient temperature (Tair). Temperatures were measured using a thermistor (RS 151-237 Radiospares, France) of 10 kΩ at 25°C fed by a 100 µA current source (REF 200, Texas Instruments USA). These environmental parameters were acquired an averaged Fs was stored (i.e. 2.27s).

Signal to noise ratio and working distance

The moderate output power of the light source implied that the target could not be too far, as the detected flux decreased proportionally to the inverse of the square of the distance. We made some tests at midday, under full sunlight conditions, pointing the Ledflex head to nadir above the pea canopy. The ground surface was fully covered by pea leaves and the mean leaf chlorophyll content was about 40 SPAD units[1]. At 4 m above the canopy, the signal was 0.8 V.

[1] SPAD units are proportional to the amount of chlorophyll present in the leaf (see section 2.1.3.5)

The measured standard deviation of the Fs signal on 70 points (3 min of measurement) was ± 0.006 V. The signal-to-noise ratio (SNR) was 133, which we considered as good. During the night, the signal decreased to 0.72 V but with a much lower noise of ± 0.002 V resulting in a SNR = 360. The noise reduction at night was a proof that most of the noise during day was due to photon noise induced by ambient light. Given the quadratic decrease of the signal with distance, we expected an Fs value of 0.2 V at 8 m with the same noise. So, the SNR would drop to 33 under full sunlight, which was assumed to be still acceptable. However, we did not make the test at this distance because of the mechanical limitations of our set-up in a vertical position. Fig. 2. 5 shows the Ledflex complete set-up in the field.

Fig. 2. 5 Ledflex in operation above grassland. The PAR sensor is fixed on a vertical rod above the boom. The boom is rigidified with ropes to avoid any movements due to wind.

2.1.3.2 Plant material and environmental

Experiments were carried out on the SIRTA (Site Instrumental de Recherche par Télédétection Atmosphérique) (48.7º N, 2.2º E) during summer and autumn of 2015. In a first experiment, plant material was *Pisum sativum* "petit provençal" variety. Seeds were planted with a distance between them of approximately 2 cm in a pot (Ø 54 cm x 16 cm deep) with universal substrate. Measurements started when a homogeneous canopy was obtained. Several days after the beginning of measurements, water stress was induced by withholding watering. To monitor the recovery from water stress, the plants were irrigated again.
Measurements were also done on mint (*Mentha spicata*) canopy planted in pots as well as on Velvet grass (*Holcus lanatus*) a natural meadow. They were grown in outdoors conditions and maintained in well watered conditions.

2.1.3.3 Water Content Index

To estimate a "water content index" (WCI), small leaf discs were extracted with a cork borer and weighted immediately to obtain fresh weight. These discs were immerged in distilled water at 4 °C and weighted after 24 h in the freezer to obtain the weight at full turgor. WCI was calculated following the relation:

$$WCI = 100 * (\text{Fresh weight}) / (\text{Turgid weight}).$$

According to Smart and Bingham 1974 there is an almost linear relationship between WCI and the relative water content defined as (RWC) = (Fresh weight−dry weight)/(Turgid weight−dry weight).

2.1.3.4 Gas exchanges measurements

The gas exchange measurements were made using the leaf chamber fluorometer of LI-6400 IRGA (Li-Cor, Lincoln, NE, USA). This chamber gives the quantum yield of PS II from chlorophyll fluorescence data in the same area where gas exchange is measured. Three to five attached leaves were measured at mid-morning during the different water treatments periods. The measurements conditions were constants with 1300 µmol/m^2·s of PAR and 390 µmol CO_2/mol of air concentration. All the measurements were carried out on fully expanded leaves at mid-morning. An additional stomatal conductance measurement at leaf level was obtained with a leaf porometer (Decagon Devices) thus increasing the number of leaves measured during the water stress induction.

2.1.3.5 Chlorophyll content

The chlorophyll content was estimated in SPAD units with the SPAD-502 (Minolta) over the campaign as the average of 20-30 measurements on different leaves.

2.1.3.6 PAR measurements

Photosynthetic Active Radiation was measured with a quantum-meter (JYP 1000, SDEC, Reignac sur Indre, France) fixed above the instrument in order to avoid any shade induced by the surrounding (Fig. 2. 5).

2.1.4 Results

2.1.4.1 Pea measurements

Measurements at canopy level require spatial integration to average the fluorescence signal over a great number of leaves. It involves also measurements at distance in order to be non-invasive. We choose to use plants in a pot, as described in the methods, for a better control of water content. To achieve this, the canopy of pea plants that were grown outdoors (full sunlight) was used to perform measurements. Plants were sowed on August 18th and maintained until October 6th. Ledflex was fixed in a vertical position 2.5 m above the target. Plants were well watered until September 8th, when we stopped irrigation.

2.1.4.2 Control measurements.

On September 10th the plants could still be considered as well-watered. Fig. 2. 6a shows, for this sunny day, a complete cycle of stationary fluorescence (Fs, red line) together with the reflected light (Rc, blue line) and measured Photosynthetic Active Radiation (PAR, black line). During the night, Fs stayed almost constant. This constant night level is denoted as Fo hereafter. After the night Fs increased with the first photons reaching the canopy until 8:30 a.m. Maximum of Fs was attained with a PAR of ≈ 250 μmol $m^{-2}s^{-1}$. Further PAR increases until solar noon (2:00 p.m.) led to a continuous decrease of Fs. Compared to the Fo value obtained during the night, Fs remained significantly higher (Fs solar noon > Fo). During the afternoon, Fs increased again to attain a second maximum (6:00 p.m.) equal to the one obtained in the morning. Notwithstanding, the PAR was still about 600 μmol m^{-2} s^{-1}. Observed Fs signal variations between 9:30 and 11:00 a.m. were a consequence of the gas exchange measurements that caused disturbances in the measuring area, due to the limited size of the target.

To illustrate the Ledflex capacity to monitor rapid changes under changing illumination conditions, we produced an artificial shade of the target around 11:30 a.m., which reduced the incoming radiation to ≈ 13% of full sunlight (Fig. 2. 6b). During the shade period lasting 8.5 min, we observed an increase of Fs followed by a decrease to a value close to that reached at full sunlight. When the shade was removed, a large increase of Fs was observed followed by a decrease to a level lower than under the shade. The increase of Fs depended, among other things, on the temporal resolution of the instrument (≈ 2.3 s) and on the speed at which the panel producing the shade was removed. After a few minutes, the effect of the shade completely disappeared.

2.1.4.3 Stress measurements

Water stress was induced by withholding watering. The water content index (WCI) was estimated as described in the methods. Leaf discs were taken periodically in the early morning to avoid differences in water content due to water loss during the day. Environmental heterogeneity was present during the experiment, with sunny and cloudy days, as well as sunny and cloudy intervals within the same day. During rainy days the pots were covered.

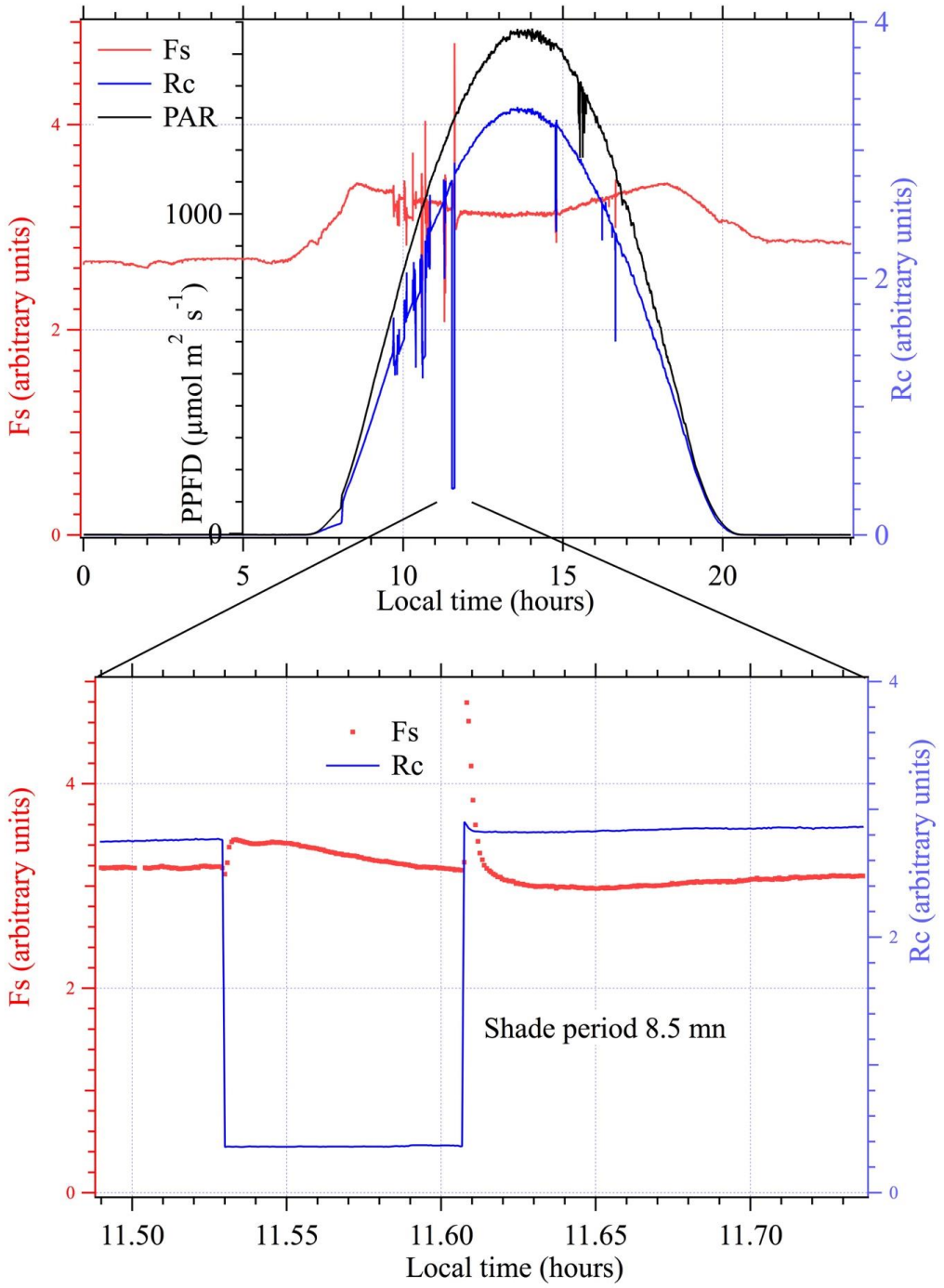

Fig. 2. 6 a Diurnal cycle of PAR, Rc (reflected light) and Fs (stationary fluorescence) above a pea canopy. **b** Detail of an artificial light transition. One may observe the small transient of Rc after the end of the shade period which is due to the fluorescence contribution.

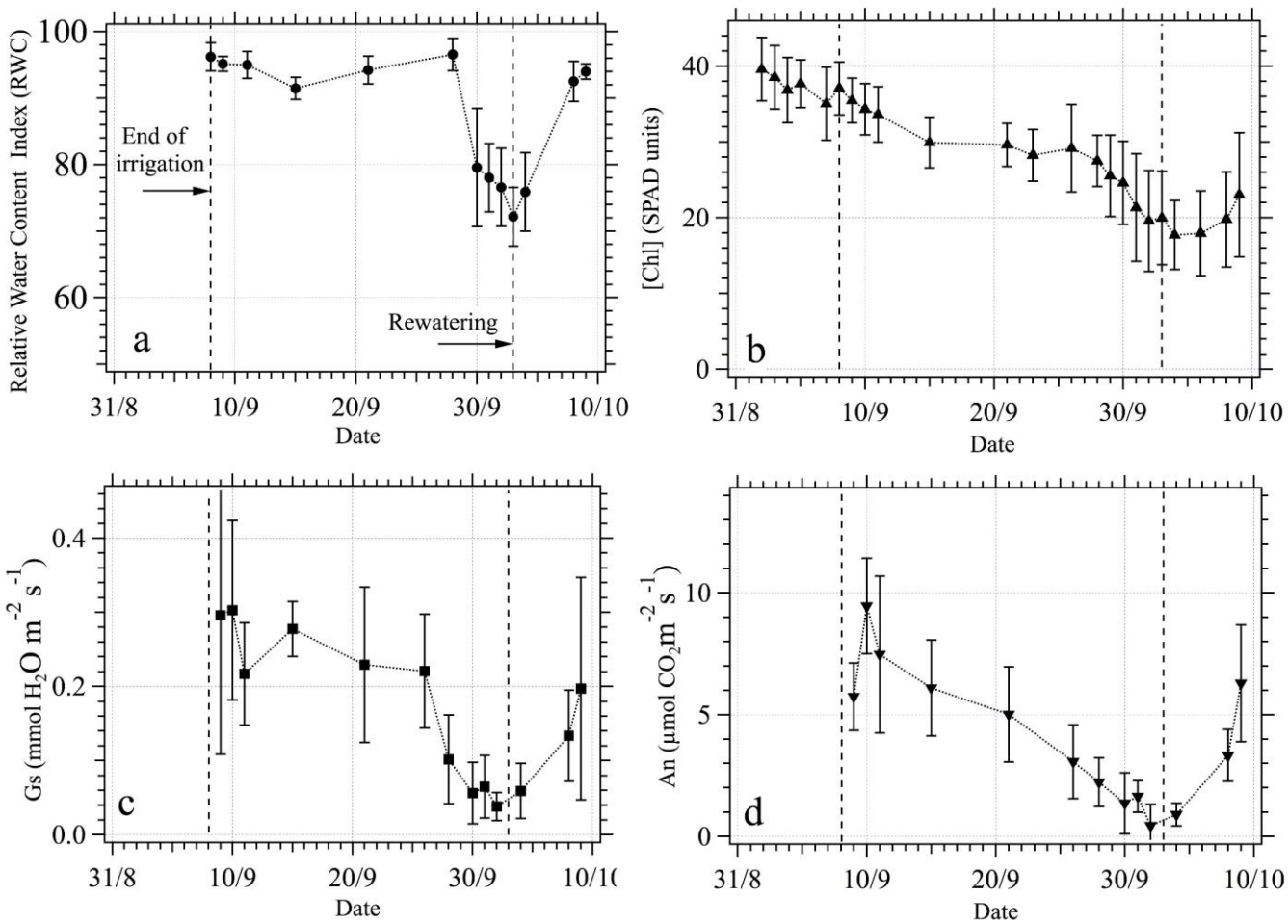

Fig. 2. 7 Pea canopy during water stress treatment. **a** Relative water content index (Decagon data). **b** Chlorophyll concentration. **c** Stomatal conductance (Decagon). **d** Assimilation (LI-6400).

Fig. 2. 7 presents the evolution of several important physiological parameters recorded during the campaign that includes water content index (WCI), chlorophyll concentration [Chl], stomatal conductance (Gs), and CO_2 assimilation (An). WCI (Fig. 2. 7a) started with a value of ≈ 90% that changed very little until September 20th, then decreased to ≈ 72% upon water stress and increased suddenly to ≈ 85% upon re-watering. Measurements started September 7th with a chlorophyll content of ≈ 37 SPAD units that decreased continuously until a minimum of 19 SPAD units when water stress was maximum and recovered partially (≈ 21 SPAD units) after re-watering (Fig. 2. 7b). Stomatal conductance dropped from ≈ 0.3 at the beginning of the experiment (control) to 0.05 mol H_2O $m^{-2}s^{-1}$ under stress. Re-watering restored stomatal conductance to ≈ 0.2 mol H_2O $m^{-2}s^{-1}$ (Fig. 2. 7c). The stress period was prolonged until assimilation fell from ≈ 8 µmol CO_2 m^{-2} s^{-1} to almost zero (Fig. 2. 7d). Then, re-watering was initiated and assimilation recovered up to ≈ 6 µmol CO_2 $m^{-2}s^{-1}$.

To illustrate the changes that occurred in the Fs signal under stress conditions, a sunny day (October 1st) was chosen (Fig. 2. 8a) to compare with the control cycle of September 10th (Fig. 2. 8b). Fs measurement was partially perturbed between 9:30 and 11:00 due to interference with gas exchange measurements as evoked above. The Fs signal stayed constant during night (Fo) and increased early in the morning, like in the control case, until 8:30 a.m. However, as PAR exceeded 120 µmol m^{-2} s^{-1}, Fs decreased continuously well below Fo, to reach a minimum of 78% of Fo at solar noon. During the afternoon, Fs increased but stayed below Fo. So we observed a large difference between control (Fig. 2. 8b) and stressed plants (Fig. 2. 8a) that can be characterized by the ratio between the peak of Fs in the morning (F_s^1) and the minimum at solar noon (F_s^2). This ratio changed from 1.1 (control) to 1.49 (stress).

2.1.4.4 Mint measurements

In order to test Ledflex with a different crop, we conducted, during two weeks, a campaign on a mint cover formed by 20 pots put together to form a target. At variance with the pea cover, the chlorophyll content stayed constant at 40 ± 4 SPAD units during the whole campaign (not shown). Assimilation and conductance measurements done with the Licor 6400 revealed values of An = 19 ± 4 µmol CO_2 m^{-2} s^{-1} and Gs = 0.23 ± 12 mol H_2O m^{-2} s^{-1}, respectively, for well-watered plants (Fig. 2. 9a). Although illumination conditions were not as constant as for peas (alternating clouds and sun), the diurnal cycle of Fs was similar to that of pea crop, M-shaped, but with a minimum at noon, well over the predawn level.

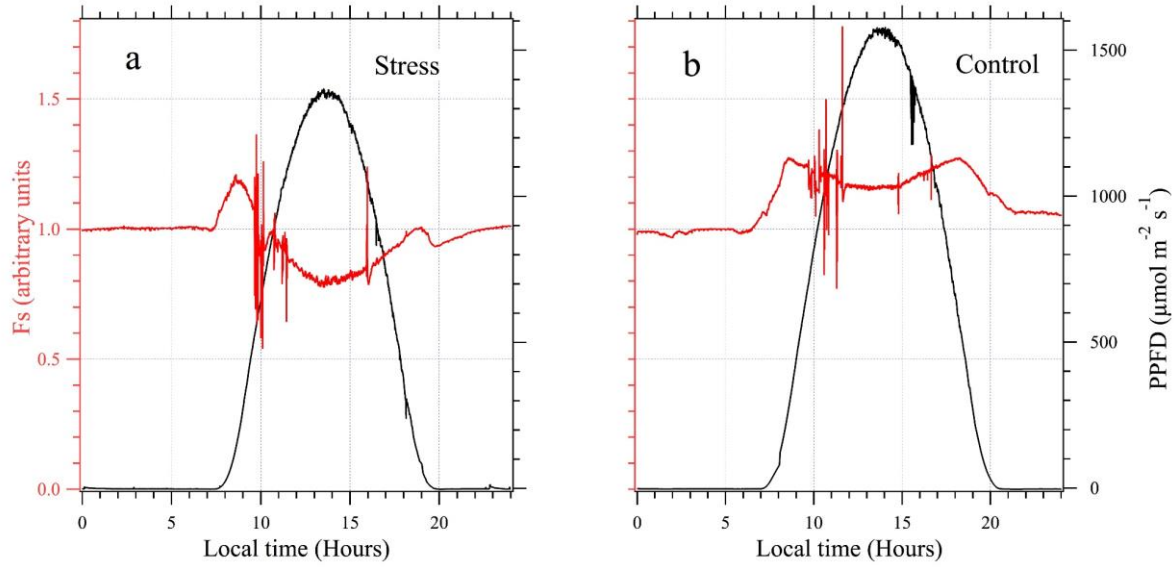

Fig. 2. 8 Diurnal cycles of chlorophyll fluorescence. **a** After several days withholding watering. Observe the decrease of Fs at noon that becomes lower than during the night (Fo). **b** The same well-watered pea canopy for comparison.

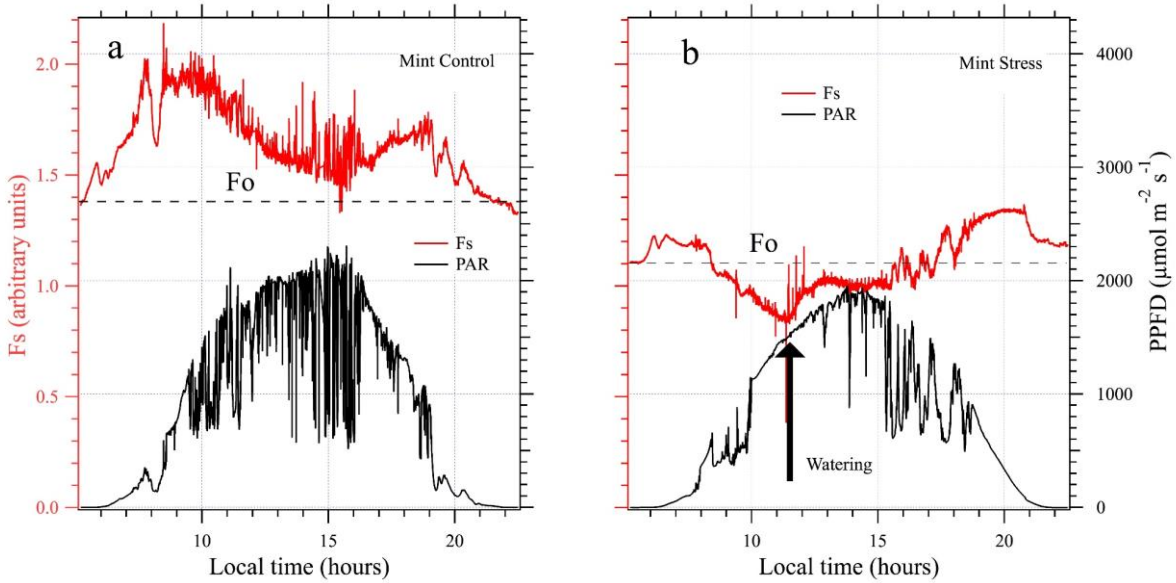

Fig. 2. 9 a Control mint cover a windy day. **b** Stressed mint cover. The rapid Fs decay has been reverted in minutes after watering.

After 2 days withholding watering (Fig. 2. 9b) we observed, in the morning, a small increase of Fs with low light rapidly followed by a strong decrease, well below Fo, when the illumination reached 500 µmol m^{-2} s^{-1}. At 11:30, fearing that the strong sun damaged irreversibly the plants, we decided to irrigate. After a few minutes Fs increased, then became higher than Fo and continued to increase despite high light conditions (PAR > 1800 µmol m^{-2} s^{-1}). The responsivity of the Fs signal also increased when light changed, for example, between 15:00 and 19:00 compared to morning conditions. These observations made on peas and mint canopies were similar to those on sweet potatoes (*Ipomea batata*) made in Lima (Peru) when testing Ledflex (not shown).

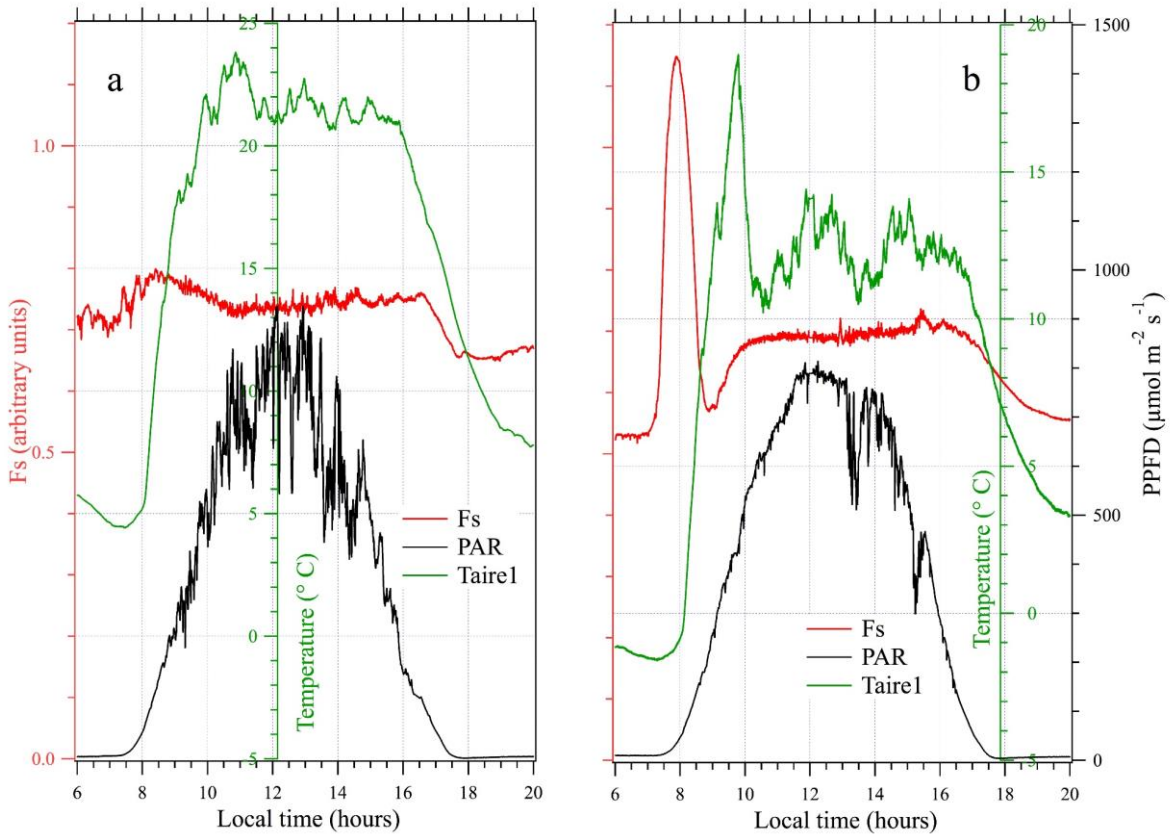

Fig. 2. 10 a: Diurnal cycle of a natural grassland. **b**: Diurnal cycle during a cold morning with negative temperatures at dawn.

2.1.4.5 Grassland measurements

Ledflex was installed pointing nadir at 3.2 m above a natural grassland. Experiments took place at the beginning of November 2016 with rain every 4 or 5 days and rare sunny days. The target was principally composed of velvet grass (*Holcus lanatus*, *Holcus mollis*) of about 4 – 5 cm height. The target contained also a large amount of dried material and debris produced by previous grass mowing. The average chlorophyll content was about 30 SPAD units. Fig. 2. 10a presents a rather sunny day (November 1st). One can appreciate the low extent of Fs variations and a general pattern rather similar to what was observed for potted pea plants. In the following days, the temperature tended to decrease with a concomitant decrease in Fo. Fig. 2. 10b shows what happened when temperature became negative during night (November 3rd). We observed a huge increase in Fs (more than twice!) in the early morning which reversed when the temperature became positive. This peculiar increment lasted about one hour, followed by a diurnal cycle similar to Fig. 2. 10b. This behavior - a prominent peak occurring in the morning - has been observed each time the temperature was negative at dawn.

2.1.5 Discussion

Our methodology consists of measuring continuously several parameters including stationary fluorescence Fs, reflectance of the target Rc, PAR, and temperature. These data are acquired from a fixed place and maintained unchanging the targeted part of the

vegetation. Also Fo is measured daily. We focus on the eventual changes of the diel cycle that could be a stress signature. The experiments may last several weeks. Although non-commercial, the instrument can be built for a cost of less than 2 000 $. The technique can be applied to the study of other stresses, including nitrogen deficiency, albeit we did not have the opportunity to do such work. Notwithstanding, other excitation wavelengths seems more adapted to study nitrogen deficiency. For example, excitation in the UV generates a blue fluorescence emission proceeding from phenolic compounds together with the chlorophyll fluorescence emission (see Cerovic et al., (1999) and Tremblay et al., (2012) for a revue).

2.1.5.1 Water stress effect on Fs

Other authors have measured the effect of water stress on fluorescence. Cerovic et al., (1996) using a modified PAM 101 (Walz, Effeltrich, Germany) monitored Fs at a distance up to 1m on an attached leaf. The authors monitored several species submitted to drought including maize, sugar beet and kalanchoë. On maize, after six days withholding watering Fs decreased at noon to a value lower than Fo. Although in this experiment the light intensity was limited to less than 350 µmol m^{-2} s^{-1} for technical reasons, these results are in line with the data presented here.

Flexas et al., (2000) studied also the effect of water stress on an attached leaf of a vine plant, during a campaign of 17 days. The authors developed a new fluorometer based on a laser diode for measuring at distance both Fs and Fm' through the window of a Licor 6400 gas analyzer. They also evidenced the M shape of the diurnal cycle of Fs with a minimum at solar noon. Under stress conditions, the evening branch was much lower than the morning one and the minimum (F_s^2) was clearly lower than Fo, in agreement with what is shown in Fig. 2. 8of the present paper. Other works including Ounis et al., (2001) and Evain et al., (2004) reported similar results. However, in the above mentioned papers only a single point of the leaf was analyzed.

Rosema et al., (1998) used a target formed by poplar trees grown in pots in a growth cabinet with glass walls inside a greenhouse. A Nd-Yag laser providing pulses of 10 mJ of 10 ns length at 532 nm was used for excitation. The laser illuminated an area of 60 cm of diameter at 12 m. During a water stress experiment lasting 5 days the diurnal cycle showed a dip at noon that developed and became lower than Fo when drought progressed. Indeed, inside a greenhouse with low radiation (< 400 µmol m^{-2} s^{-1}), the water stress signature was evidenced at canopy level. Although, unnoticed to the authors, a small peak on Fs can be observed at dawn in Fig. 2. **7** of their publication, as it is evidenced in the present work.

Bright light conditions prevailed in an outdoors vineyard work presented by López González, (2015). They used a laser-diode µLIDAR, developed at LMD (Laboratoire de Météorologie Dynamique, Paris), which was able to measure Fs from a distance of a few meters, over a plant section containing several leaves. Field work was conducted during the summer, for 45 days, at Barrax, in the South of Spain. Fs was continuously measured from well-watered conditions (Gs = 0.18 µmol H_2O m^{-2} s^{-1}) to stress conditions (Gs = 0.05 µmol H_2O m^{-2} s^{-1}). During this long period of good weather, neither the chlorophyll content nor the reflectance were modified. The authors observed a progressive decrease

of Fs at noon, which dropped below Fo at the end of the treatment. Importantly, 12 h after re-watering, a diurnal cycle similar to control plants was obtained. These results were very similar to those obtained on mint plants or peas and presented in this work, although they were obtained with different plant species.

2.1.5.2 Effect of negatives temperatures at dawn on Fs

Ledflex uses the shelf supplies and is robust, sensible, and efficient. It can measure fluorescence outdoors continuously, during prolonged periods of time, under full sunlight conditions. It is worth noting that the installed warming system allowed us to measure under negative temperatures (°C) without water condensation on the front-end windows. Under normal conditions (positive temperatures and well watered plants) we observed a very small peak (≈ 5% of Fo) that often occurs at dawn, when the first photons reached the system. We interpreted this small increase as a transitory reduction of QA occurring when light hits the target. It disappeared after complete activation of photosynthesis. This small peak at dawn has also been observed by Flexas et al., (2000) and by López González, (2015). Under "normal conditions," Fs variations were between 5 to 20% of Fo. When temperature was low at dawn, enzymatic reactions were slower and a larger reduction of Q_A occurred as soon as light increased. This phenomenon ended when temperature increased; in turn, following further increase of daylight after 8:00 a.m., allowing the reoxidation of QA. We did not find any other reference in literature describing this phenomenon. The effect of cold and light stress on photosynthesis parameters was studied using the LIFT approach (Pieruschka et al., 2010). An impairment of the photosynthetic efficiency was observed on some species under cold stress including *L. esculentum* and *C. annuum*. However, in other species like grass the authors did not report any change on the fluorescence under cold treatment. In particular they did not observe our dawn occurring peak. Compared to Ledflex, LIFT used high intensity light pulses with high duty cycle periods to saturate photosynthetic activity within PS II reaction centers. To avoid accumulation of possible harmful excess light, sampling frequency is necessarily limited, so rapidly occurring events can be missed with the LIFT approach. This is not the case with Ledflex which continuously samples stationary fluorescence level at high rate. The sampled area is also larger with Ledflex (around 1 m^2 at 8 m distance) compared to LIFT (around 100 cm^2).

2.1.6 Conclusions

We presented in this work a non-commercial instrument dedicated to continuous measurement of chlorophyll fluorescence of vegetation under natural conditions. All the electronics and optics were encapsulated within a PVC drainage pipe of 160 mm of diameter and 550 mm length connected to a solar panel by a single 12V power line. Data were collected using a wireless connection. The measuring range was more than 8 m, depending on the target, but it can be increased easily using a greater number of diodes.
A simple signature of water stress emerged, based on a strong increase (35 %) of Fs(9h) - Fs(noon) on stressed plants compared to the control, associated with a Fs(noon) below

Fo. These facts have been established for several crops. Thanks to a simple warming system, it was possible to work with negatives ambient temperatures that revealed new fluorescence features like a conspicuous peak at dawn.
The device has been duplicated and currently applied for the study of potatoes and sweet-potatoes, in parallel with a spectrometer based passive instrument in Peru.

Acknowledgments: The authors acknowledge the Bill & Melinda Gates Foundation (Grant Number: OPP1070785) and the International Potato Center (CIP- Lima, Peru) through the subgrant agreement SGA 7821-000-00-FX-01 for the *Development of a remote sensing system to quantify water-stress fluorescence signatures of crop fields* and the *CNES TOSCA ECOFLUO* project. The authors also thank professor Alfonso Calera and the Remote Sensing and GIS-Unit—University of Castilla-La-Mancha (Albacete, Spain) for the loan of a Decagon porometer.

Compliance with ethical standards

Conflict of Interest: The authors declare that they have no conflict of interest

Open Access This article is distributed under the terms of the Creative Commons Attribution 4.0 International License (http://creativecommons.org/licenses/by/4.0/), which permits unrestricted use, distribution, and reproduction in any medium, provided you give appropriate credit to the original author(s) and the source, provide a link to the Creative Commons license, and indicate if changes were made.

CHAPTER 3

SIF and LIF measurements at canopy level

In this chapter we studied the diurnal cycles of ChlF, as measured by the two different methods, active and passive. For active measurements, we used the Ledflex instrument described in the previous chapter. For passive measurements, a new instrument was built: Spectroflex2, which is described in this chapter. Spectroflex2 is able to work in outdoor conditions and perform fluorescence measurements at canopy level. The first version of Spectroflex was presented by Fournier et al., (2012). However, in the frame of my thesis work a fully new version of this instrument was developed. Similar to work done with Ledflex, Spectroflex2 was conceived by Ismael Moya – the co-advisor of my thesis project – and my main contributions were: a) to develop the software to control the instrument and the algorithm to allow it work in loops under outdoor condition., 2) to perform temperature regulation tests of Spectroflex2 in laboratory and open field, and 3) to perform calibrations and tuning of different instrument parts: the optic, to manage the electronic shutter and synchronize the spectrometer dark measurements, and to control a rotatory solenoid that synchronize the movement of reference panel.

Spectroflex2 and the second Ledflex were underwent to a field experiment in the facilities of International Potato Center (CIP) in Lima – Peru. Both instruments were setup with a fix geometry, and for several days at a same spot LIF and SIF measurements were carried out on potato crops canopy. This study, including a deep description of Spectroflex2, were published in Photosynthesis Research Journal (Loayza et al., 2022).

3.1 Article: Active and passive chlorophyll fluorescence measurements at canopy level on potato crops. Evidence of similitude of diurnal cycles of apparent fluorescence yields.

Hildo Loayza[1], Ismael Moya[2], Roberto Quiroz[3], A. Ounis[2], Yves Goulas[2]

3.1.1 Abstract

We performed active and passive measurements of diurnal cycles of chlorophyll fluorescence on potato crops at canopy level in outdoors conditions for 26 days. Active measurements of the stationary fluorescence yield (Fs) were performed using Ledflex, a fluorescence micro-LIDAR described in Moya et al. (2019), Photosynthesis Research, 142, 1-15, DOI: 10.1007/s11120-019-00642-9, capable of remote measurements of chlorophyll fluorescence under full sun-light in the wavelength range from 650 to 800 nm. Passive measurements of solar-induced fluorescence (SIF) fluxes were performed with Spectroflex, an instrument based on the method of filling-in in the O_2-A and O_2-B absorption bands at 760 nm (F760) and 687 nm (F687), respectively.

Diurnal cycles of Fs showed significant variations throughout the day, directly attributed to changes in photosystem II yield. Contrasting patterns were observed

according to illumination conditions. Under cloudy sky, Fs varied in parallel with Photosynthetically Active Radiation (PAR). By contrast, during clear sky days, the diurnal cycle of Fs showed a “M” shape pattern with a minimum around noon.

F687 and F760 showed different patterns, according to illumination conditions. Under low irradiance associated with cloudy conditions, F687 and F760 followed similar diurnal patterns, in parallel with PAR. Under high irradiance associated with clear sky we observed an increase of the F760/F687 ratio, which we attributed to the contributions in the 760 nm emission of photosystem I fluorescence from deeper layers of the leaves, on one end, and by the decrease of 687 nm emission as a result of red fluorescence re-absorption, on the other end.

We defined an approach to derive a proxy of fluorescence yield (FYSIF) from SIF measurements as a linear combination of F687 and F760 normalized by vegetation radiance, where the coefficients of the linear combination were derived from the spectral transmittance of Ledflex. We demonstrated a close relationship between diurnal cycles of FYSIF and Fs, which outperformed other approaches based on normalization by incident light.

Keywords LED-induced fluorescence, solar-induced fluorescence, fluorescence yield, steady-state fluorescence, potato.

Abbreviations

SIF	Solar-induced fluorescence
LIF	Laser or LED-induced fluorescence
ASFY	Apparent Spectral Fluorescence Yield
ChlF	Chlorophyll fluorescence
PAR	Photosynthetically active radiation
Fs	Stationary fluorescence
F760	Fluorescence fluxes at 760 nm
FY760	Fluorescence Yield at 760 nm
ASFY760	Apparent spectral fluorescence yield at 760 mn
F687	Fluorescence fluxes at 687 nm
FY687	Fluorescence Yield at 687 nm
ASFY687	Apparent spectral fluorescence yield at 687 mn
IDE	Environment Development Software
DAQ	Data Acquisition
SNR	Signal to Noise Ratio
SSR	Sum of squared residuals
O_2-A	Oxygen A absorption band
O_2-B	Oxygen B absorption band
PS I	Photosystem I
PS II	Photosystem II
NQP	Non-Photochemical Quenching

3.1.2 Introduction

The chlorophyll fluorescence (ChlF) of the vegetation is becoming a principal tool for monitoring the photosynthetic activity at the canopy level. This signal is related to the existing competition for the absorbed light energy between several deactivation pathways within the collecting antenna of photosystem I (PS I) and photosystem II (PS II). They encompass 1) the photosynthetic conversion at the reaction centers, 2) the internal conversion into heat, and 3) the fluorescence emission. Information on photochemistry can be inferred from the variation of the fluorescence emission (Genty et al., 1990; Kautsky & Hirsch, 1931).

Chlorophyll fluorescence in natural conditions (outdoor and under full sun-light) varies much less than during an induction after dark adaptation but depending on stress conditions and their variations are readily detectable (López González, 2015; Moya et al., 2019).

For the last 20 years, passive fluorescence has been preferentially detected using the filling-in of the atmospheric absorption band B (O_2-B) at around 687 and band A (O_2-A) at 760 nm (Moya et al. 1999). Band B is located almost exactly at the first peak of the fluorescence emission, whereas band A is not far from the second fluorescence peak. The interest in the passive method has grown because, although attenuated by the terrestrial atmosphere, the filling-in of these bands was still detectable from a sensor carried by a satellite. However, we voluntarily limited our interest to field measurements.

3.1.2.1 Diurnal cycles of passive fluorescence measurements

Significant progress has been made in solar-induced chlorophyll fluorescence (SIF) diurnal cycles at the canopy level and reported flux measurements on different crops. For instance, Louis et al., (2005); Goulas et al., (2017); Du et al., (2019), with different instruments, presented diurnal cycles of SIF at O_2-B and O_2-A on pines of the boreal forest, wheat, or maize fields, respectively, showing different shapes along the day. Other works also reported fluorescence flux diurnal cycles within the two bands (Daumard et al., 2010; Xu et al., 2021), but the resolution of the data presented is relatively low.

PS II predominantly produces the fluorescence flux retrieved in the O_2-B band, while the O_2-A band has fluorescence contributions of PS II and PS I (Boardman et al., 1966; Govindje, 1995). Reabsorption plays also an important role. The red fluorescence emission comes principally from the upper layers of the leaf, whilst the far red fluorescence is emitted from much deeper layers of the leaf, as compared to red fluorescence. As a result, the fluorescence flux retrieved in the O_2-B band and O_2-A band are sampled in different layers of leaf with different light intensities. In consequence, their kinetics are different.

In addition, recent works with dilute suspensions of green unicellular algae (*Chlorella vulgaris*) using a highly sensible Multi-Color-PAM fluorimeter (Heinz Walz

GmbH, Germany) reported evidences a variable fluorescence of PS I (Schreiber & Klughammer, 2021). However, in this work, a contribution of variable PS I fluorescence emission was not considered since we worked with green leaves and under natural light conditions that didn't allow an induction with completely oxidized plastoquinone.

To study the diurnal kinetics of fluorescence retrieved from O_2 bands, we built a new version of Spectroflex, first described by Fournier et al., (2012). It is a spectrometer-based passive instrument to continuously recover chlorophyll fluorescence emissions within O_2-A and O_2-B bands from potato crops.

We chose the potato crop due to its importance as a food security crop, as indicated by the Food and Agriculture Organization of the United Nations (FAO), due to its widely adaptive range, excellent yield potential, and high nutritional value (Devaux et al., 2014). In addition, to our knowledge, there are only a few studies of SIF measurements on potato crops at the canopy level, except for recent studies performed by Xu et al., (2021).

3.1.2.2 Active fluorescence measurement at canopy level

In contrast to SIF measurements, only a limited number of works on light-induced fluorescence (LIF) measurements in outdoor conditions are reported. For example, Rosema et al., (1998) presented diurnal cycles of Fs measured on poplar trees placed inside a growth cabinet with a glass wall. Recently Moya et al., (2019), using Ledflex, a diode-based micro-LIDAR to measure continuously at a distance (4 m) and canopy level, reported first time Fs diurnal cycles on pea, mint, and grass plants for several days under natural conditions. In addition, they presented a straightforward methodology to detect water stress by comparison of Fs values at darkness and noon.

In this work, we used a Ledflex replica. For 26 days, diurnal LIF cycles were measured on potato crops' foliage over the same target as Spectroflex2.

3.1.2.3 Diurnal cycle of passive and active measures of ChlF

Combined LIF and SIF measurements at the foliage scale are scarce, and we found just one such study. Louis et al., (2005) measured scot pines with both methods. They presented the first approximation of passive fluorescence measurements using the Passive Multi-wavelength Fluorescence Detector (PMFD), described by Evain et al., (2001), together with the active fluorescence measurements using the micro-LIDAR FIPAM (Flexas et al., 2000). The comparisons showed a discrepancy at solar noon, and the authors attributed it to differences in the structure of the targets measured by both instruments. For example, FIPAM saturates and measures fluorescence at 2 m covering an area of 3x20 mm. In comparison, PMFD covers a full tree at 40 m.

In this study, we present, for the first time, a comparison of active and passive diurnal cycles of stationary fluorescence at the canopy level. The objectives of this work were the following:

- To retrieve cycles of passive fluorescence from potato canopy O_2-A and O_2-B bands and compare their diurnal variations.
- Using the same target, we perform active fluorescence measurements to gain insights into stationary fluorescence variations.
- Compare active and passive fluorescence yields of potato plants.

3.1.3 Materials and methods

3.1.3.1 Environment and plant material

The field experiment was carried out at the International Potato Center (CIP) experimental station in Lima-Peru (12.08°S, 76.95°W, 244 m.a.s.l.), from July 5th to October 03th, 2017. The study site is a subtropical arid desert climate with cloudy skies during the first hours of the day (autumn-winter), 19.7 °C of average annual Temperature, and 6.0 mm of annual total precipitation (2013-2017, CIP Meteorological Station). The potato variety studied was UNICA (CIP code: 392797.22), an improved genotype with partial salt and high-temperature tolerances, PVY virus resistance, and susceptibility to leafminer fly (*Liriomyza huidobrensis*) (Gutiérrez-Rosales et al., 2007).

Chlorophyll content

Leaf chlorophyll content was estimated with a chlorophyll meter SPAD-502 (Minolta, Ramsey, NJ, USA). It is expressed as SPAD units and it was recorded as the mean value of 20-30 measurements per leaf.

3.1.3.2 Active instrument: Ledflex

Ledflex is a laboratory-designed fluorescence micro-LIDAR for continuous open field measurement of relative stationary fluorescence yields (Fs) from vegetation foliage. Fluorescence is induced by a pulsed artificial light source synchronized with a fast detection system. This type of technique is known as light-induced fluorescence (LIF). For a detailed description of Ledflex, see Moya et al., (2019).

A Ledflex replica was implemented for this work, and its main features include:

The excitation light source.

The light source consists of four identical blue light-emitted diodes (LEDs) (LED470L, Thorlabs, Maisons-Laffitte, France). These LEDs emit at a central wavelength of 470 ± 5 nm with a full width at half-maximum (FWHM) of 22 nm, mounted in series and powered under 3 A by a source of 22 V. The light source is controlled by an electronic circuit that adjusts the light intensity and the operation mode of the LEDs to work in pulses with a repetition rate of 10 ms. Although the frequency is low, it is sufficient to follow the variations of natural light, whose transition time is about 1s. The pulse duration was tuned to 4.5 µs; thus, the mean value of irradiated light from Ledflex avoids generating any change in plant photosynthesis. In addition, the power supply board generates digital outputs to synchronize the acquisition system with the fluorescence pulses induced by the LEDs.

The fluorescence detection optics

It is based on a 6-inch diameter Fresnel lens (Edmund Optics, France) that focuses the fluorescence light on a 10 mm x 10 mm PIN photodiode (S3590-01, Hamamatsu, France) associated with a combination of a long-pass filter (Schott RG665, Edmund Optics, U.K.) and a short pass filter (λ < 800 nm, Edmund Optics, U.K.) that limits the spectral detection range from 650 to 800 nm. Furthermore, a 3 inches focal was chosen to collect a surface of about 55 cm in diameter at a distance of 4 m. Such an area is large enough to provide an excellent spatial integration in the case of potato crops. Finally, a PVC (polyvinyl chloride) tube of 6 inches in diameter was used to enclose both the optic and detection system in a waterproof case.

The fluorescence acquisition system

Signal conditioning is based on an electronic card at the bottom of the fluorescence detection optics. Its function is to transform the output current of the PIN photodiode into signals directly measurable by the acquisition system. The detected signal at the output of the optical sensor is the sum of a slowly varying signal corresponding to the solar irradiance in the filter bandwidth reflected by vegetation and a fast varying signal corresponding to the LEDs-induced fluorescence. After voltage conversion by a trans-impedance amplifier, the two signals are electronically separated by an arrangement of two operational amplifiers with different cut-off frequencies. A fast sample and hold circuit, synchronized with the LEDs' light pulses, maintains the LEDs' peak value-induced-fluorescence during analog to digital conversion. A data acquisition device (34970A, Keysight Technologies, Santa Rosa, CA, USA) is used to convert signals to digital numbers either synchronously with a trigger signal to detect Fs or asynchronously for the acquisition of vegetation radiance reflected in the range from 650 to 800 nm, ambient Temperature (thermistor RS151–237, Radiospares, France) and incident photosynthetically active radiation (PAR) (radiometer, JYP 1000, Sdec, France). The data was recorded on a portable computer with an average sampling frequency of 1.8 seconds.

The signal-to-noise ratio (SNR) of LIF measurements

Tests were performed to measure the ratio between the Fs signal recovered from different targets and the noise. Under open field conditions at approximately solar noon and with Ledflex located about 4 meters away and pointing nadir to the canopy of peas plants whose leaves presented SPAD values of 40 (on average), an SNR of 133 was reached. (Moya et al., 2019). Therefore, the SNR value obtained was considered acceptable for the objectives of this study.

Spectral transmittance of the detection optics

A laboratory test was performed to measure the light transmitted through the Ledflex optics, including the Fresnel lens and the filters, and finally reaching the photodiode. The optics transmittance was measured with a cosine corrector (Ocean Insight, Orlando, FL, USA) adapted to a VIS-NIR spectrometer (H.R. 2000+, Ocean Insight, Orlando, FL,

USA). The corrector was located at the focal point – corresponding to the position of the PIN photodiode – and using a 600 W white light tungsten lamp as a source.

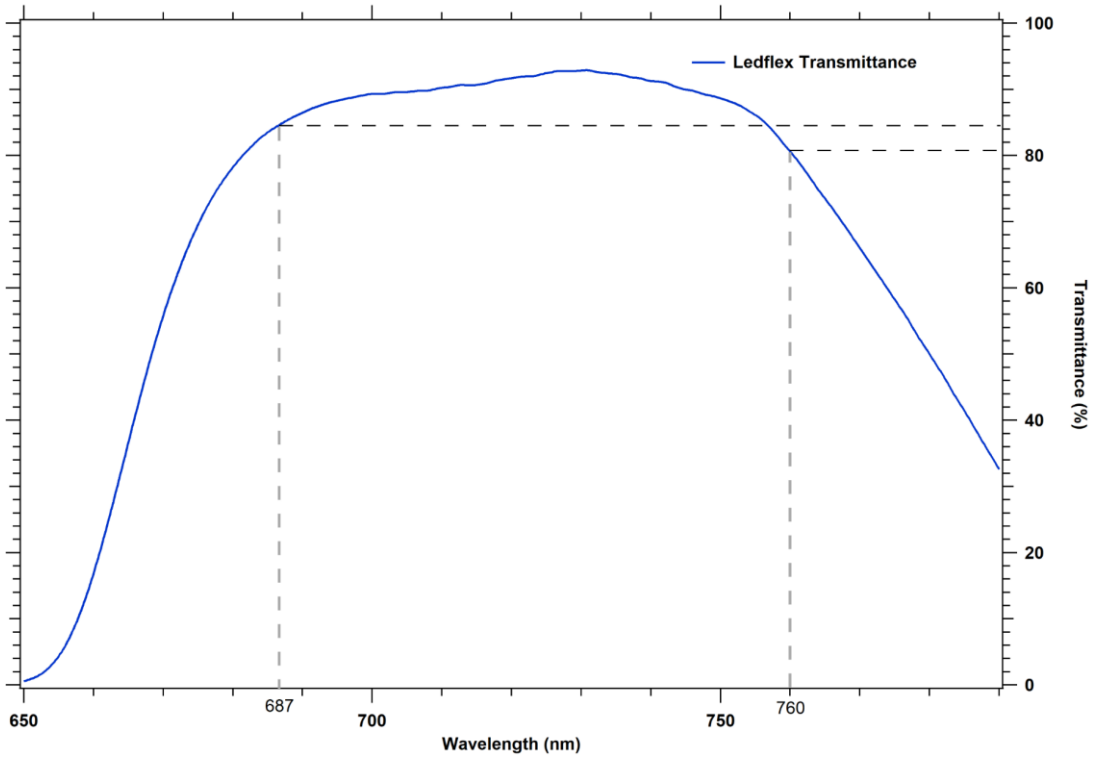

Fig. 3. 1 Transmittance of the Ledflex detection optics (blue line). The gray dash lines indicate the positions and intensities corresponding to 687 and 760 nm wavelengths.

Fig. 3. 1 shows the transmittance spectrum of the Ledflex optics and highlights the contributions corresponding to the wavelengths 760 and 687 nm, giving a transmittance ratio of 0.95.

3.1.3.3 Passive Instrument: Spectroflex

Spectroflex is a laboratory-made instrument designed to accurately and continuously measure the radiance of the vegetation at a high spectral resolution compared to a reference panel under outdoor conditions. With this information, we recovered the solar-induced ChlF (SIF) fluxes at the foliage level using the filling-in method in the A and B absorption bands of atmospheric oxygen (Moya et al., 1998, 2004).

The first version of Spectroflex was presented and described by Fournier et al., (2012), and inspired by this work, a new version, hereafter Spectroflex2 was implemented and adapted for this study. A DC rotary solenoid (Magnet-Schultz, Old Woking Surrey, UK) alternated the radiance measurements on the reference panel and vegetation. At the same time, a data acquisition (DAQ) board (NI-USB 6210, National instrument, Texas USA) allowed the incorporation of the PAR sensor (JYP 1000, Sdec, France) readings at each loop of the Spectroflex2 measurements.

Fig. 3. 2 shows a scheme of Spectroflex2 installed in open field conditions. The light is transmitted through an optical fiber, placed and fixed on a tripod, with one of its ends pointing in the nadir direction. In the rest condition, it collects the radiance of a reference panel installed on the rotary solenoid, which is managed by the Spectroflex2 program, which in turn changes the target in a synchronized way. The essential accessories of Spectroflex2 are described in Figure 3. 2.

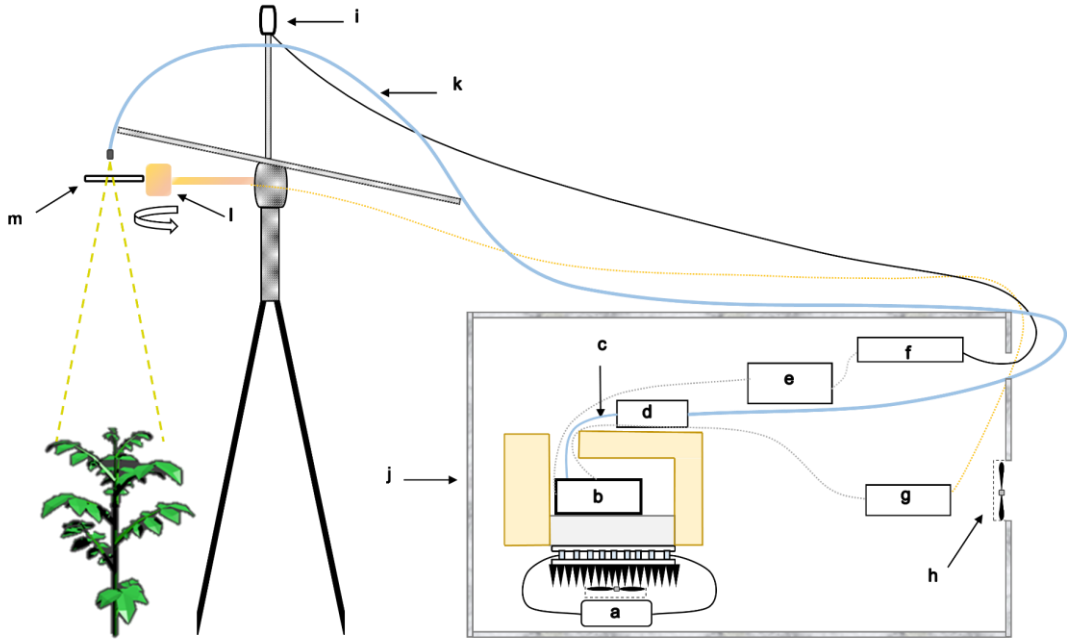

Fig. 3. 2 Spectroflex instrument. Electronic devices are placed inside an insulated box to protect them from weather conditions. The different optical and electronic accessories of Spectroflex are: **a**) temperature controller, **b**) USB 2000+ spectrometer, **c**) optical fiber of 13 cm, **d**) electronic shutter, **e**) minicomputer, **f**) Data Acquisition (DAQ) card, **g**) power supply for both solenoid and fan, **h**) fan, **i**) PAR sensor, **j**) waterproof, **k**) optical fiber of 5 meters and collimating lens, **l**) rotatory solenoid, stroke up to 95º, and **m**) reference panel (PVC).

The spectrometer

A USB2000+ user-configured miniature spectrometer (Ocean Insight, Orlando, FL, USA) was used. A lightweight spectrometer of 190 g was selected since the ultimate goal is to collect passive measurements from a unmanned aerial vehicle (UAV). The spectrometer optic was defined to optimize the radiance measurements in the spectral region around the A-band of atmospheric oxygen absorption. These measurements are achievable with 1200 lines grating blazed at 750 nm, a focusing lens, a 25-µm entrance slit, a long-pass filter (OF1-GG475), and 16 bits analog to digital (A/D) converter. Furthermore, the detector is a 2048-pixel CCD (Sony ILX511 linear silicon) with a spectral sampling interval of 0.19 nm, resulting in an FWHM of 0.63 nm. Measuring vegetation indexes such as the Photochemical Reflectance Index (PRI) was planned from the onset; therefore, the spectral range was set from 510 to 818 nm.

In addition, the USB 2000+ features a high-speed FPGA controller programmable onboard, a 22-pin connector, and 8-user programmable digital I/Os, also known as General Purpose Input Output (GPIO). It provided the necessary resources to synchronize data acquisition from the spectrometer with the movements of the reference panel controlled by a rotary solenoid (see Fig. 3. 2) and manage the passage of light through an electronic shutter (INLINE-TTL-S model, Ocean Insight, Orlando, FL, USA) both configured in external trigger mode.

To focus and define the field of view (FOV) integrated by the spectrometer, a lens (# 64-772 Edmund Optics, Barrington, NJ, USA), 0.4 numerical aperture (N.A.), and 6.24 mm effective focal length at 780 nm was used. This setting defines a FOV of 17.5 cm in diameter at a distance of 1 meter, verified experimentally.

A relative radiometric calibration was applied to the setup using a calibrated light source LI 1800-02 (LICOR, Lincon, NE, USA). In addition, a wavelengths calibration was performed with a Hg (Ar) calibration lamp (6035 model, ORIEL Instrumentation, Irvine, CA, U.S.) with the support of the NIST Atomic Spectra Database Lines Form.

Dark measurements

The dark measurements ranged from 2 to 10% of the spectrometer counts, depending on the spectral region and integration time. Therefore, each radiance measurement – whether from vegetation or reference – was accompanied by a dark measurement with the same integration time.

Reference measurements

A white-roughened PVC board was used as a reference surface to acquire the high-resolution spectrum of incident light. Its reflectance spectrum was previously measured in the laboratory using an ISS-REF model integrating sphere (Ocean Insight, Orlando, FL, USA), obtaining a value of 0.96 +/- 0.1% in the VIS / NIR range. The board was then installed on the rotary solenoid and configured to rotate by 90º upon receiving a TTL signal managed by the spectrometer's GPIO.

A close linear relationship was observed between the radiance of the reference panel at 584 nm ($L_{ref}(584)$) which corresponds to the maximum of the reference panel radiance and the readings of the PAR sensor. Hence, after cross-calibration with the PAR sensor, we used $L_{ref}(584)$ as an indicator of the irradiance level, in tight synchronization with the high-resolution spectral information.

Temperature regulation of spectrometer

The spectrometer was placed inside a tightly closed box made of expanded polystyrene. In order to facilitate heat dissipation, it was fixed on a pile of elements that successively comprised a metal base, a Peltier module (CP1.0-127-05L-RTV, Laird Thermal System, North Carolina, US), a radiator, and finally, a fan to accelerate the cooling of the entire assembly.

A high stability temperature controller (TEC 2000, Wavelength Electronics, Bozeman, Montana, US) collected in real-time the temperature data of a thermistor

(TCS610, Wavelength Electronics, Bozeman, Montana, US) of 10 KΩ NTC installed in direct contact between the surface of the conductive base and the spectrometer. The temperature regulation of Spectroflex2 was tuned for optimal performance of radiance measurements, reaching a diurnal temperature drift of 0.18 ºC on sunny days.

Spectroflex2 software

Spectroflex2 is controlled by a custom program developed in C ++ language, which was implemented in the free Integrated Development Environment (IDE) CodeBlocks 16.01 on a miniature fanless P.C. (Fitlet iA10, Compulab, Yokneam, Israel).

The Spectroflex2 program allowed the system to record daily cycles of the vegetation's radiance and reference panel's radiance and their respective dark currents, accompanied by a measure of the incident PAR. The measurements dynamic range was established and adjusted to reach 85% of the maximum number of counts measured over a reference spectral region corresponding to the reference panel and for vegetation, thus improving the SNR. These spectral regions were defined experimentally in tests performed outdoors under natural light conditions.

The exposure times were estimated considering a linear relationship between the measured light and the number of counts obtained on the respective reference spectral region. Moreover, the number of spectra acquisitions was calculated considering a total of two seconds for each measurement cycle. Finally, Spectroflex2 worked continuously and autonomously at a frequency of 12 seconds per loop from 07:00 to 18:00 hours.

3.1.3.4 Fluorescence retrieval method

The method used to retrieve fluorescence fluxes from radiance spectra was described by Daumard et al., (2010). It is based on the filling-in method of atmospheric oxygen bands A and B proposed by Moya et al., (1998, 2004).

The fluorescence flux corresponding to the atmospheric oxygen absorption band A (O_2-A) was recovered at the bottom of the band at 760.41 nm and hereafter called F760. At the same time, the flux corresponding to the absorption band B of atmospheric oxygen (O_2-B) was recovered at 686.97 nm and referred to as F687 (see Table 3. 1). The following three assumptions were considered:

- a) the shape of fluorescence emission spectrum at the canopy level in the vicinity of the O_2-A and O_2-B bands is assumed to be the same as the shape of emission spectrum at the leaf level as discussed by Fournier et al., (2012). The form factors (K_i) were determined experimentally using a leaf spectrum and are listed in Table 3. 1,
- b) the reflectance of vegetation in the vicinity of the O_2-A band is assumed to vary linearly with wavelength,
- c) the reflectance of vegetation in the vicinity of the O_2-B band is assumed to vary in a quadratic way.

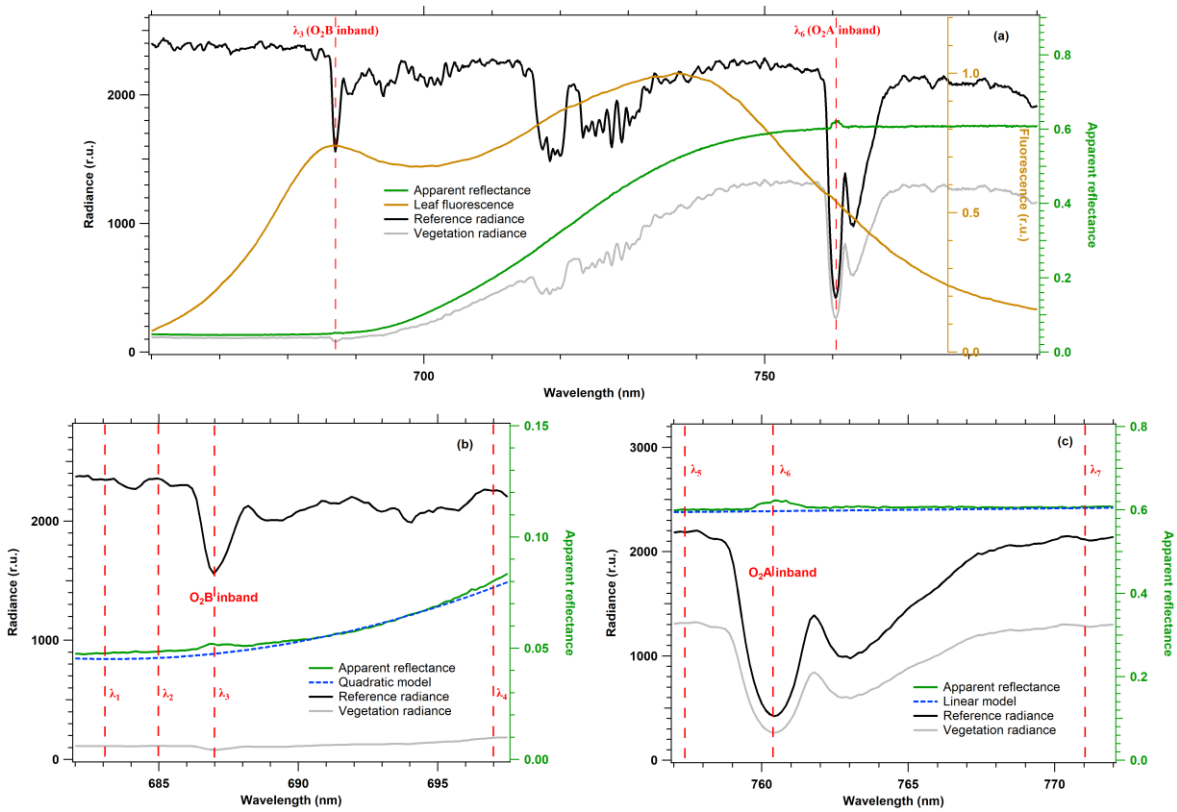

Fig. 3. 3 (**a**) Vegetation and reference panel radiances acquired by Spectroflex2 (gray and black, respectively). The figure also shows the apparent reflectance at the canopy level (green) and a fluorescence spectrum at the leaf level (SPAD value 31.5) acquired under full sun-light with a fluorimeter already described in Moya et al., (2006) (brown). The position of the O_2-B and O_2-A bands are emphasized (red dotted lines), showing the oxygen absorption features and the small peak in the apparent reflectance induced by the fluorescence filling-in. Bottom panels: Zooms in the vicinity of O_2-B and O_2-A bands, respectively. The position of the channels used for fluorescence retrieval in each oxygen band is indicated (red dotted lines) and the retrieved true reflectance (blue).

F760 can be retrieved by computing the vegetation radiance in the vicinity of the O_2-A band using three channels, two out-band and one in-band, and solving a system of three equations. On the other hand, four channels are used for the O_2-B band, three out-band and one in-band, to retrieve F687 by solving four equations. Selected channels to retrieve F687 and F760 and their respective form factors, $K_{i,}$ are presented in Table 3. 1. More details can be found in Daumard et al., (2010); Fournier et al., (2012).

An example of data from a measurement cycle of Spectroflex2 and the corresponding retrieval results are shown in Fig. 3. 3.

Table 3. 1 Spectral channels used to retrieve fluorescence fluxes in the O_2-B and O_2-A absorption bands and associated form factors of the fluorescence shape.

Channels	Central wavelength (nm)	Wavelengths range (nm)	Form factors (K_i)
O_2-B outband	λ_1= 683.08	682.77 to 683.34	0.93
O_2-B outband	λ_2= 684.95	684.64 to 685.26	0.99
O_2-B inband	λ_3= 686.97	686.81 to 687.12	1
O_2-B outband	λ_4= 696.97	696.66 to 697.28	0.90
O_2-A outband	λ_5= 757.38	756.97 to 757.80	1.13
O_2-A inband	λ_6= 760.41	760.14 to 760.55	1
O_2-A outband	λ_7= 771.16	770.76 to 771.57	0.60

3.1.3.5 Experimental design and setup to measure fluorescence

The experimental plot had an area of 5m^2, 05 furrows containing ten plants per furrow. The furrow's direction was 16º N, and plants were watered with drip irrigation. Aiming to have a green cover capable of avoiding border effects in active and passive fluorescence measures, the distance among furrows and plants was established at 0.2 m and 0.5 m, respectively.

Fluorescence measurements started once the plants reached their maximum canopy cover. The effective period of fluorescence measurements at canopy level was between 48 and 82 days after planting (DAP), which corresponded from August 22nd to September 25th, 2017, and where the maximum solar height varied from 66.38º to 76.85º. A schematic representation of the configuration of both instruments located in the field is shown in Fig. 3. 4.

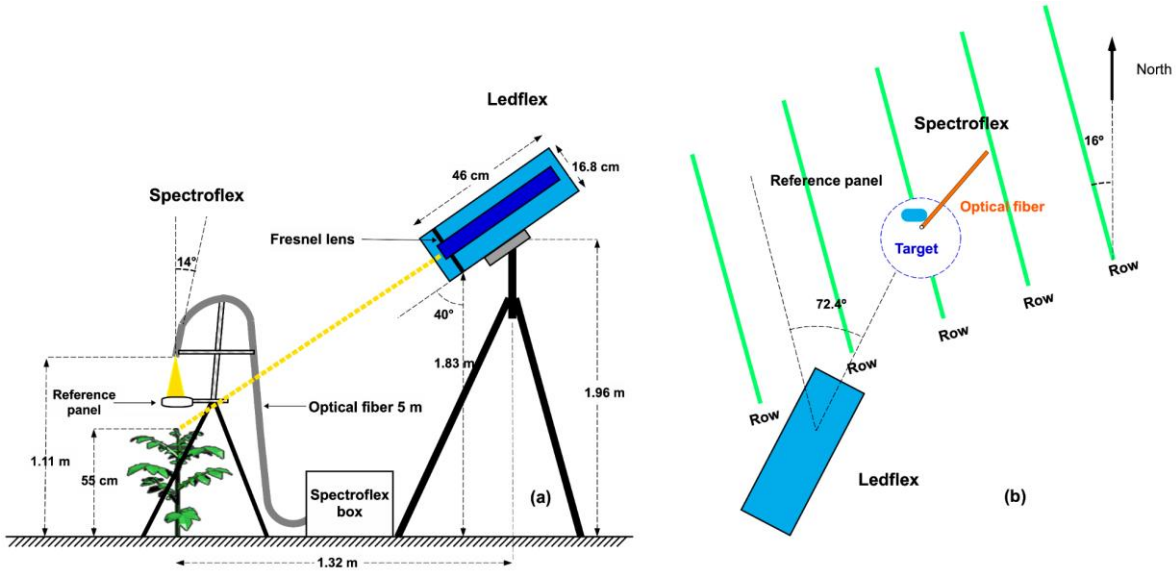

Fig. 3. 4 Schematic representation of the geometric configuration of Spectroflex2 and Ledflex measuring devices as conducted on the plot: **a** Front view and **b** top view. Fluorescence measurements – passive and active – started once the plants reached an average of 55 cm height (maximum vegetation cover).

The Spectroflex2 and Ledflex FOV were adjusted to point and measure on the same target. The calibrations were carried out at night to take advantage of the spot generated on the green cover by Ledflex's blue LED source. To pinpoint and define the Spectroflex2 FOV, the end of the primary optical fiber was unplugged and coupled to a tungsten halogen light source (H.L. 2000-FHSA-LL model, Ocean Insight, Orlando, FL, USES). The Spectroflex2 FOV was contained and aligned to the center of the Ledflex FOV, as shown in Fig. 3. 5b.

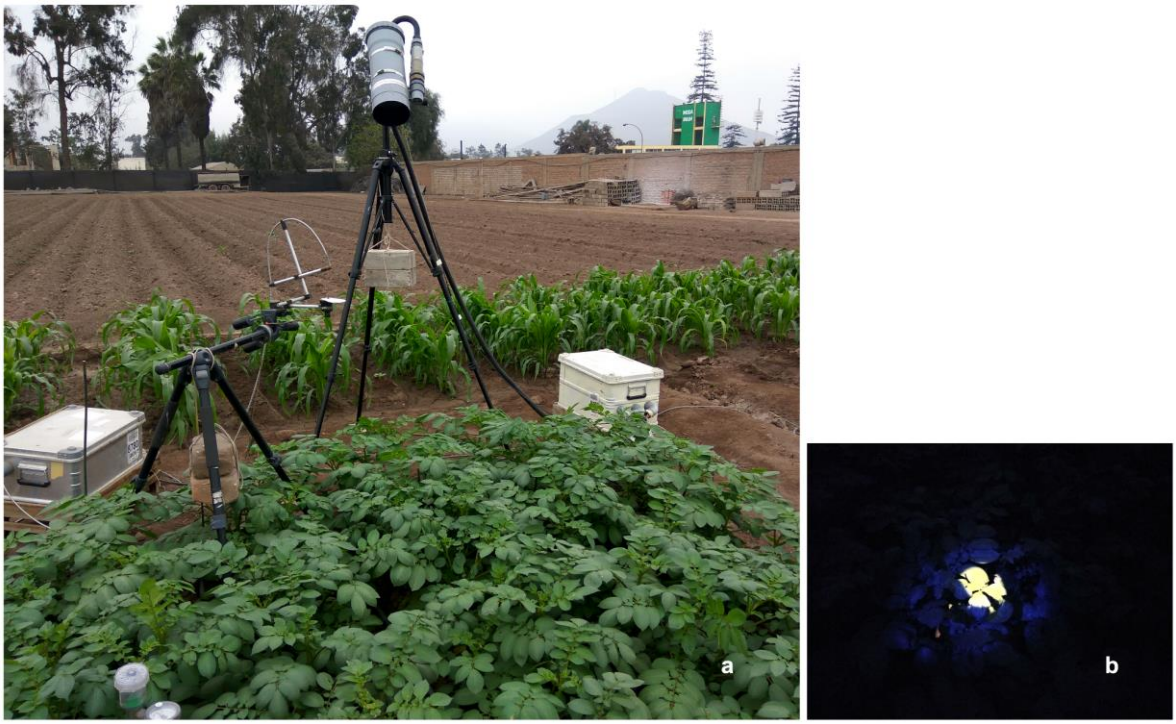

Fig. 3. 5 a Measurement configuration of Ledflex and Spectroflex2 over the vegetation cover of a potato plot. **b** Photograph of the plot acquired at night showing the effective area measured by both instruments. The blue color corresponds to the Ledflex FOV (16 cm of radius) and in its interior – in yellow – the Spectroflex2 FOV (7 cm of radius).

3.1.3.6 Estimation of fluorescence yields with passive methods

Spectroflex2 accurately measures the radiances on the reference panel and the vegetation cover, and with this information, it recovers the time series of the fluorescence fluxes in O_2-A and O_2-B bands in relative units. However, the photosynthetic activity is commonly related to ChlF through fluorescence yields, defined as the ratio of the number of photons emitted by fluorescence to the number of photons absorbed by photosynthetic pigments.

The accurate computation of changes in the light absorbed by vegetation under natural illumination during the day in the FOV of the instrument is a challenge. One was to consider the complex interaction between canopy structure and incident light. In addition, re-absorption of fluorescence in the radiative transfer from the leaf surface to the sensor could also play a role. However, we can approximate SIF yields by computing an apparent spectral fluorescence yield (ASFY) as:

$$ASFY687 = \frac{F687}{APAR} \qquad (3.1a)$$

$$ASFY760 = \frac{F760}{APAR} \qquad (3.1b)$$

Where: APAR is the PAR absorbed by the vegetation, which varies during diurnal cycles.

In this work, we tested different approximations for APAR to compute diurnal cycles of ASFYs. The results were compared with time series of relative fluorescence yields measured by Ledflex.

Two approximations of APAR were used: 1) Incident PAR, assuming that, given the high fractional vegetation cover of the crop, most of the incident light is absorbed by photosynthetic pigments 2) Radiance of vegetation integrated into a spectral range similar to PAR. The latter approach is motivated by the assumption that, at constant pigment content and leaf position, a close positive relationship is expected between absorbed and reflected light at each surface element of the canopy. We used the data acquired by the Spectroflex2's spectrometer to compute: 1) a proxy of the PAR obtained by cross-calibration of the radiance of the reference panel at 584 nm (maximum radiance of panel reference, $L_{ref}(584)$ against the PAR sensor, 2) the integrated vegetation radiation. Since the spectral range of the spectrometer is limited to the range 510 nm to 818 nm, the spectral portion of the PAR that can be measured covers results from integrating from 510 to 700 nm. Hence, two apparent fluorescence yields per emission channel can be defined and tested for SIF normalization, which are:

$$FY687\_PAR = \frac{F687}{PAR} \sim \frac{F687}{L_{ref}(584)} \quad (3.2a)$$

$$FY687\_Veg = \frac{F687}{\sum_{\lambda_i=510}^{700} L_{veg}(\lambda_i)} \quad (3.2b)$$

$$FY760\_PAR = \frac{F760}{PAR} \sim \frac{F760}{L_{ref}(584)} \quad (3.2c)$$

$$FY760\_Ref = \frac{F760}{\sum_{\lambda_i=510}^{700} L_{veg}(\lambda_i)} \quad (3.2d)$$

Where: $L_{ref}(\lambda_i)$ and $L_{veg}(\lambda_i)$ are the radiance of the reference panel and vegetation, respectively.

3.1.3.7 Assessments of performance fluorescence retrieval

The performance of Spectroflex2 and the fluorescence flux recovered by Daumard et al., (2010) model were subjected to preliminary open field tests. A material with a known and constant fluorescence emission was used instead of vegetation as the target. It allowed – by comparison – to determine the performance of the set (hardware and software). The material chosen was a white PVC panel whose fluorescence emission was zero.

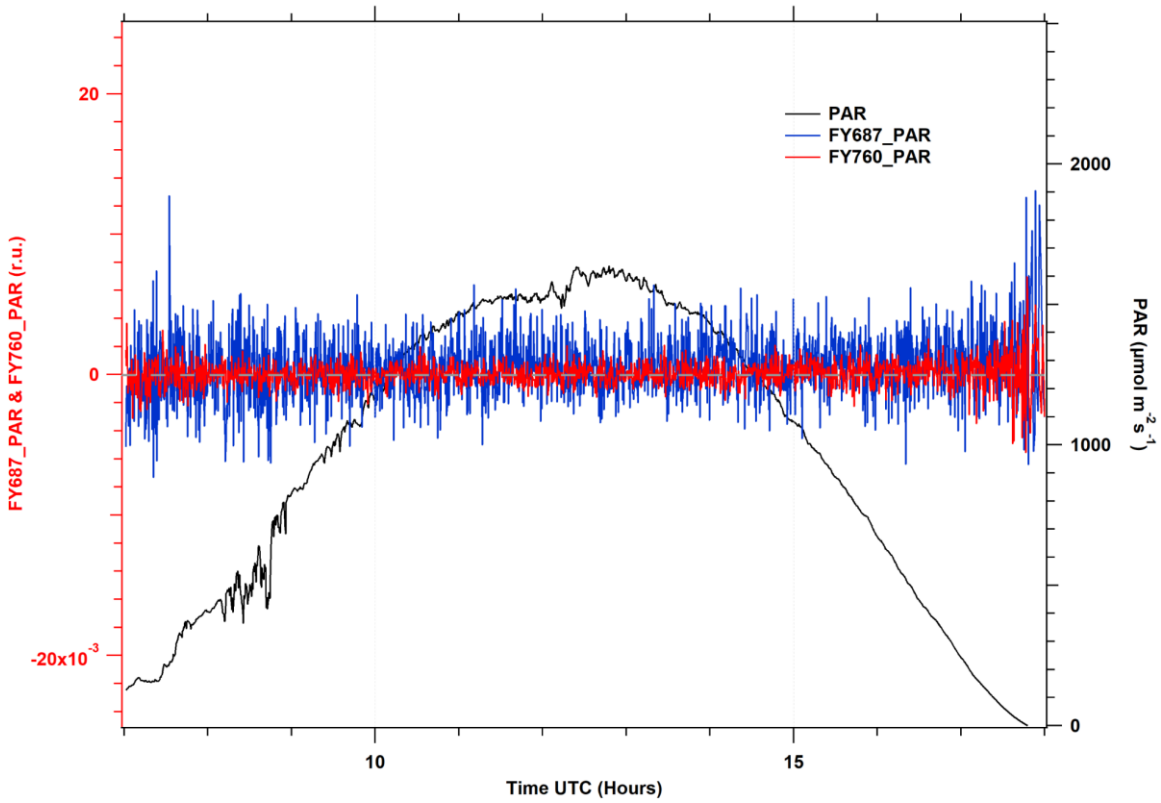

Fig. 3. 6 Diurnal cycle of SIF measurements recovered from a white PVC panel. Where: FY760_PAR (red line) refers to ASFY in O_2-A, FY687_PAR (blue line) corresponds to the ASFY in O_2-B and r.u. (relative units).

As it is shown in Fig. 6 the ASFY estimated with incident PAR in O_2-A and O_2-B and measured on a white PVC panel during whole day had a mean value of almost zero.

3.1.4 Results

3.1.4.1 Active fluorescence measurements

Diurnal cycles of relative fluorescence yield at canopy level over potato plants were measured throughout a campaign (26 days) with Ledflex. These time series were classified according to the sun-light conditions between sunny and cloudy days to show the relationship between Fs changes and incident PAR. One example of each category is shown in Fig. 3. 7.

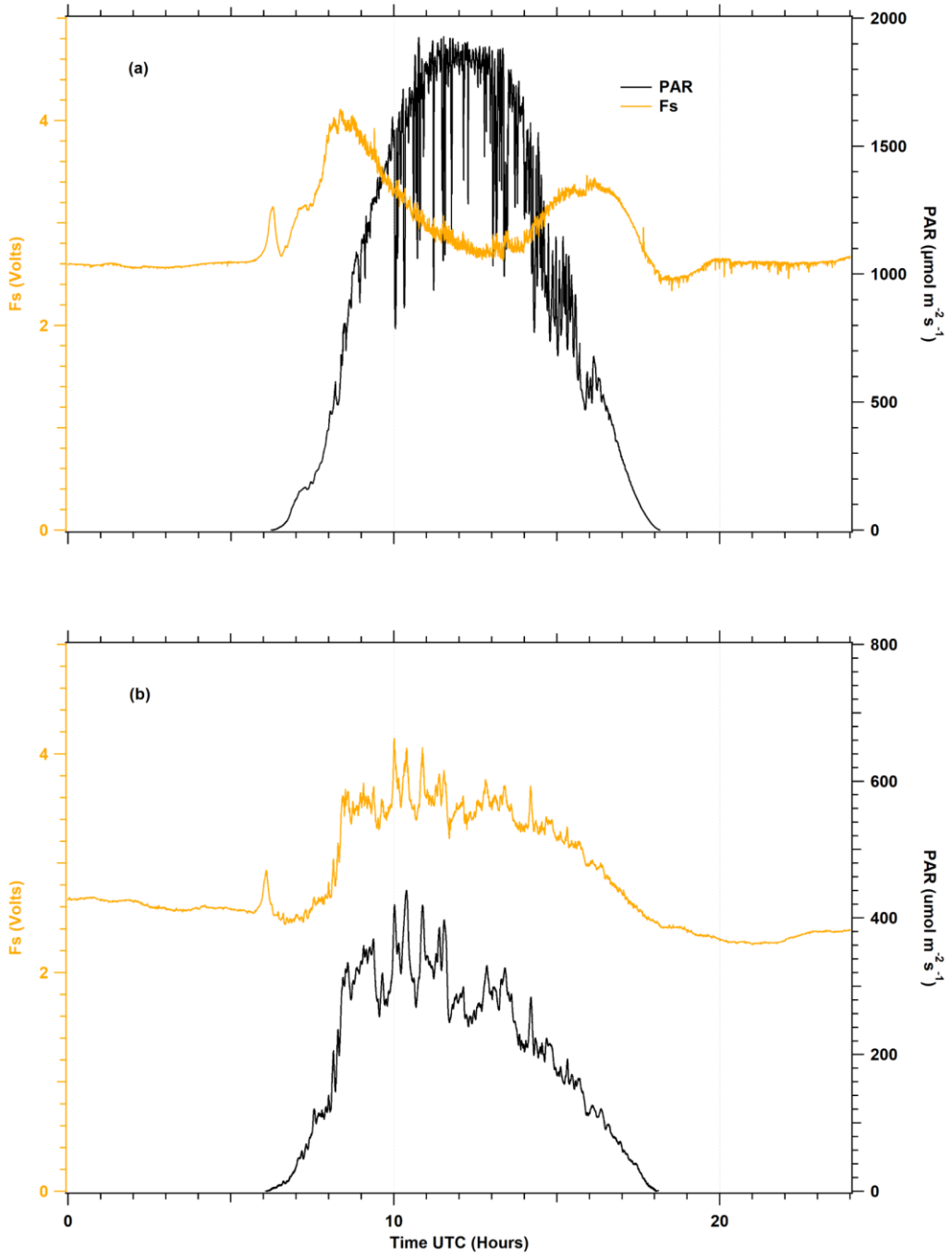

Fig. 3. 7 Diurnal cycles of stationary fluorescence (Fs) measured over potato canopy under sunny conditions at 56 DAP (**a**) and under cloudy conditions at 71 DAP (**b**). Fs time series changed according to intensity changes of incident PAR.

The cycles (Fig. 3. 7) show that at pre-dawn, i.e., in complete darkness, Fs is relatively constant, at a fluorescence level that can be associated with the Fo level (the minimum fluorescence value in the dark when all PS II reaction centers are open, see van Kooten & Snel, 1990). Nonetheless, with the first sun-light striking the potato's foliage, a small and reproducible peak appeared in all recorded cycles, as in Moya et al., (2019). Furthermore, according to PAR intensity, the Fs signal showed different patterns and responses to the incident light.

Under sunny conditions (Fig. 3. 7a), the Fs signal followed the natural changes of PAR until it reached the first maximum value when PAR amounted to around 600 µmol photons $m^{-2}s^{-1}$. Then it decreased until it reached a minimum local value, whereas incident PAR continued to increase up to the solar noon (maximum intensity). Once this Fs minimum was reached, the signal increased while PAR decreased. When the PAR intensity lowered to around 600 µmol photons m^{-2} s^{-1}, Fs finally reached a second local maximum to decrease and followed natural illumination changes. The three extrema of the Fs diurnal cycle generated an M-shape that characterizes the Fs series under sunny conditions, with the second maximum in the afternoon being of lower amplitude compared to the morning one. The experiment obtained similar results for Fs cycles on all sunny days.

Under cloudy conditions (Fig. 3. 7b), the Fs signal closely followed the incident PAR's natural changes over the day. Fs permanently changed in correlation with incident PAR whenever PAR intensity was less than 300 µmol photons $m^{-2}s^{-1}$.

3.1.4.2 Passive fluorescence measurements in O_2-A and O_2-B bands

During the campaign, time series of fluorescence fluxes from the vegetation cover of potato plants were recovered from two independent channels using the filling-in method of atmospheric oxygen absorption bands at A and B described in the Materials and Methods section. In addition, these diurnal cycles (see Fig. 3. 8) were retrieved using Spectroflex2 with the method proposed by Daumard et al., (2010).

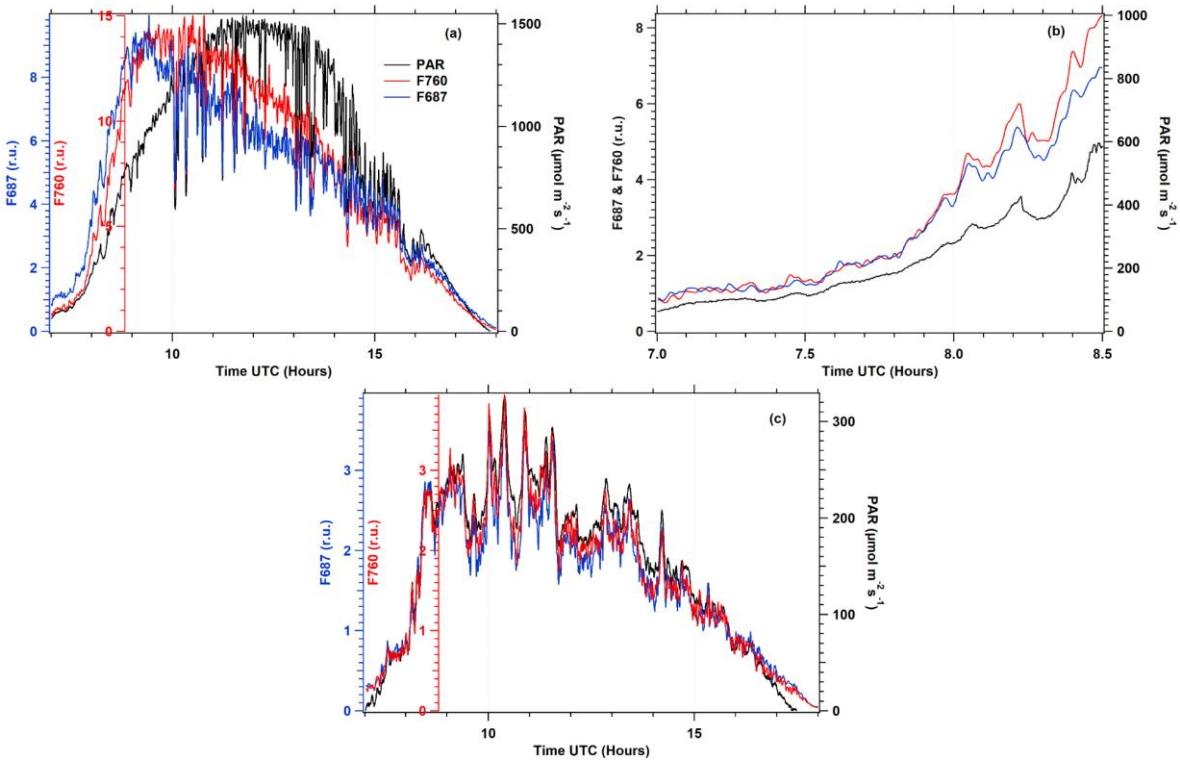

Fig. 3. 8 Diurnal cycles of fluorescence fluxes F687 (blue line) and F760 (red line), under sunny day conditions (**a**, **b**) at 56 DAP and a cloudy day (**c**) at 71 DAP. Following the

pattern of direct light, the fluorescence fluxes differed in amplitude and shape, whereas under cloudy conditions, both fluorescence fluxes closely followed changes in PAR.

Fig. 3. 8a shows a diurnal cycle example of fluorescence fluxes retrieved under clear days, plotted with independent axes to show their variations with respect to incident PAR. Both diurnal cycles showed similar patterns that changed due to intensity changes of incident light. These diurnal variations were observed in all recorded diurnal cycles. Although similar, F687 and F760 were not identical. During the morning, both time series continued to increase with the increase of PAR until about 1000 µmol photons m^{-2} s^{-1}. Nevertheless, after reaching this PAR level, the fluxes continuously decreased while PAR intensity increased. Between 10 and 14 hours, F687 decreased faster than F760, and the aspect ratio (F760/F687) was roughly 1.5, whereas it was near one at the beginning of the day (Fig. 3. 8b).

Under cloudy conditions and during the sunrise and sunset of sunny days with PAR intensity less than about 400 µmol photons $m^{-2}s^{-1}$ (see Fig. 3. 8b, c), the diurnal cycles of fluorescence fluxes in red and far-red were very similar in shape and amplitude and closely followed the changes of incident PAR intensity.

On the other hand, considering the whole diurnal cycles measured in this campaign (not shown), we observed that ASFY in 687 nm showed the most significant variations, which may better characterize the PS II electron transfer rate.

3.1.5 Discussion

3.1.5.1 Active measurements of fluorescence cycles

Diurnal cycles of relative fluorescence yields (Fs) were acquired using the active fluorimeter Ledflex. Among several factors that may influence Fs are chloroplast movements as they change leaf absorption and consequently leaf fluorescence (Brugnoli & Björkman, 1992; Wada, 2013). However, these effects were of small amplitude and occurred at low light (Brugnoli & Björkman, 1992). So it was neglected in the following. Measurements were done on a well-watered potato crop and under high light conditions (Fig. 3. 7), similar to those already published using active instruments. See, for example, the works of Rosema et al., (1998), Flexas et al., (2000), and Evain et al., (2004). The comparison with the data presented in Moya et al., (2019) is vital as the micro-LIDAR used in both studies are identical.

As in Moya et al., (2019), Fs reached a maximum at about 8:30 am when PAR exceeded 600 µmol photons m^{-2} s^{-1} (see Fig. 3. 7a), then decreased as Non-Photochemical Quenching (NPQ) developed. NPQ is the regulatory mechanism by which the plants can cope with the excess incident radiation when it exceeds the capabilities of the electron transfer chain (Müller et al., 2001). It involves conformational changes within the light-harvesting proteins of PS II that causes the formation of energy traps. The conformational changes are stimulated by combining a transmembrane proton gradient, PsbS protein, and

the carotenoid violaxanthin conversion to zeaxanthin. When PAR decreased in the afternoon, Fs increased due to the relaxation of NPQ (Horton & Ruban, 2005).

Further decrease of PAR induced a concomitant decrease of Fs until a level close to F_0. The M shape of the diurnal cycle is not symmetrical: the second maximum observed in the afternoon is lower than the first one observed in the morning. We suggest that part of NPQ formed before noon does not fully reverse during the afternoon and needs the entire night to dissipate and start again a new cycle the day after. Fig. 3. 7b shows the situation during an overcast day where the PAR stays under 300-400 µmol photons m^{-2} s^{-1}. In this case, Fs always closely follow PAR changes. In short, our results agree with the few LIDAR data available in the literature.

3.1.5.2 Passive measurements of fluorescence cycles

Using the method defined by Daumard et al., (2010), the fluorescence fluxes were determined from the solar spectrum reflected by the target and compared with the light reflected by a flat white horizontal board as described in the Materials and Methods section. In Fig. 3. 8a, we observed that the fluxes at 687 and 760 were similar in shape but different in amplitude. Several facts should be taken into account that may explain a different behavior:

- F687, peaking at almost the first peak of the fluorescence emission spectrum, reflects mainly PS II fluorescence and is fully affected by the development of NPQ under the high light conditions prevalent in Fig. 3. 8a. One may also observe that at light intensities under 300 µmol photons m^{-2} s^{-1}, that is, under relatively low light, F760 and F687 are almost superimposed (see Fig. 3. 8c), whereas, at 1000 µmoles photons m^{-2} s^{-1}, F760 is about 1.5 times F687. The reabsorption of ChlF also plays an important role. Fluorescence emission recorded at 687 nm comes principally from the upper layers of the leaf, as the contribution from the deeper layers are strongly reabsorbed by chlorophyll itself due to the overlap between absorption and emission spectra. This is not the case at 760 nm where re-absorption does not occur and the recorded signal is enhanced by the contribution of the deeper layers of the leaf, as compared to 687 nm. As the effective irradiance experienced by these deeper layers is significantly reduced from its value at the very surface, they are supposed to be less affected by the development of NPQ. In fact, these two wavelengths are sampling different parts of the leaf which are excited with different light intensities.

- F760 is, like F740, close to the second maximum of the fluorescence emission. This wavelength is strongly affected by the contribution of the constant PS I fluorescence emission, as shown in several works (Agati et al., 2000; Franck et al., 2002; Pfündel, 1998). These authors concluded that PS I fluorescence contributes around 35 to 40 % of Fo. In our case, under high light conditions, the fluorescence level is also close to Fo (see Fig. 3. 7a).

In addition, we should consider that the F760 excitation wavelength domain includes the spectral range over 700 nm that no one uses to excite chlorophyll fluorescence as it is impossible to excite and detect fluorescence at the same wavelength. This wavelength range is absorbed by PS I and contributes to the emission at F760, but it does not excite PS II. Thus, the contribution of PS I fluorescence at F760 is reinforced (Laisk et al., 2014; Zhen & Bugbee, 2020).

3.1.5.3 Comparison between active and passive diurnal cycles

At variance with the LIF technique, where the excitation source and experimental conditions are fixed and allow to define of a relative fluorescence yield, the SIF method retrieves fluorescence fluxes that should be divided by the radiation absorbed by the vegetation to compute a relative yield (see equations 1a and 1b in Materials and Methods 5th section). However, calculating the radiation absorbed by the vegetation using remote sensing methods results in a big challenge. Nevertheless, we can get an apparent spectral fluorescence yield (ASFY) considering approximations of absorbed radiation.

We thoroughly tested two choices that we compared in Fig. 3. 9:
1) Incident PAR (Fig. 3. 9b). Regarding incident PAR, we used the radiance of the reference panel as this signal is measured by our spectrometer each time we measured the radiance of the vegetation (see Materials and Methods, 5th section). It is based on the fact that fluorescence fluxes are recovered using radiances measured over the reference panel as a proxy of the incident light, and besides that, the capture times of each measurement involved in computing passive fluorescence can be obtained using a unique sensor. Furthermore, we used the difference between the reference panel's and vegetation's radiance with almost identical results.
2) Vegetation radiance in the 510-700 nm range as described in Materials and Methods 5th section (Fig. 3. 9a).

We compared the fluorescence fluxes after normalization by PAR or vegetation radiance with Fs (Fig. 3. 9). The time series of apparent spectral fluorescence yields and Fs were restricted to a time window from 8:00 to 16:00 local time to avoid artifacts in the passive data due to lower solar illumination angles. In addition, these patterns were observed on different sunny days.

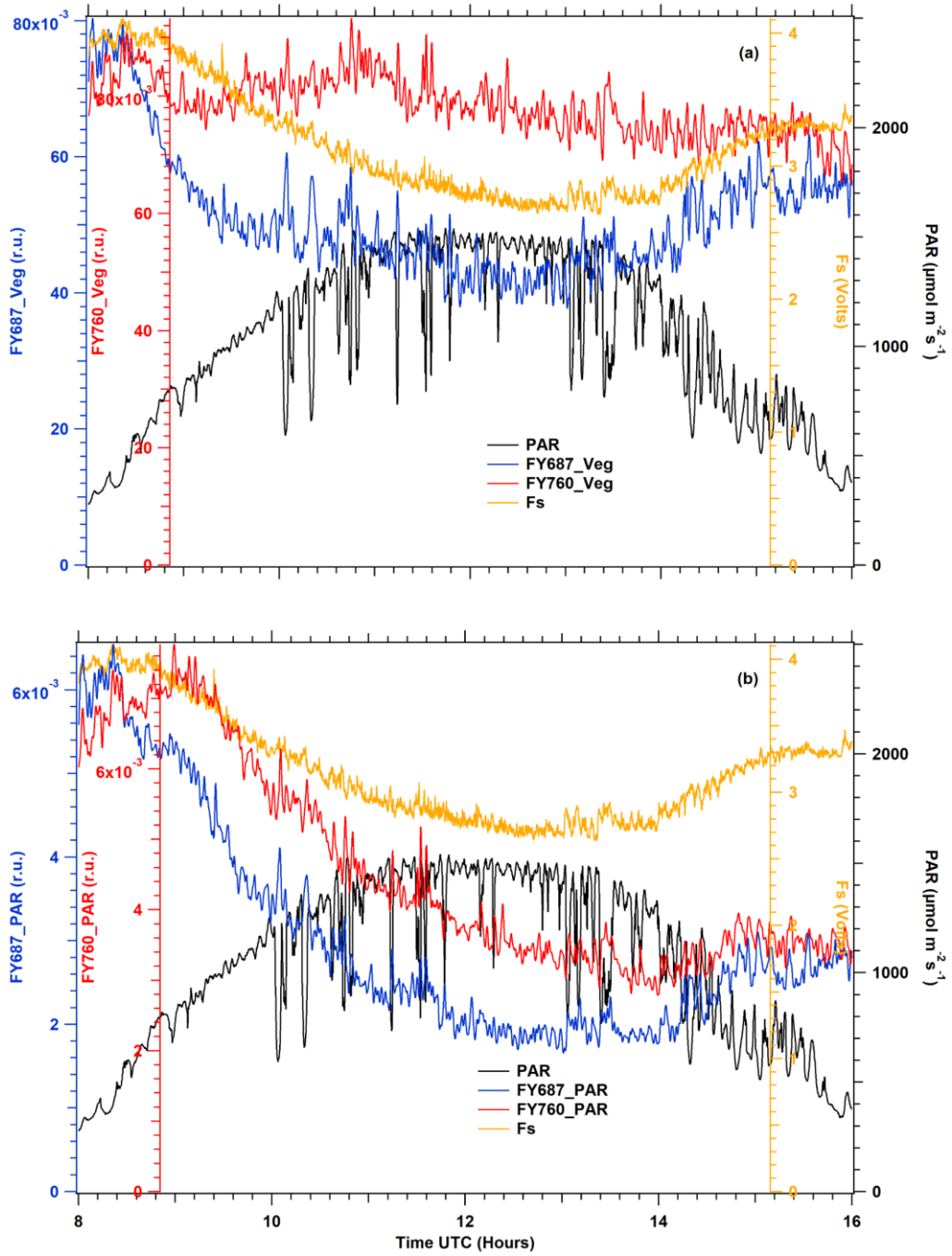

Fig. 3. 9 Comparisons at 56 DAP between fluorescence yields measured with the active method (orange) versus apparent fluorescence yields at 687 nm (blue) and 760 nm (red) retrieved by passive methods: (**a**) apparent fluorescence yields normalized by radiance of vegetation (**b**) apparent fluorescence yields normalized by incident PAR. Significant differences are observed between the patterns of the diurnal time courses. Similar results were obtained in all the measurements under sunny conditions.

Daily cycles were normalized with their respective maximum Fs_{max} and FY_{max}. Furthermore, cubic splines were applied to calculate statistics that allow measuring the differences between Fs and the apparent yields derived from passive measurements (F.Y.s). The distances between Fs and all F.Y.s were calculated using the sum of squared

residuals (SSR, see equation 3.3 below) as a criterion in model selection, which means that an SSR value closer to zero results in a better fit.

$$SSR = \frac{\sum_{t_i=8:00}^{16:00}[Fs(t_i)-FY(t_i)]^2}{Fs_{max}FY_{max}} \qquad (3.3)$$

Time series resulting from cloudy day measurements were dropped from the analysis since no significant differences were found between the F.Y.s calculated with the incident PAR.

Considering the average of all diurnal cycles recorded, the SSR ratio between FY760_PAR and FY760_Veg is 2.62, while that between FY687_PAR and FY687_Veg is 3.13. Therefore, F.Y.s computed with vegetation radiance are significantly better than F.Y.s obtained with incident PAR (Table 3. 2). Hence, these later ones were excluded from the following analysis.

3.1.5.4 Optimized SIF versus LIF measurements

Leaves movements due to wind may also contribute to decorrelate signals of Spectroflex2 (period of measurements 12 seconds per loop) and Ledflex (period 2 seconds per loop). Furthermore, Ledflex detects fluorescence emission over the whole spectral band between 650 nm and 800 nm (Fig. 3. 1), which mixes the red and the far-red emissions of ChlF. To better represent the whole ChlF with the passive method, we combined the FY687 and FY760 apparent yields into a single indicator, considering their values as representative of the emission of the red and far-red ChlF bands, respectively. This approach is supported by the fact that the total emission is mainly controlled by the two independent factors related to the PS I and PS II emissions.

Ledflex transmission calculated a correction coefficient for each passive signal: 1 for FY687_Veg and 0.95 for FY760_Veg (see Materials and Methods, 2nd section, Fig. 3. 1), and an equivalent F.Y. was calculated with the aim to more closely fit Fs time series with passive measurements. This improved F.Y. was called FYSIF and is defined as:

$$FYSIF = FY687_{Veg} * 1 + FY760_{Veg} * 0.95 \qquad (3.4)$$

FYSIF time series were compared with Fs under different natural light conditions. Good agreements were found between the variables (see examples in Fig. 3. 10). The SSR indicator was computed for all F.Y.s and sunny days of the experiment (Table 3. 2). The last row of Table 3. 2 shows the SSR average of each F.Y.

Table 3. 2 Measure of the normalized difference between apparent fluorescence yields derived from passive measurements and Fs over a diurnal cycle (Sum of squares of residuals, SSR) according to emission wavelengths (687 nm, 760 nm) and normalization method (PAR: irradiance; Veg: vegetation radiance). FYSIF combined the two

wavelengths, 687 nm and 760 nm, normalized by vegetation radiance. Again, only sunny days of the experiment are reported.

DAP	FY687_PAR	FY687_Veg	FY760_PAR	FY760_Veg	FYSIF
48	677.07	409.37	112.94	157.49	**133.32**
51	490.76	311	380.85	258.43	**234.36**
52	998.98	422.32	726.5	238.95	**147.8**
53	797.51	232.67	364.83	23.94	**51.15**
54	340.74	128.98	212.99	100.65	**50.53**
56	1704.73	222.49	750	349.34	**57.77**
57	595	295.04	578.7	200.32	**107.69**
64	632.2	198.92	248.14	65.60	**61.15**
73	182.82	47.28	130	337.1	**169.56**
74	162.66	41.47	233.95	61.52	**23.05**
80	543.55	305.76	899.52	325.51	**177.21**
81	637.6	185.6	661.8	126.74	**95.69**
82	1309.19	92.78	744.26	65.84	**42.15**
SSR (average)	697.91	222.59	464.96	177.8	**103.96**

Except for the data corresponding to 53 DAP where the SSR computed for FY760_Veg is less than FYSIF and for 73 DAP where SSR computed for FY687_Veg is less than FYSIF, the SSR corresponding to FYSIF is less than other F.Y. models presented in Table 3. 2.

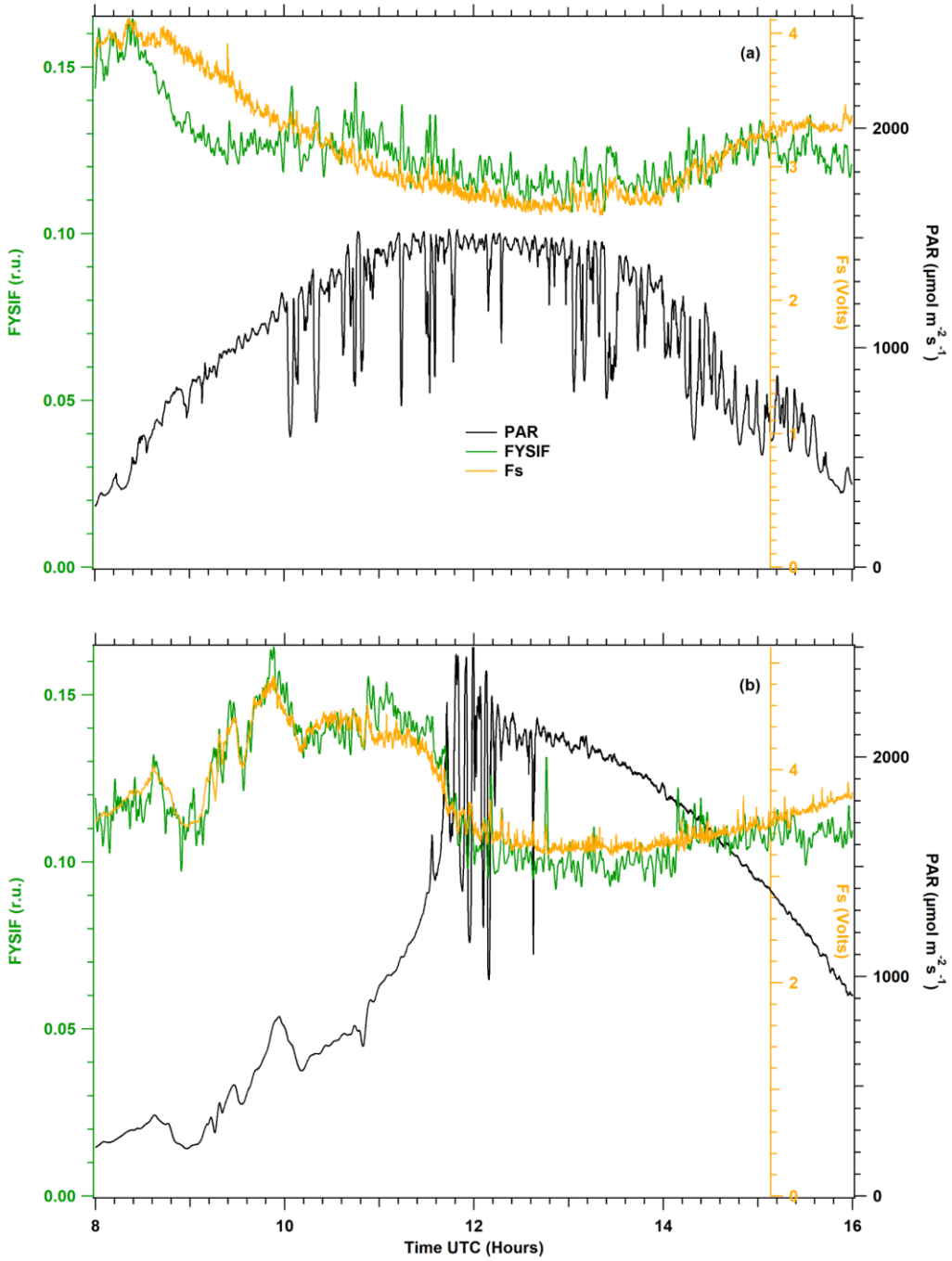

Fig. 3. 10 Diurnal cycles of FYSIF and Fs under sunny conditions at 56 and 64 DAP. Similar results were obtained for other days of the experiment.

Considering the average SSR computed for each passive fluorescence yield described in this work, the mix of passive fluorescence measurements at 687 nm and 760 nm divided by vegetation radiance (FYSIF) resulted by far in the best fit to Fs, with an SSR value of 103.96. In addition, the close results between fluorescence yields retrieved with active and passive methods implies that leaves movement seems to have only a negligible effect.

3.1.6 Conclusions

The present work constitutes the first report comparing active and passive measurements of chlorophyll fluorescence by filling-in atmospheric oxygen absorption bands at 687 and 760 nm at the canopy level.

Diurnal cycles of fluorescence fluxes at 687 and 760 nm showed a similar signal-to-noise ratio but differed in magnitudes. To extract relative fluorescence yields from passive fluorescence fluxes, we used two different approaches of normalization:
- by the flux reflected by a flat and white reference surface - i.e. representative of the incident radiation,
- by the flux reflected by the vegetation.

The resulting diurnal cycles of the relative fluorescence yield at 687 nm and 760 nm significantly differed from the fluorescence yield obtained by the active method. Furthermore, dividing the fluxes by the radiance of the vegetation was found to reproduce better the actual fluorescence yield than dividing them by the radiance of the white panel. In order to better represent the spectral detection range of the active sensor, we combined the two passive fluorescence yields in the red and far-red after normalization by the vegetation radiance. This approach was successful as a good agreement was found between fluorescence yields derived from active and passive methods. Moreover, we confirmed the differences between fluorescence yields diurnal cycles at 687 nm and 760 nm that we explained by the contribution of PS I to the 760 nm emission and the reabsorption of red fluorescence, which limits the contribution of the deeper layers of the leaf at 687 nm. This also improved the confidence in the retrieval method proposed by Daumard et al., (2010), which computes fluorescence fluxes using only four channels to retrieve fluorescence at 687 nm and three channels for fluorescence at 760 nm. Additionally, the low computational cost allows to retrieve fluorescence in real time.

Acknowledgement The core of this work was supported by the Bill & Melinda Gates Foundation [OPP1070785]. Under the grant conditions of the Foundation, a Creative Commons Attribution 4.0 Generic License has already been assigned to the Author Accepted Manuscript version that might arise from this submission. In addition, this research was undertaken and partially funded by the CGIAR Research Program on Roots, Tubers, and Bananas (RTB) and the CGIAR Plant Health Initiative, supported by CGIAR Trust Fund contributors (https://www.cgiar.org/funders/).

Data Availability statement The data that support the findings of this study are openly available in Dataverse CGIAR repository at: Diurnal cycles of passive and active fluorescence measurements at canopy level in potato crops. https://doi.org/10.21223/5RL85W

CHAPTER 4

Water stress detection using proximal remote sensing of chlorophyll fluorescence at field level and airborne SIF measurements.

In this chapter is described a water stress experiment on fescue meadowland carried out in the facilities of Provincial Agronomic Technical Institute (ITAP) in Barrax – Spain. We used Ledflex to determine the water stress effect on fluorescence of fescue field. In addition to the fluorescence data, surface temperature was also measured using infrared radiometers. And for SIF measurements, a new version of Airflex, a passive fluorometer measuring the filling-in of the atmospheric oxygen absorption band at 760 nm, described first by Moya et al. (2006), was installed in an ultralight plane and flown during the most critical days of the campaign.

The full description of this study was published in the Photosynthesis Research Journal (Moya et al., 2023).

4.1 Article: Active in situ and passive airborne fluorescence measurements for water stress detection on a fescue field

Ismael Moya[1], **Hildo Loayza[2]**, María-Llanos López[3], Juan Manuel Sánchez[4], Yves Goulas[1], Abderrahmane Ounis[1], Roberto Quiroz[5], Alfonso Calera[4]

4.1.1 Abstract

Ledflex is a fluorometer adapted to measure chlorophyll fluorescence at the canopy level. It has been described in detail by Moya et al., (2019), Photosynthesis Research. DOI: 10.1007/s11120-019-00642-9. We used this instrument to determine the effect of water stress on the fluorescence of a fescue field under extreme temperature and light conditions through a 12 days campaign during summer in a Mediterranean area. The fescue field formed part of a lysimeter station in "las Tiesas," near Albacete-Spain. In addition to the fluorescence data, the surface temperature was measured using infrared radiometers. Furthermore, "Airflex," a passive fluorometer measuring the filling-in of the atmospheric oxygen absorption band at 760 nm, was installed in an ultralight plane and flown during the most critical days of the campaign.

We observed with the Ledflex fluorometer a considerable decrease of about 53 % of the stationary chlorophyll fluorescence level at noon under water stress, which was well correlated with the surface temperature difference between the stressed and control plots. Airflex data also showed a decrease in far-red solar-induced fluorescence upon water stress in agreement with surface temperature data and active fluorescence measurements after correction for PS I contribution. Notwithstanding, the results from airborne remote sensing are not as precise as *in situ* active data.

Keywords chlorophyll fluorescence, water stress, LED-induced fluorescence, airborne measurements, sun-induced fluorescence, fescue

Abbreviations

SIF	Solar-induced fluorescence
PAR	Photosynthetically active radiation
O_2-A	Oxygen A absorption band
O_2-B	Oxygen B absorption band
D760	The atmospheric oxygen band depth at 760 nm
F_yield	Apparent fluorescence yield at 760 nm
Fs	Stationary fluorescence
Fo	Minimum dark-adapted fluorescence yield
Fmin	Minimum of stationary fluorescence at around solar noon
Tair	Air temperature measured by a thermistor outside Ledflex
NDVI	The normalized difference vegetation index
PS I	Photosystem I
PS II	Photosystem II

4.1.2 Introduction

Remote sensing is becoming a prerequisite for monitoring the photosynthetic vegetation state at the field level. Among available methods for plant studies, chlorophyll fluorescence plays an essential role as this emission is directly linked to photosynthesis. Light absorbed by plants between 350 and 750 nm ultimately leads to an excited state of chlorophyll *a* at the reaction center. Several ways of de-excitation are possible: photochemistry and the subsequent CO_2 fixation are highly probable under favorable conditions, but the energy can also be dissipated as heat or emitted as fluorescence emission. Because these three deactivation pathways compete, fluorescence is highly variable, and its variations reflect the variations of the photosynthetic activity.

The efficiency of the fluorescence emission *in vivo* is very low (less than 1 - 2% of absorbed energy). Nevertheless, chlorophyll fluorescence is widely used in the laboratory as it is a specific emission of green plants. In addition, chlorophyll is probably one of the rare constituents of the biosphere to fluoresce in the red and far-red parts of the spectrum.

For the last 30 years, several modulated fluorometers have been proposed to the community. Among them, the Pulse Amplitude Modulation (PAM) fluorometer (Walz, Effeltricht, Germany) was the most popular (Schreiber et al., 1986). At the basis of this success was the "light-doubling" technique (Quick & Horton, 1984), in which a faint (non-actinic) modulated light generates a synchronously detected fluorescence emission that changes when a continuous actinic light is superimposed. In addition, the possibility to saturate photosynthesis with intense sub-second light pulses allows for calculating several parameters like the effective yield of photosystem II photochemistry, the yield of non-photochemical energy dissipation, or the apparent electron transport rate. The drawback of these measurements is the need to work at the leaf level and near contact.

It is impossible to saturate the fluorescence by using large target sizes of > 1m in diameter to integrate the spatial heterogeneity at the canopy level. One of the most accessible parameters is stationary fluorescence (Fs), as shown by Cerovic et al., (1996). Fs variations are much smaller in amplitude than the maximum fluorescence (Fm); however, obtaining qualitative but valuable information on the vegetation's physiological state by measuring Fs continuously from a fixed and constant position is possible. For example, one can consider the Fs/Fo ratio (Fo is the Fs signal measured during the night) to characterize water stress, as shown by Moya et al., (2019). In the present work, the authors used the same "Ledflex," a LED-based micro-LIDAR able to measure Fs continuously at several meters, in full sunlight, and over a target size of up to $1m^2$.

We decided to use this instrument during reversible water stress in a well-controlled fescue field of a lysimeter station in "las Tiesas," near Albacete-Spain. In addition to the fluorescence data, the surface temperature was measured using infrared radiometers (IRTs) (MI-210, Apogee Instruments Inc., Lugan, UT, USA). Last but not least, "Airflex," a passive fluorometer measuring the filling-in of the atmospheric oxygen absorption band (Daumard et al., 2015; Moya et al., 2006; Rascher et al., 2015), was installed in an ultralight plane and flown during the most critical days of the campaign.

The aims of this work were:

1. To test the capacity of stationary fluorescence at canopy scale (Fs) measured by Ledflex to discriminate between well-watered and water-stressed conditions. The case of a natural crop under full sunlight is of particular scientific interest.

2. To compare active Ledflex measurements of fluorescence changes with passive Airflex measurements of fluorescence changes.

3. To compare canopy temperature changes with Ledflex fluorescence changes.

4.1.3 Material and methods

4.1.3.1 Experimental area

The study was conducted in a flat country near Albacete in the South-East of Spain. The first measuring campaign in this zone was done in the summer of 2005 in the framework of the Earth Observation Envelope Programme of the European Space Agency (ESA) (Moya et al., 2006). The actual campaign lasted one month, from July 3 to August 2 during the summer of 2017. It occurred near Barrax (Albacete-Spain) in the experimental farm "las Tiesas," situated at 39.06º north, longitude 2.099º west, altitude 698 m. A lysimeter station was installed in the center of a ≈1-hectare plot of a fescue meadow (*Festuca arundinacea Schreb.*), Fig. 4. 1, maintained in optimum growth conditions with the object of measuring reference evapotranspiration (ET_O) values. The crop was kept between 0.08 and 0.12 m in height through weekly mowing (Fig. 4. 3). The field was maintained in optimum growth conditions to measure reference evapotranspiration values and was irrigated regularly for three hours every two or three days from July 3rd until the end of the experiment by an automated sprinkler system of total underground coverage. Climatic data were recorded by the agro-meteorological station "Anchor station" thanks to an STA-212-PVC sonde. The agro-meteorological

station was situated in the vicinity of the Ledflex instrument. In the actual campaign, the field was divided into two parts: i) A first part delineated by a blue line which was kept well-watered (Fig. 4. 1) and ii) a second part delineated by a yellow line in Fig. 4. 1 (hereafter named stressed plot) where the irrigation was interrupted for several days to generate a controlled drought. The Ledflex fluorometer was installed in the stressed plot when it was still well-watered, as shown in Fig. 4. 3. Irrigation of the stressed plot was interrupted from July 13 (last irrigation) until July 25, except for 1-hour irrigation on July 21 and three hours on July 24. No rain occurred during this period. So, we assumed that on July 16, control conditions still prevailed for both plots and that maximum stress was obtained on July 24 in the stressed part.

An automated agrometeorological weather station (Anchor Station) was also used that provided 10-min, hourly, and daily recordings of the climatic data. In particular, the air temperature was measured at 0.5, 2, and 10 m above ground with an accuracy of $\pm$ 0.1 °C.

The original plan was to use a portable photosynthesis meter (LI-6400, Licor, USA) to gather gas exchange information to complement fluorescence measurements. However, this measurement was not taken because the fescue leaves were too small to fit the LI-6400 window. So instead, we used infrared thermometry (Apogee MI-210) in both parcels (control and stress) to continuously monitor surface temperatures day and night.

Fig. 4. 1 The fescue (*Festuca arundinacea Schreb*.) meadowland. The plot was maintained in optimum growth conditions to measure reference evapotranspiration values (ETo) and has an automated sprinkler irrigation system of total underground coverage. The yellow line delineates the portion of the field where the irrigation was interrupted for several days to generate a controlled drought (stressed plot). (Figure modified from

Google earth Pro V 7.3.4 (July 29, 2017). Las Tiesas, Barrax, Spain. 39° 03’ 37.45” N, 2° 05’ 58.45” W, Eye alt 901 meters. July 01, 2022).

4.1.3.2 Ledflex

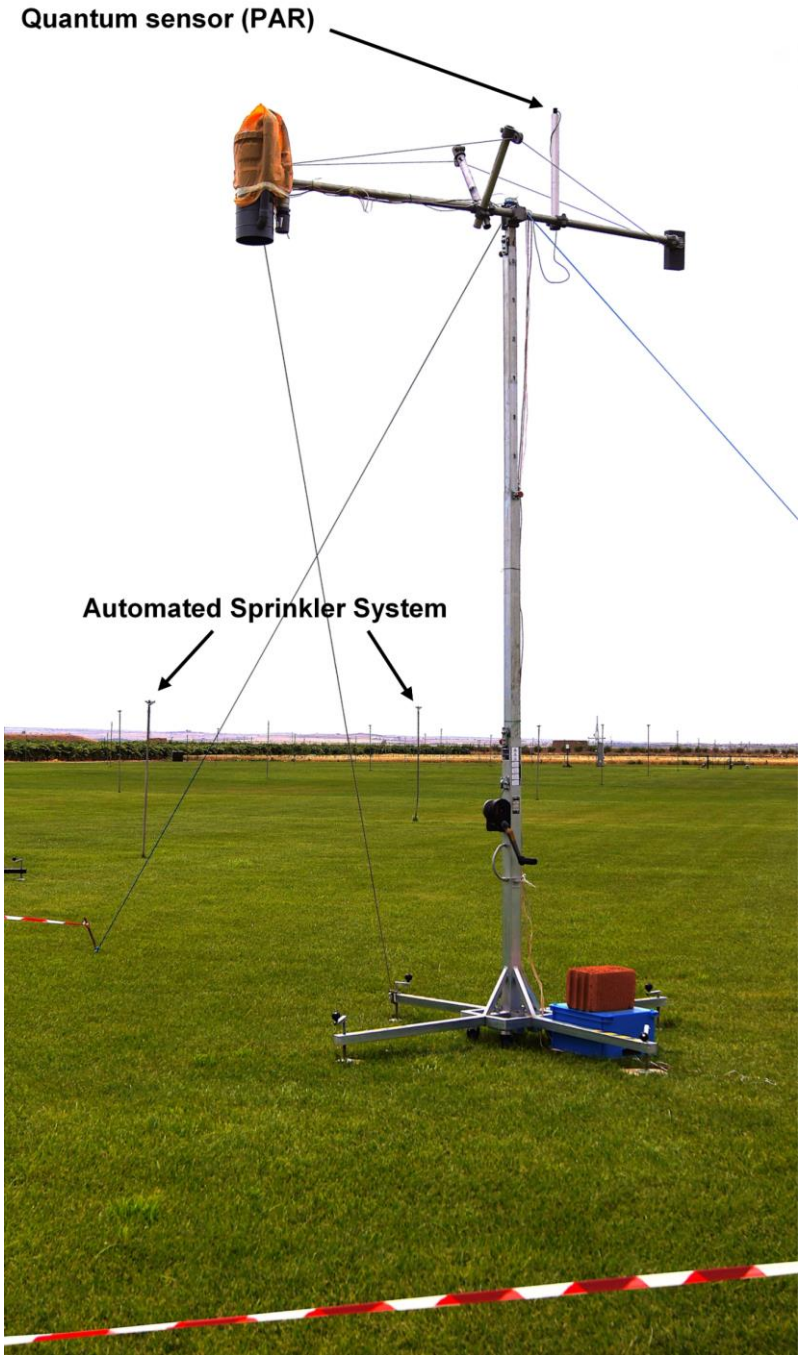

Fig. 4. 2 Ledflex in position over the fescue field.

This instrument has already been described by Moya et al., (2019). Briefly, Ledflex is a hardened fluorometer for continuous chlorophyll fluorescence measurements under natural illumination at distances up to 8 m. It has been designed to integrate the fluorescence emission of a target diameter of about 1m. The light source consists of a group of pulsed blue Light Emitting Diodes (LEDs) (Thorlabs, Maisons-Laffitte, France)

with peak emission at 470 nm and a full width at half maximum (FWHM) of 22 nm. The fluorescence emitted in response to the 5μs width pulses of excitation light is separated from the reflected ambient light through a synchronized detection. The fluorescence signal is also spectrally selected with the combination of a high-pass filter (Schott RG665, 3 mm, $\lambda > 665$ nm, Edmund Optics, UK) and a low-pass filter ($\lambda < 800$ nm, Edmund Optics, UK) to reduce the detected spectral range to the functional zone (665 – 800 nm) where fluorescence is emitted. The target's reflected sunlight and LED-induced fluorescence were acquired simultaneously in the same field of view and the same spectral band. The incident photosynthetic active radiation (PAR) was acquired thanks to a quantum sensor (JYP 1000, SDEC-France, Tours, France) situated on a pole at the top of the Ledflex set-up. The Ledflex sensor was fixed on a vertical mast with a nadir viewing 4 m above ground (Fig. 4. 2). The Ledflex sensor arm was directed south to avoid shadows in the target area. All the instruments were powered by a 12 V car battery recharged by a solar panel, allowing continuous measurements during night and day.

Fig. 4. 3 Detail of the fescue cover about 8 – 10 cm deep.

4.1.3.3 Thermal-Infrared Radiometers

This experiment used two thermal-infrared radiometers (IRTs), Apogee MI-210 (Apogee Instruments, Inc.). These instruments have a broad thermal band (8–14 μm) with a field of view of 22º, a response time of 0.6 s, and an accuracy of ± 0.2 K. Calibration was assessed using a blackbody source (Hyperion R 982, Isotech, England). One of the IRTs was installed near Ledflex on the stressed plot. The second IRT was located in the "well-watered" control plot (see Fig. 4. 1). The IRTs were fixed on a mast, at the height of 1.5 m above the ground, with a viewing angle of 45º, defining a surface target area of about 6.4 m^2. Acquisition mode was set to perform a measurement every 30 seconds and then record an average every 30 minutes. This work did not apply atmospheric and emissivity corrections since only relative differences between well-watered and stressed crops were required.

The use of these broad-band IRTs is widespread in agronomic applications such as plant water status estimation or surface energy balance modeling (Sánchez et al., 2008, 2011, 2014, 2015, 2019) and also in surface temperature monitoring for remote sensing calibration/validation activities (Niclòs et al., 2015; Sánchez et al., 2020; Sobrino & Skoković, 2016).

4.1.3.4 Passive fluorescence measurements using Airflex

Airflex is an interference-filter-based airborne sensor developed in the Earth Observation Preparatory Program of the European Space Agency (ESA) framework and first described by Moya et al., 2006. See also Rascher et al., (2009) and Daumard et al., (2015). It is a 6-channel photoradiometer that measures the filling-in of the atmospheric oxygen bands. Nevertheless, since its first development, its design has been substantially modified. In this new version, a set of 3-channels, equipped with specific interference filters from Alluxa (Santa Rosa, California - US), was used to monitor the spectral profile of the O_2-A absorption band (Fig. 4. 4a). The transmission band of one filter is centered at the minimum of the O_2 absorption band (in-band), and the other two are placed right before and after the O_2 absorption feature (out-band). The three filters dedicated to monitoring the O_2-B band in the first version of the instrument were replaced by two narrow bandpass filters in the green (523.8 nm and 566.7 nm) to measure the photochemical reflectance index (PRI). Unfortunately, electronic failures at the campaign's onset precluded signal measurements in the 566 nm channel, and thus PRI could not be calculated. In addition, a third red filter at 672.6 nm and one of the far-red filters used for the O_2-A band profile (770.64 nm) were devoted to determining NDVI. The peak positions, spectral bandwidth (FWHM), and peak transmittance of these filters are listed in Table 4. 1. This new filter set has better transmission and durability than the previous ones. The Airflex objective and the filters are maintained at 40 ± 0.1°C by a regulated heating system to prevent thermal drifts.

The former Airflex was a cylinder of ≈ 1 m in length; its central part was a hub in front of the objective. The hub contained a set of black-painted baffles to prevent stray light from entering the Airflex objective (Fig. 4. 4). At the end of this cylinder was the photometer itself (Moya et al., 2006).

Table 4. 1 Peak wavelength (λ_i), Full Width at Half Maximum (FWHM), and Transmission for the filters used in the Airflex sensor.

	Airflex sensor filters		
Band	**Peak wavelength (nm)**	**FWHM (nm)**	**Transmittance**
PRI	λ_1 = 532.8	9.4	95 %
PRI	λ_2 = 566.7	10.2	91 %
NDVI	λ_3 = 672.6	10.8	94 %
O_2-A out band	λ_4 = 757.93	1.13	88 %
O_2-A in band	λ_5 = 760.80	1.02	91 %

O_2-A out band / NDVI	λ_6 = 770.64	1.10	85 %

The Airflex splitter and the fiber optics

The Airflex hub was removed and replaced by an optical fiber that feeds the light to the objective through a light "splitter" to fit the reduced available space inside the ultralight plane (see Fig. 4. 4b, c). The fiber has a 2 m length and a numerical aperture of 0.37 and 0.94 mm in diameter (SEDI-ATI Fibres Optiques, Courcouronnes, France). The fiber etendue is calculated as the product of the solid acceptance angle by the entrance pupil and is 0.31 mm^2 rad in our case. This value is greater than the etendue of the native Airflex, which was 0.27 mm^2 rad. As a fully optimized optical system produces an image with the same etendue as the source, we should provide at least this value. So, we lost a small amount of the collected light that is not accepted by the Airflex etendue.

The splitter is a complex piece of machined aluminum that has been specially designed and built in the lab's workshop (Fig. 4. 4c, d). It contains several mirrors, beam splitters, and dichroic filters and divides the flux collected by the optical fiber into six beams corresponding to the six channels described in Table 4. 1. As a result, the optical fiber and splitter system is much more flexible than the original Airflex hub and can fit easily in the cabin of a small airplane, as shown in Fig. 4. 5b.

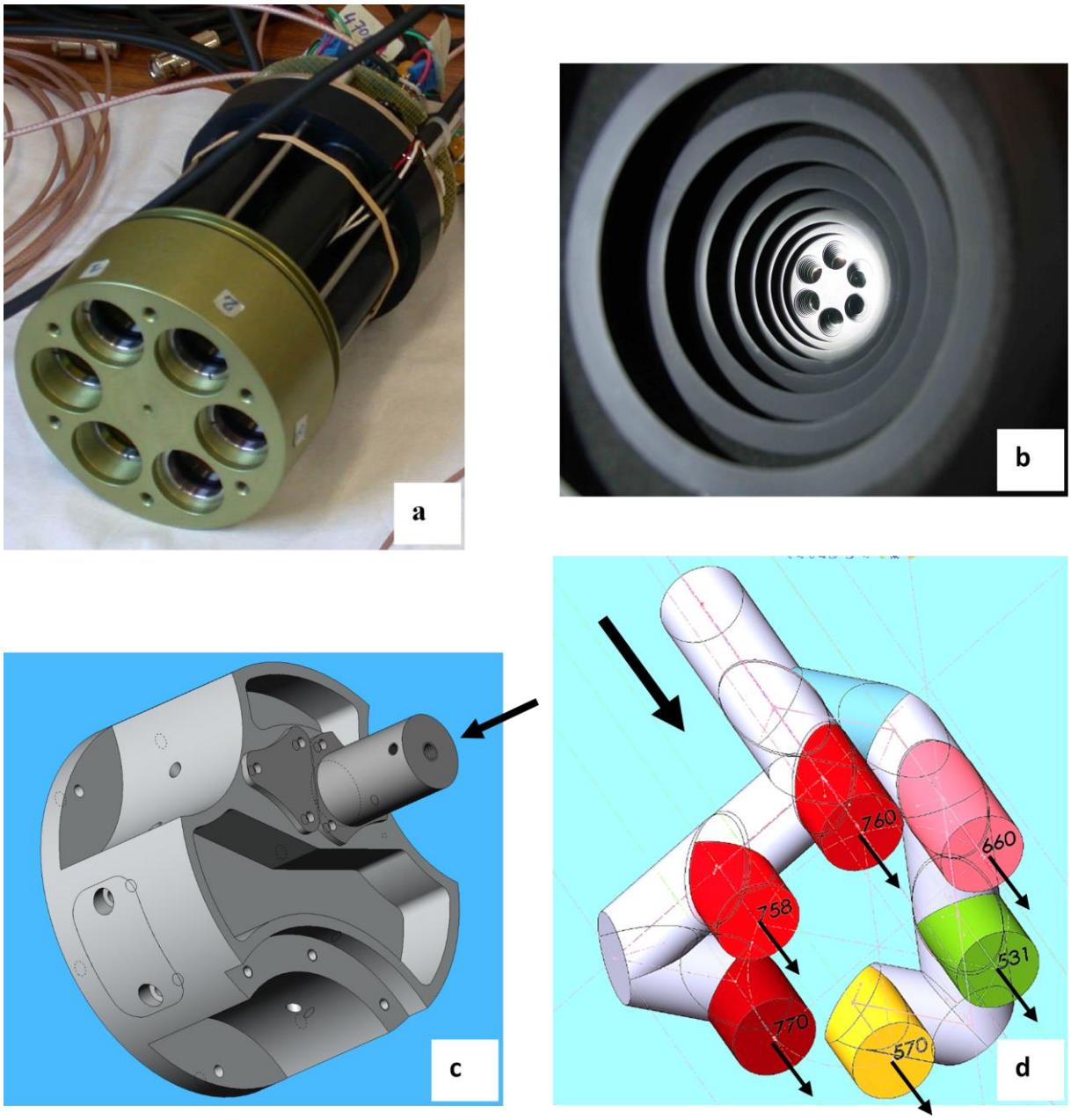

Fig. 4. 4 a Heart of the sensor, the objective exhibits six cavities containing the set of filters and the collimating lenses. The objective is maintained at 40 °C by a regulated heating system. **b** Hub. The objective is visible behind the baffle. A fiber optic replaced the black-painted baffle system's entrance to minimize stray light. **c** Beam splitter of the new version of Airflex. **d** Scheme showing the beam splitter interiors and how the beam collected by the optical fiber is divided into six channels thanks to a set of mirrors and dichroic filters.

Each channel signal was measured by a low noise amplified silicon photodiode (HUV 1100 BG, Perkin-Elmer, France). Thanks to an aspheric objective of 25 mm in diameter and 31.25 mm of focal length (Edmund Optics, France), the field of view was set to 3.0 m from an altitude of 100 m. This altitude was maintained more or less constant (±10 m) during all flights.

Data acquisition was ensured by a data acquisition board (USB NI 6356, National Instruments, France) having eight simultaneous differential inputs with 16 bits encoding capacity. The acquisition software was managed using LabVIEW (National Instruments, France). In addition, a USB monochrome video camera (Chameleon, 1.3 MP CCD, FLIR systems U.S.) was added to record a synchronized image of the field of view context for each Airflex measurement. The video camera was externally triggered by a TTL signal generated by the LabVIEW program. Recording and transferring images were managed by a program developed in C language using libraries of the FlyCapture 2.0 software development kit (SDK) from FLIR Systems that allowed the data acquisition synchronization.

The new version of Airflex with fiber optic, splitter, and a video camera was flown on the 16th (control days), 24th (stress), and 25th (reversion day) of July 2017. During these days, measurements were taken around noon to minimize changes in the atmospheric oxygen absorption band during the flight. The speed was maintained as low as possible within security limits at 25 - 30 $m.s^{-1}$ (i.e., ≈100 $km.h^{-1}$) at an altitude of approximately 100 m. The ultra-light plane was a Micro Aviation Pulsar III, capable of carrying two persons (Fig. 4. 5c).

The new version of Airflex was radiometrically calibrated just before the airborne campaign with a calibration source (Licor 1800-02, NE, USA) and a second time at the end of the experiment. Both calibrations were in agreement, except for the failure of the PRI channel, which was out of order.

4.1.3.5 Canopy reflectance measurements

Canopy reflectance spectra were recorded using a portable fiber optic spectrometer (HR 4000, Ocean Insight, USA). Measurements were taken on the stressed area before starting the water stress period (see Fig. 4. 13 of the appendix). The target size was about 0.7 m in diameter. Measurements on the target were immediately preceded and followed by a similar measurement on a horizontal white-roughened PVC board whose reflectance spectrum was determined in the laboratory against a Spectralon (Labsphere, USA) reflectance standard.

4.1.3.6 Chlorophyll fluorescence measurements on the ground.

The shape of the fluorescence emission spectrum (Fig. 4. 13 of the appendix) is needed to retrieve the SIF level according to the retrieval method used by Daumard et al., (2010). Therefore, we used the entire sunlight leaf-level emission spectra as a proxy for the canopy level emission, as Fournier et al., (2012) suggested. Before starting the water stress period, measurements were taken on the stressed area. The spectra were acquired with a fluorometer already described by Moya et al., (2006), Rascher et al., (2009), and Daumard et al., (2010), using the sun as the source of excitation. It is based on a portable spectrometer (HR2000+, Ocean Insight, USA) equipped with a high-pass red filter (RG665, Schott, France) to select wavelengths only corresponding to chlorophyll fluorescence.

The solar radiation was filtered in the illumination system by a low-pass filter (Corning 4.96, 5 mm, Corning, USA), blocking excitation at $\lambda > 600$ nm. A plano-convex lens

focuses the sun on the leaf to compensate for the light attenuation introduced by the filter and the optics. As a result, measurements were taken at total sunlight excitation. Measurements were performed after a light adaptation period of 10 – 15 min when a stationary state was reached. Raw emission spectra were corrected for the spectrometer's instrumental response function and the red filter's transmission.

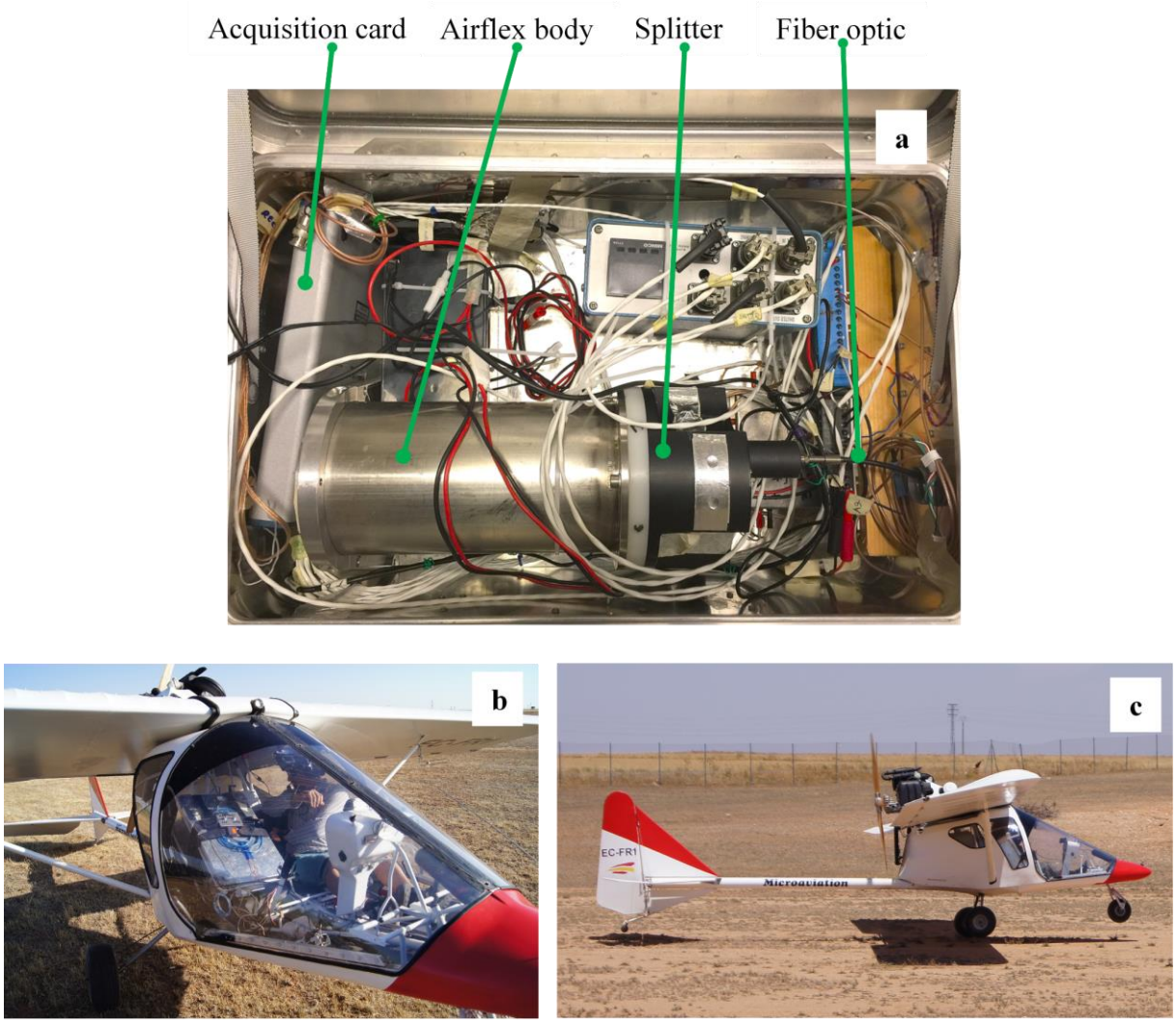

Fig. 4. 5 a Airflex and associated electronics inside the instrumental box. **b** The Airflex box in the airplane cabin. **c**. The ultralight airplane at take-off.

4.1.3.7 Statistics

Mean values of stationary fluorescence level measured by Ledflex were computed at two specific times of the diurnal cycle:

- The fluorescence level in the dark-adapted state (Fo) was derived as the mean of fluorescence in a time interval of 15 min lasting from 05:53 to 06:08 local time. It corresponds to the fluorescence level just before the morning induction curve resulting from the first increase in PAR level.
- The minimum fluorescence level in the day (Fmin) was derived as the mean in a time interval of 15 min around the minimum fluorescence level that occurs around solar noon (Fig. 4. 6).

The standard deviation of Fo and Fmin were also computed on the same sample of data. The number of measuring points included in the computation of each fluorescence level (Fo, Fmin) was between 462 and 470, corresponding to a mean sampling rate of raw data of 0.52 Hz.
Linear regression and other statistical analyses were performed using Igor Pro (Wavemetrics, Portland, OR, USA).

4.1.4 Results

The active fluorometer Ledflex was continuously operated throughout the campaign at about 4 m above ground and monitored the transition of the restricted watering zone from a well-watered situation to stress conditions. The restricted watering phase lasted from July 13 through July 26 (Fig. 4. 6 shows a typical control day, July 15). The stationary fluorescence is in red. In black is the Photosynthetic Active Radiation (PAR) measured with a quantum sensor over the Ledflex instrument (see Fig. 4. 2). The air temperature measured with the meteorological station is green.

Fig. 4. 6 shows an experiment that starts at midnight and lasts 24 hours. Except for some spurious morning variations, the PAR variation describes a very smooth curve close to a cosine curve with a maximum of about 1900 µmol of photons $m^{-2}s^{-1}$. Fs stays almost constant during the night. This constant night level is denoted hereafter as Fo. Fs increases in the morning when PAR increases. A maximum is reached around 9:00 local time with a PAR of 650 µmol of photons $m^{-2}s^{-1}$, then Fs decreases to a minimum (Fmin) slightly above Fo. As light decreases in the afternoon, Fs increases in a somewhat symmetrical way as in the morning but with a smaller amplitude.

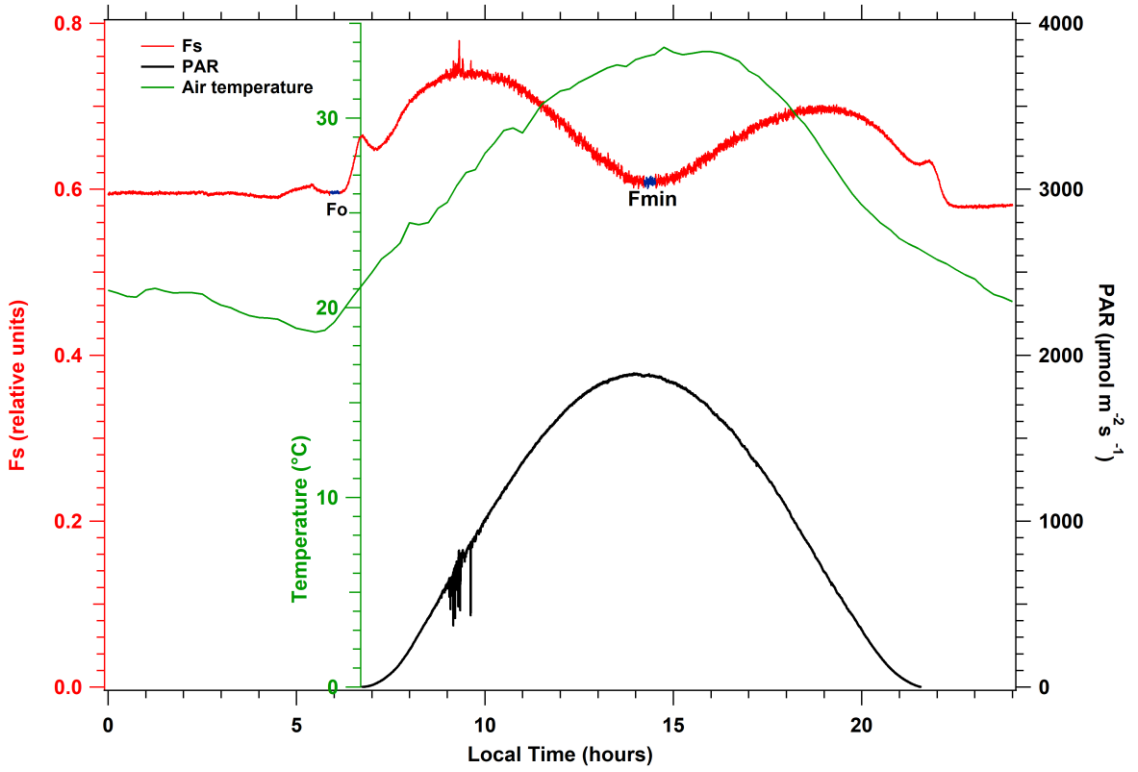

Fig. 4. 6 Diurnal time courses of acquired signals during the control day of July 15. Stationary fluorescence is in red. Points in blue on the Fs curve indicate the time interval for the computation of Fo and Fmin (see M&M). In black is the Photosynthetic Active Radiation (PAR). In green is the air temperature measured by the lysimeter meteorological station. Each parameter is associated with a vertical axis of the same color.

The irrigation was applied regularly every 2 - 3 days until July 13, when the interruption of irrigation started for the stressed plot. After July 15, Fs continuously declined in the absence of irrigation or rain until July 21, when watering started again. During this period, sunny conditions were pervasive, as can be seen in the PAR plot of Fig. 4. 7. This drought period induced a significant fluorescence decrease illustrated by the temporal series in which the value of Fs at noon is, at the end of the drought period (July 24), about 53% of its initial value (control day on July 15). On July 21, 1-hour night irrigation was implemented to prevent damage to the fescue field. The exact irrigation time can be detected by a decrease in Fs (see Fig. 4. 7). It is interesting to note that just a few hours after watering, the daily cycle of July 22 presents a noticeable Fs increase, showing a pattern very similar to those of July 19. After this temporary increase, Fs decreased again at a similar rate until the night of July 24, when more extended irrigation (3 h) took place. The almost instantaneous effect of watering is better illustrated by comparing the cycles from July 24th and 25th, as shown in Fig. 4. 8. The significant increase of Fs after watering is illustrated by Fmin, which changes from ≈ 0.305 to 0.466 under a similar illumination level. However, despite the irrigation, Fmin stays lower than Fo.

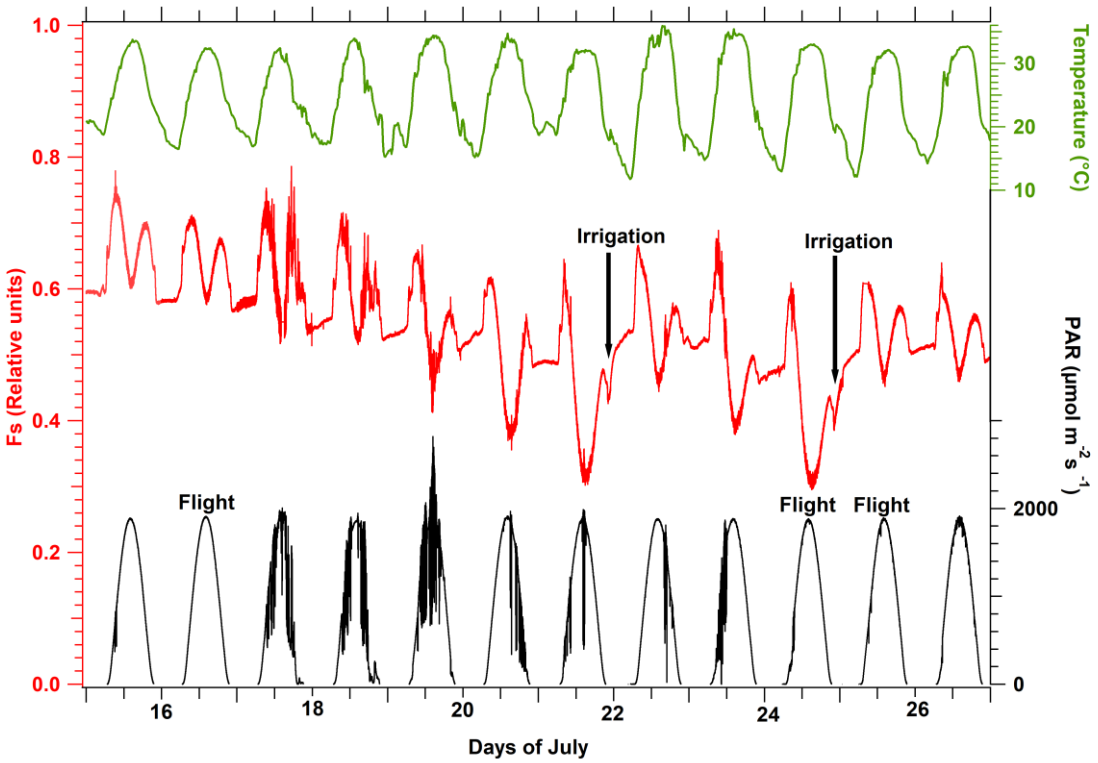

Fig. 4. 7 Effect of water stress on stationary fluorescence and recovery after irrigation. From top to bottom: air temperature measured by the meteorological station (green), stationary fluorescence level Fs (red), and PAR (black). The irrigation and airborne observation events are also indicated. Observe the decrease of Fs and the somewhat reproducible diurnal time course of PAR.

The temporal series of surface temperature recorded by the infrared Apogee thermometers situated in both control and stressed parts of the fescue field showed identical measurements until July 16. After this date, the diurnal temperatures of the stressed plot went up to 10 °C above the control. Notwithstanding, night temperatures were identical (Fig. 4. 9).

As shown in Fig. 4. 10, Fo and Fmin decreased concomitantly with the temperature difference between control and stressed plots measured by the IRTs. One may observe the continuous decrease of both Fo and Fmin until July 21 and the partial recovery after the first irrigation, followed by a second monotonous decrease until the second irrigation on July 24. It is worth noting that the surface temperature difference between control and stressed plots followed precisely the same pattern (Fig. 4. 10). Linear regressions between fluorescence data and surface temperature difference result in a coefficient of determination R^2=0.87 and 0.57 for the prediction of ΔT(Control – Stressed) by Fmin and Fo, respectively.

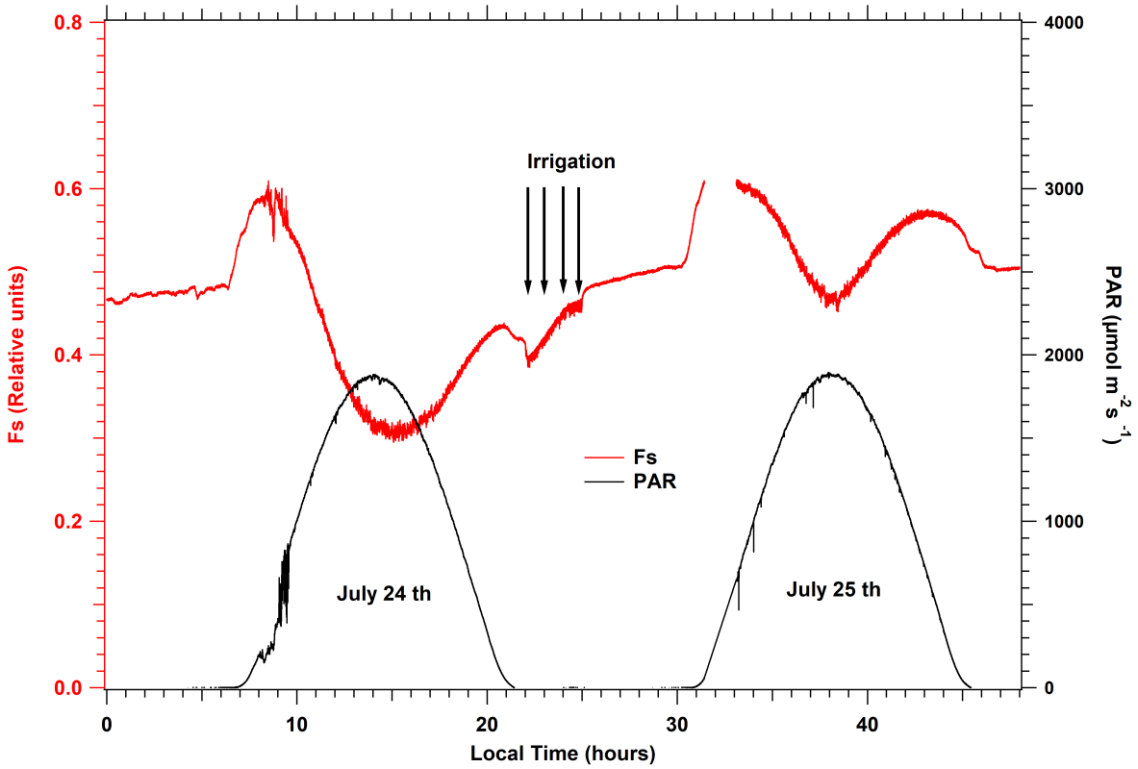

Fig. 4. 8 Effect of three hours of irrigation at the end of the water stress period. The minimum fluorescence level (Fs, red) during the day (Fmin) is strongly enhanced, despite similar PAR conditions (black). Observe also the transient decrease of Fs during watering.

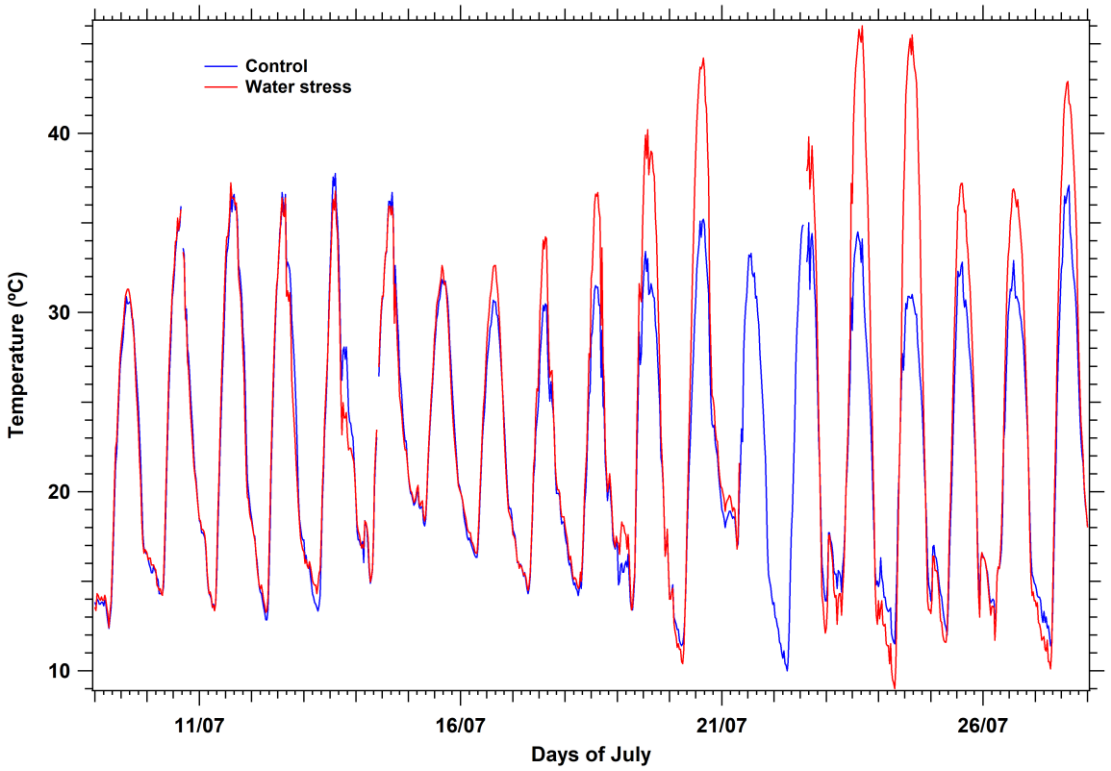

Fig. 4. 9 Temporal series of surface temperatures as measured by the Apogee thermometers. While minimal temperatures are unchanged, maximal temperatures of the stressed plot increased more than ten °C during the stress period from July 16 to July 25.

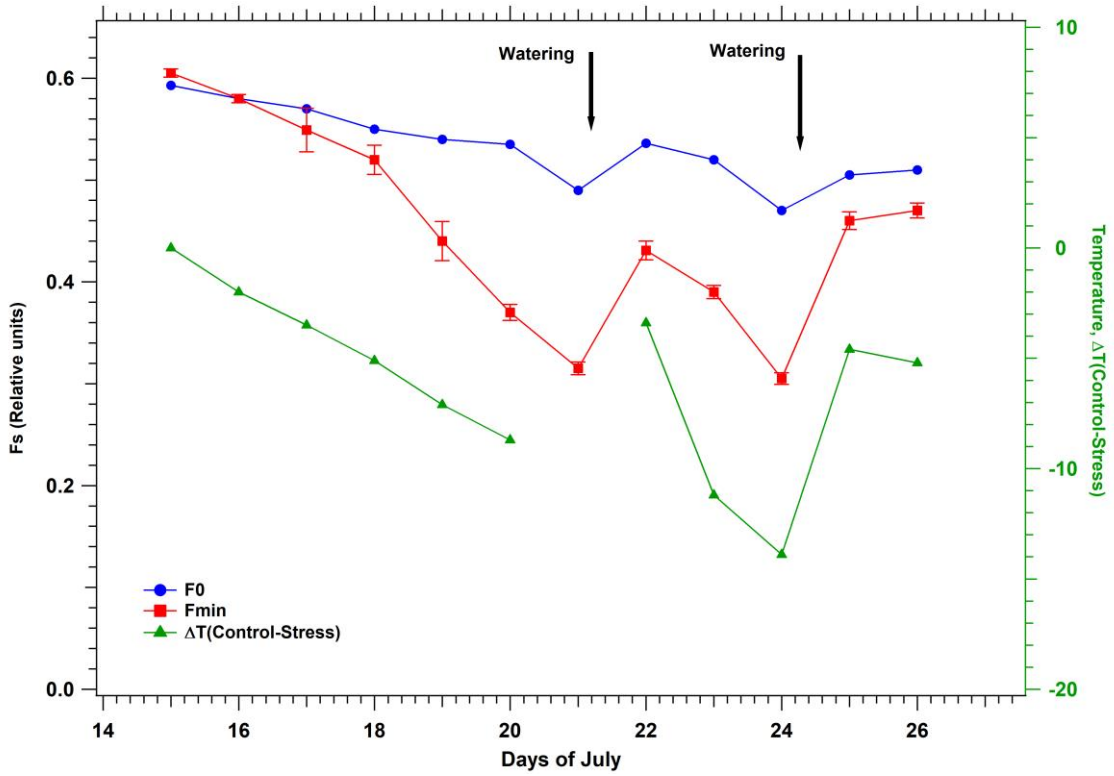

Fig. 4. 10 Temporal series of Fo (blue), Fmin (red), and surface temperature difference between control and stressed plots (green) at noon.

4.1.4.1 Airflex data

Airplane data were collected around or just after solar noon, where fluorescence quenching was supposed to be maximum, as shown by the occurrence of Fmin in the Ledflex data (Fig. 4. **7**). The plane flew alternatively and several times over empty and fescue fields. As in other works (Daumard et al., 2015; Moya et al., 2006), the atmospheric oxygen band depth at 760 nm (D_{760}) was characterized by the ratio of the out-band signal $F_{757.93}$ (at 757.93nm) to the in-band signal $F_{760.8}$ (at 760.8 nm):

$D_{760} = F_{757.93} / F_{760.8}$

D_{760} at the sensor level was in the order of 3.5 over bare soil (without vegetation), and we took this value as the reference to calculate the vegetation fluorescence fluxes (Daumard et al., 2015; Moya et al., 2006). The contribution of the fluorescence to the vegetation radiance led to a decrease of D_{760} from bare soil to vegetated fields. Over the fescue parcel, this decrease was about 0.13 - 0.15, corresponding to a filling-in of the atmospheric O_2 band (not shown).

Table 4. 2 Summary of flight data. Apparent fluorescence yield (F_yield) was computed over the stressed plot where Ledflex was situated.

Date of flight	NDVI Control	NDVI Stress	D760 bare field	D760 Control	D760 Stress	D760 (Stress) - D760 (Control)	F_yield *10-3
July 16th 2017	0.683	0.651	3.455	3.315	3.329	0.014	5.57 ± 0.64
July 24th 2017	0.764	0.575	3.52	3.369	3.414	0.045	4.42 ± 0.47
July 25th 2017	0.790	0.663	3.511	3.382	3.414	0.032	4.46 ± 0.38

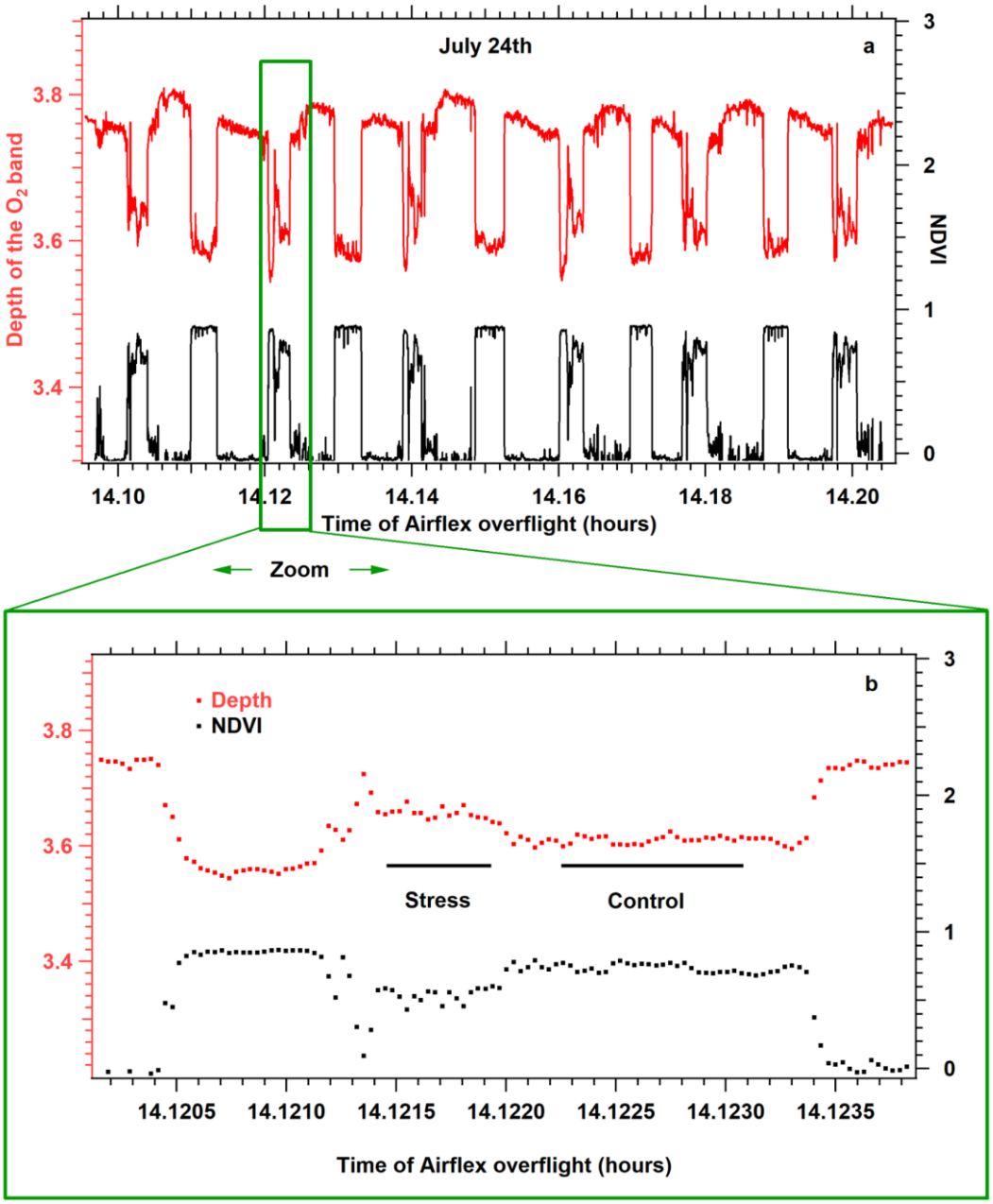

Fig. 4. 11 a Reproducibility of depth measurements (red) and NDVI (black). **b** Enlarged detail of a consecutive measurement of both stress and control plots.

Depth measurements are illustrated in Fig. 4. 11a, representing a 10 min flight over a succession of empty and green fields. Two curves directly calculated from measured radiances are presented: the band depth D_{760} (in red) and the normalized difference vegetation index (NDVI) (Bannari et al., 1995) in black. One may appreciate both curves' good reproducibility despite the pilot's difficulty reproducing exact overflights. In our case, NDVI was defined according to Airflex filters:

$NDVI = (F_{770.64} - F_{672.6}) / (F_{770.64} + F_{672.6})$

Where: $F_{672.6}$ and $F_{770.64}$ represented the radiance in the 672.6 and 770.64 nm channels, respectively.

NDVI was almost zero for empty fields, whereas vegetation parcels (maize) had an NDVI of about 0.9, and fescue fields had a lower NDVI, between 0.6 and 0.8. Fig. 4. 11b shows an example of the identified zones thanks to the images of the context taken for each measuring point (not shown) and from which depths and NDVI were extracted.

In Table 4. 2, the main results of the flight campaign are reported, including NDVI's and depths for fescue under stressed and watered conditions. The reproducibility of the flights can be judged by the depth measured over bare soils, which changed by only 1.85 % during the nine days of the airborne campaign. However, it was difficult to get a constant depth level over bare soils, as illustrated in Fig. 4. 11a for July 24 (stressed case), and this is also true for the other days. Several reasons can be invoked to explain this difficulty, including loops made by the plane to repeat the same trajectory, the wind always present in the afternoon, and the weakness of the navigation tools that equipped this tiny plane. For the control plot, NDVI increased continuously from 0.683 to 0.790 (13.5 %), probably due to growth during the nine days of the airborne measurements. At the same time, stressed plot NDVI initiated the campaign with a lower value (0.651), decreased during the drought period reaching 0.575 (July 24), and seemed to rise upon irrigation (0.663) on July 25 (see Table 4. 2).

The O_2 band depth for the control plot showed a variability (1.98 %) similar to the band depth variation of the bare soils. The depth of the O_2 band increased on July 24 compared to July 16. An increase in the depths is expected if the amount of fluorescence decreases. In all cases, D_{760}(stress) > D_{760}(control) indicates a decrease in the stressed plot fluorescence compared to the control (Table 4. 2).

By chance, both control and stressed plots were measured consecutively with 2 - 3 seconds of delay, ensuring identical measuring conditions that were not guaranteed when comparing different days. For this reason, the differences between depths of stressed minus control plots were emphasized (Table 4. 2).

The fluorescence flux at the ground was computed using the method of Daumard et al., (2010), which combines a linear model of the reflectance spectrum in the vicinity of 760 nm and the shape of the fluorescence emission spectrum measured on the ground as described in the methods (see Appendix) to decouple reflectance and fluorescence emission in the vegetation radiance. The vegetation radiance at three wavelengths (one in-band at 760.8 nm and two out-bands at 757.93 and 770.64 nm) and the same data from bare soil allowed us to calculate the fluorescence flux at 760.8 nm using the equations of Daumard et al., (2010). The Modtran 4 model was used to correct the atmospheric

absorption along the path from the vegetation to the sensor (≈100 m) in the airborne signals (Daumard et al., 2007). Results of fluorescence flux were divided by the actual Photosynthetic Active Radiation at the time of measurements to be converted into apparent fluorescence yields (F_yield) and are shown in the last column of Table 4. 2 and Fig. 4. 12.

F_yield = F / PAR

Apparent fluorescence yields were computed only over the stressed plot as measurements with Ledflex were done at this location.

4.1.5 Discussion

4.1.5.1 Ground measurements:

Until July 2017, Ledflex was mainly used with potted plants to control irrigation conditions better. For this reason, we took advantage of having a field campaign in the hot conditions of mid-summer prevailing in the center of Spain (Barrax). The results in Fig. 4. 6 were similar to those shown in Moya et al., (2019) for control conditions on potted pea plants. It can be interpreted as follows (Flexas et al., 2000): photochemical quenching (qP) primarily determines the actual fluorescence level when the stomata are open. A light intensity increase modifies the equilibrium of the electron transport chain in the direction of a reduction, which is accompanied by an increase in ChF. After approximately 9.30 am, the light intensity increases, and the plant needs another mechanism to cope with the increase of light. A non-radiative (heat) dissipation of the excess absorbed energy mechanism occurs at the LHCII antennae (NPQ) level that also involves the violaxanthin cycle, inducing a decrease of Fs. Reciprocally, Fs increases when the NPQ relaxes after a light intensity decrease in the afternoon, reproducing an Fs cycle similar to the morning but with slightly lower amplitude because some NPQ persists. Therefore, it will need the night to relax.

Fig. 4. 8 (July 24th) presents the situation of the same fescue field after several days of water stress. Again, one may observe the same steps for Fs qualitatively except that the maximum in the morning is reached one hour before, and under a lower light intensity, the minimum at noon is strongly decreased, and Fs always stays lower than Fo.

Other similar results have been found in the literature. For example, in a similar experiment, Rosema et al., (1998) used a target formed by poplar trees grown in pots in a growth cabinet with glass walls inside a greenhouse. An Nd-Yag laser providing pulses of 10 mJ of 10 ns length at 532 nm was used for excitation. The laser illuminated an area of 60 cm in diameter at 12 m. During a five-day water stress experiment, the diurnal cycle showed a dip at noon that developed and became lower than Fo when drought progressed. Indeed, inside a greenhouse with low radiation (< 400 μmol m^{-2} s^{-1}), the water stress signature was evidenced at the canopy level.

Cerovic et al., (1996) used a modified PAM 101 (Walz, Effeltrich, Germany) to monitor Fs at a distance of up to 1 m on an attached leaf. The authors monitored several species submitted to drought, including maize, sugar beet, and kalanchoë. After six days of withholding watering on maize, Fs decreased at noon to a value lower than Fo. Although in this experiment, the light intensity was limited to less than 350 μmol m^{-2} s^{-1}

for technical reasons, these results align with the data presented here.

Flexas et al., (2000) also studied water stress's effect on an attached vine plant leaf during a campaign of 17 days. The authors developed a new fluorometer based on a laser diode for measuring at a distance both Fs and Fm' through the window of an LI-6400 gas analyzer. They also evidenced the M shape of the Fs diurnal cycle with a minimum at solar noon. Under stress conditions, the evening branch was much lower than the morning one, and the minimum was lower than Fo, in agreement with what is shown in Fig. 4. 8 of the present paper.

Bright light conditions prevailed in an outdoors vineyard work presented by López González, (2015). They used a laser-diode μLIDAR, developed at LMD (Laboratoire de Météorologie Dynamique, Paris), which was able to measure Fs from a few meters distance over a plant section containing several leaves. Fieldwork was conducted during the summer, for 45 days, at Barrax, in the South of Spain. Fs was continuously measured from well-watered conditions (stomatal conductance Gs = 0.18 mol H_2O m^{-2} s^{-1}) to stress conditions (Gs = 0.05 mol H_2O m^{-2} s^{-1}). During this long period of good weather, neither the chlorophyll content nor the reflectance was modified. The authors observed a progressive decrease of Fs at noon, which dropped below Fo at the end of the treatment. Notably, 12 h after re-watering, a diurnal cycle similar to control plants was obtained.

Nevertheless, fescue results showed that Fmin is close to or just below the Fo level even under well-watered conditions at noon, whereas in the control pea experiment shown in Moya et al., (2019), Fmin ≈ 1.16 Fo under similar conditions. Up to now, only a few species, including peas, sweet potato, mint, and grapevine, have been tested, and we always found Fmin > Fo under well-watered conditions. At least three reasons can be evoked to explain the low Fmin value observed on the fescue crop: i.) The weekly mowing strongly reduces the height of the crop and tends to reduce the shade within the fescue canopy and increases the illumination, ii.) the high irradiance conditions prevailing near the summer solstice in the South of Spain, and iii.) the high average temperature associated with this continuous high irradiance. The co-occurrence of these three conditions may produce a substantial decrease in Fs, even lower than the level registered at noon.

To conclude, with ground-based measurements in the fescue experiment, it is evident that both Ledflex and temperature difference data measured at noon (with the help of a control plot) demonstrated a high sensitivity to detect reversible water stress. Fig. 4. 10 is a good summary of measurements at ground level. Then, why not use just temperature rather than fluorescence to detect water stress, as temperature measurements are much easier and cheaper to install? The answer could be that we need a reference (control) field to calculate a temperature difference, whereas a single stressed plot is enough for Ledflex fluorescence measurements as we can compare the minimum fluorescence level reached during the day (Fmin) with the Fo level observed overnight.

4.1.5.2 Airborne measurements

Data shown in Fig. 4. 12 and Table 4. 2, evidence the capacity of passive measurements to detect a decrease in apparent fluorescence yield during a water stress period. More precisely, the fluorescence yield for the control observed on July 24 was ≈ 0.79 ± 0.126

of the value measured on July 16 (Table 4. 2). A slightly recovering signal can be observed on July 25 after three hours of watering. Although having only three points, the overall pattern of Fig. 4. 12 can be compared with data changes shown in Fig. 4. 10**.**

On the other hand, the Fmin value measured with Ledflex on July 24 (maximum stress) was 0.53 of the value reached on July 16. Therefore, we should conclude that the Airflex and Ledflex data do not match quantitatively. In order to get an explanation for these differences, let us emphasize some essential differences in the chlorophyll excitation between the Ledflex and Airflex instruments.

Active methods like Ledflex use traditionally narrow band excitation often produced by lasers or LEDs. The energy is usually concentrated in a narrow spectral domain, which helps to isolate fluorescence from excitation spectrally. For instance, Ledflex excites fluorescence at 470 ± 5 nm with a narrow bandwidth of ≈ 20 nm. This wavelength is well absorbed by photosystem II (PS II) and by carotenoids (Louis et al., 2006) and corresponds to a minimum absorption of photosystem I (PS I) (see Fig. 4. 2 of Laisk et al., 2014). This figure allowed us to compare the blue excitation of PS I that coincides with depression around 470 nm with other more efficient wavelengths to excite PS I. Assuming the contribution of PS I excitation to be 35 % at longer wavelengths (Agati et al., 2000; Franck et al., 2002; Pfündel, 1998), the lower absorption of 470 nm leads to a lower excitation of PS I. We concluded with an overall contribution of 19 % of PS I for Ledflex fluorescence measurements.

Airflex uses a passive method to detect sun-induced chlorophyll fluorescence in the O_2-A absorption band at 760 nm in a narrow band of ≈ 1nm, excited by the whole solar spectrum. Considering the several works already cited concerning the participation of PS I in the far-red fluorescence emission, we guess it is also the case at 760 nm (Franck et al., 2002). It is worth noting that F760 also benefits from a unique excitation by wavelengths between 690 nm and 750 nm that is predominantly absorbed by PS I, compared to PS II. Laisk et al., (2014) stated that the excitation spectra of PS I electron transport are strongly favored at wavelengths greater than 690 nm compared to PS II. This work estimates an extra excitation of ≈ 15% in favor of PS I. This extra excitation does not exist in active methods, especially in the case of Ledflex. In other words, PS I emission can account for approximately 35x1.15 ≈ 40% of the emission at 760 nm. On the control day (July 16), we have Fs = Fo at noon (see Fig. 4. **7**). We then assume a constant PS I emission of ≈ 40% of Fs superimposed to the PS II emission.

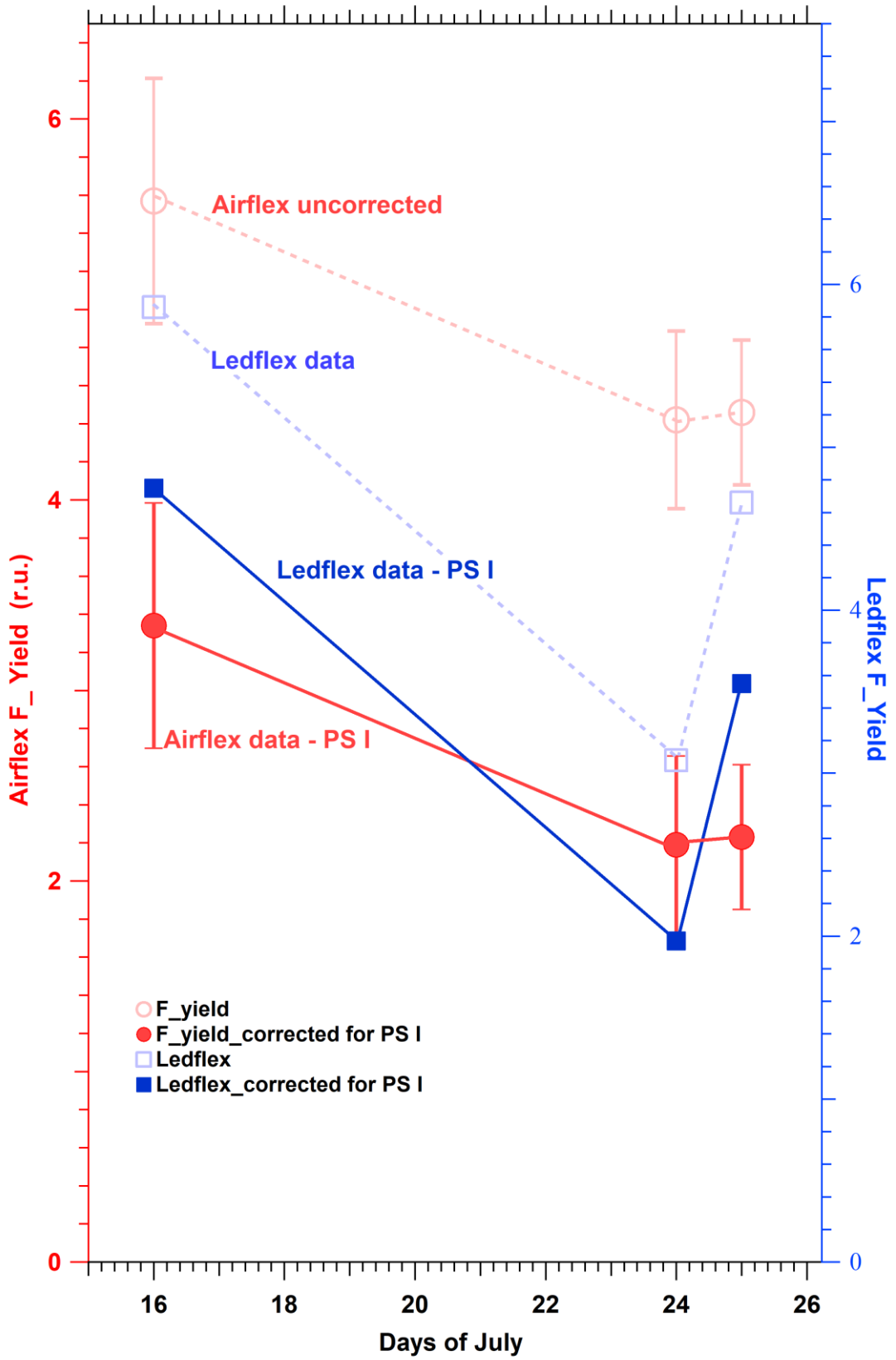

Fig. 4. 12 Red empty circles, dashed lines, and left axis correspond to the total fluorescence yield measured by Airflex. Red solid circles: after subtracting PS I fluorescence contribution (≈ 40%). Right axis empty blue squares correspond to Ledflex

fluorescence data. Solid blue squares: Fluorescence yield after subtracting PS I fluorescence emission (≈ 19%).

After nine days of withholding watering, Airflex data shows a decrease in the apparent fluorescence yield at noon to 0.79 compared to the control day on July 16 (see Table 4. 2). This decrease can be due to a decrease in PS II fluorescence or PS I fluorescence, or both. It has been shown (Dau, 1994; Trissl, 1997) that open or closed PS I reaction centers are equally efficient in trapping the excitation energy from the antennae; hence, there is no variable PS I fluorescence. As a result, we tentatively attribute the fluorescence decrease of 0.79 to the quenching of PS II, and we supposed that the PS I contribution remained unchanged during the nine days of water stress.

As both instruments were differently affected by the contribution of PS I fluorescence emission that we did not measure, the comparison becomes delicate. Therefore, we presented in Fig. 4. 12 an attempt to compare both results after removing the supposed PS I contribution that accounted, as described, for ≈ 40 % of Fmin for Airflex and ≈ 19 % of Fmin for Ledflex. Although these values are speculative, considering the error bars, they seem realistic and compatible with a decrease of ≈ 53 %, as shown by Ledflex active data.

4.1.6 Conclusions

Although active and passive chlorophyll fluorescence measurements are qualitatively in agreement, the accuracy and sensitivity of the active method are much better. It also provides additional information as it can detect fluorescence at night and under low light. Under solar excitation, passive measurements using the filling-in of the atmospheric oxygen band at 760 nm do not seem to be an appropriate wavelength to detect water stress due to the significant contribution of the PS I fluorescence, which is always superimposed with PS II emission, and rather under-documented. A more effective wavelength should be to use the O_2-B band at 687 nm, where the contribution of PS I is marginal. However, due to several factors, fluorescence detection in the O_2-B band is considered more complex than in the O_2-A band. One of these factors is the non-linear shape of the reflectance spectrum over the O_2-B band, which implies using not three but at least four wavelengths to correctly describe the curvature of the reflectance spectrum with multi-channels photoradiometers like Airflex (Daumard et al., 2012).

However, alternative retrieval methods, such as the spectral fitting method (SFM) (Cogliati et al., 2019), take advantage of the comprehensive information contained in high spectral resolution radiance spectra to retrieve both the red and far-red emissions of chlorophyll fluorescence. Such a method will be implemented in the data processing chain of the future FLuorescence EXplorer (FLEX) space mission of the European Space Agency (ESA) to provide the full fluorescence spectrum, including the red band (Drusch et al., 2017). Our results, considered from the perspective of future fluorescence space missions, open new possibilities for water stress detection from space.

Acknowledgments: The core of this work was supported by the Bill & Melinda Gates Foundation [OPP1070785]. Under the grant conditions of the Foundation, a Creative Commons Attribution 4.0 Generic License has already been assigned to the Author's Accepted Manuscript version that might arise from this submission. In addition, this research was undertaken and partially funded by the Bill and Melinda Gates Foundation investment 'SweetGAINS: Genetic Advances and Innovative Seed Systems for Sweet Potato' (ID PP1213329/INV-002971) and the CGIAR Plant Health Initiative, supported by CGIAR Trust Fund contributors (https://www.cgiar.org/funders/). Finally, the authors also would like to acknowledge I.T.A.P (Provincial Agronomic Technical Institute) for allowing us to develop the experiment at the "Las Tiesas" experimental site (Barrax, Albacete, Spain).

Data Availability Statement: The data supporting this study's findings are available in the Dataverse CGIAR repository at Active in situ and passive airborne fluorescence measurements for water stress detection on a fescue field. https://doi.org/10.21223/7QY6KU

4.2 APPENDIX

4.2.1 Fluorescence retrieval method

Here, we briefly describe the retrieval method used to recover solar-induced fluorescence from airborne radiance measurements obtained with the Airflex sensor. More detailed information can be obtained from Daumard et al., (2010, 2012, 2015).

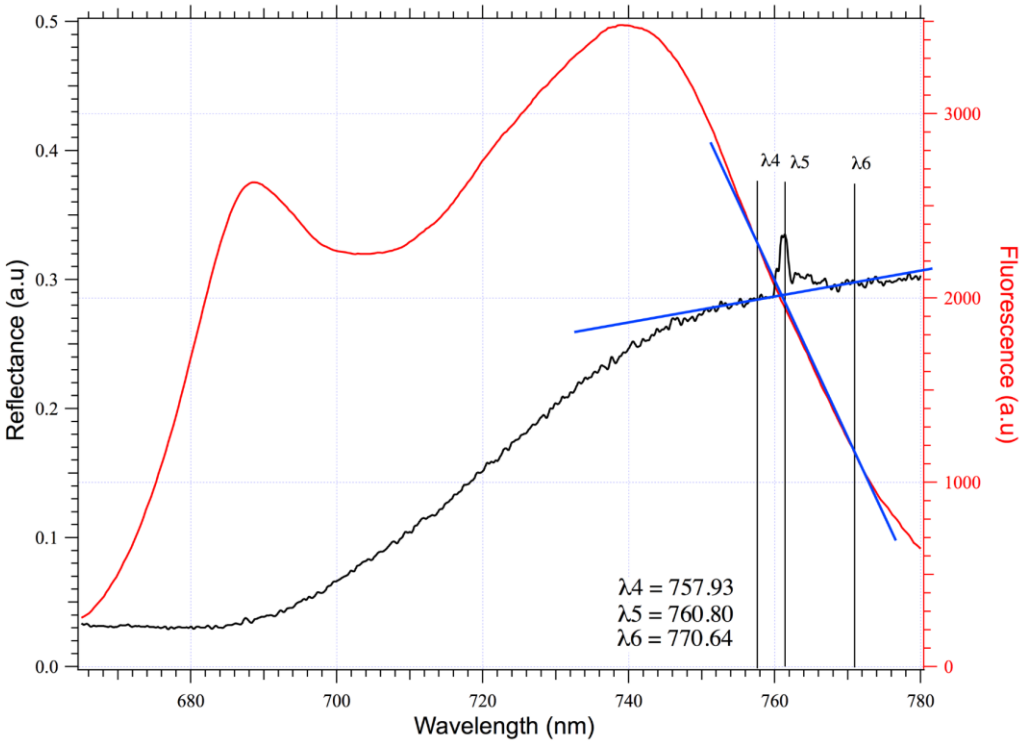

Fig. 4. 13 Reflectance spectrum (black) and fluorescence emission spectrum (red) of a well-watered fescue field. Blue lines indicate the linear models of reflectance and fluorescence emission used for fluorescence retrieval in the O_2-A absorption band. Chlorophyll concentration ≈ 20 SPAD units.

At the ground level, the vegetation radiance in the vicinity of the O_2 absorption band can be described as:

$$L(0,\lambda) = \rho(\lambda)\, I(0,\lambda) + F(0,\lambda),\ \lambda \in \{\lambda 4, \lambda 5, \lambda 6\} \qquad (4.\ 1)$$

where $\rho(\lambda)$ is the reflectance factor, defined as the ratio of the energy flux reflected by the target to the energy flux reflected by a white Lambertian reference board in the same configuration, $I(0,\lambda)$ is the solar irradiance on the target expressed in radiance units (i.e., the solar irradiance divided by π) and $F(0,\lambda)$ is the fluorescence radiance generated at the surface by the $I(0,\lambda)$ excitation. In equation (1), $L(0,\lambda)$, $\rho(\lambda)$, $I(0,\lambda)$ and $F(0,\lambda)$ represent their respective spectral values integrated over the spectral bandwidth of the Airflex filters and λ is the peak wavelength of the corresponding filter (see Table 4. 1 and Fig. 4. 13).

It is worth noting that because $\rho(\lambda)$, and $F(0,\lambda)$ are both unknown, equation (4. 1)

cannot be solved, in a general case, whatever the number of wavelengths considered. As a consequence, additional information is necessary to retrieve fluorescence flux. To solve equation (4. 1), we employed the method described by Daumard et al., (2010) and further applied it in Fournier et al., (2012) and Daumard et al., (2012). In short, the method uses complementary information obtained on the ground to model $\rho(\lambda)$, $F(0,\lambda)$ and $I(0,\lambda)$ spectra.

The solar excitation model. The solar spectrum $I(0,\lambda)$ was measured at the ground level at the time of the flight using a white PVC board calibrated against the Spectralon board reference, as stated in the methods section. Here we assumed $I(0,\lambda)$ to be constant during the flight period.

The reflectance model. Under sunlight excitation, only apparent reflectance $r(\lambda)$ can be measured, which may contain some fluorescence contribution.

$$r(\lambda) = L(0,\lambda) / I(0,\lambda) = \rho(\lambda) + F(0,\lambda) / I(0,\lambda)$$

The Chl fluorescence contribution to the radiance of the vegetation is known to be < 2% of the continuum radiance at 760 nm (Moya et al., 2004). We decided to neglect such a small contribution. This leads us to choose a linear model for $\rho(\lambda)$ in the vicinity of the O_2-A band as in similar studies (Daumard et al., 2010, 2012; Fournier et al., 2012).

Fig. 4. 13 shows apparent reflectance at the ground measured as stated in the methods section. Although reflectance spectra are relatively smooth, one may observe a prominent peak at wavelength $\lambda 5$**.** This peak is produced by the fluorescence contribution to the vegetation radiance and showed a maximum effect at the bottom of the O_2 absorption bands. This peak is not observed when measuring the reflectance of empty fields (not shown). As suggested in Fig. 4. 13, we took a linear model.

$$\rho(\lambda) = a\,\lambda + b,\ \lambda \in \{\lambda 4, \lambda 5, \lambda 6\} \qquad (4.\ 2)$$

Where a and b are the coefficients of the reflectance model.

Fig. 4. 13 also shows the emission spectrum of the fescue taken before the water stress period. One may observe that the slope of the fluorescence spectrum is remarkably constant between $\lambda 4$ and $\lambda 6$. This allows us to model the $F(0,\lambda)$ by a linear function that we characterize by two constant parameters:

$A(\lambda 4) = F(0, \lambda 4) / F(0, \lambda 5) = 1.15$ and
$A(\lambda 6) = F(0, \lambda 6) / F(0, \lambda 5) = 0.6$.

By definition $A(\lambda 5) = 1$.

The system (1), which corresponds to ground parameters, can be rewritten as follows:

$$L(0, \lambda 4) = \rho(\lambda 4)\, I(0, \lambda 4) + F(0, \lambda 5)\, A(\lambda 4), \qquad (4.\ 3)$$
$$L(0, \lambda 5) = \rho(\lambda 5)\, I(0, \lambda 5) + F(0, \lambda 5),$$

$L(0, \lambda 6) = \rho(\lambda 6)\, I(0, \lambda 6) + F(0, \lambda 5)\, A(\lambda 6)$,
$\rho(\lambda 4) = a\, \lambda 4 + b$,
$\rho(\lambda 5) = a\, \lambda 5 + b$,
$\rho(\lambda 6) = a\, \lambda 6 + b$

As measurements were taken at the airplane altitude, we should introduce some corrections for the contribution of the air mass between the sensor and the ground. The target radiance at altitude h ($L(h,\lambda)$) can be expressed in terms of ground irradiance $I(0,\lambda)$ and fluorescence $F(0, \lambda 5)$, taking into account absorption and scattering of reflected solar radiation and fluorescence by the atmospheric column between ground and sensor.

The Modtran4 model was used to calculate the mean attenuation $Ts(\lambda i)$ over the filter spectral bandwidth of the solar radiance flux reflected by the target. As the filter bandwidth is narrow (about 1 nm, see Table 4. 1), the solar radiance at the airplane level can be formulated as:

$$Is(h,\lambda i) = Ts(h,\lambda i)\, I(0,\lambda i),\ \lambda i \in \{\lambda 4, \lambda 5, \lambda 6\} \qquad (4.\ 4)$$

It can be observed that only inband radiance was significantly modified. Indeed higher altitudes affected all the channels, but they are out of the scope of the present work. Calculating the attenuation undergone by the fluorescence emission generated from the surface $F(0,\lambda i)$ in the path from the ground to the sensor is also necessary. The transmission of the air column for the fluorescence $Tf(h,\lambda)$ is calculated using the Modtran4 model in the transmission mode between the ground level and the airplane altitudes:

$$F(h,\lambda i) = Ts(h,\lambda i)\, F(0,\lambda i),\quad \lambda i \in \{\lambda 4, \lambda 5, \lambda 6\} \qquad (4.\ 5)$$

Table 4. 3 Ai coefficients, transmission factors of solar radiation, and fluorescence along the path from ground to sensor were calculated according to (Daumard et al., 2015).

Wavelength channel	**Airflex filter peak wavelength (nm)**	**Form factors of the fluorescence emission spectrum (A(λ))**	**Transmittance of solar radiation (Ts) calculated with Modtran4**	**Transmittance of fluorescence (Tf) calculated with Modtran4**
λ4	757.93	1.15	0.99	0.989
λ5	760.80	1	0.983	0.882
λ6	770.64	0.6	1	0.989

The attenuation of fluorescence flux induced by atmospheric corrections was 12 % (Table 4. 3). Finally, by introducing equations (4. 4) and (4. 5) into the system (4. 3), we obtain the following system of linear equations (4. 6) relating solar irradiance and Chl fluorescence at the ground to the measured onboard radiances at the airplane altitude:

$$L(h, \lambda 4) = \rho(\lambda 4)\, I(0, \lambda 4)\, Ts(h, \lambda 4) + F(0, \lambda 5)\, A(\lambda 4)\, Tf(h, \lambda 4) \qquad (4.\ 6)$$

$$L(h, \lambda 5) = \rho(\lambda 5)\, I(0, \lambda 5)\, Ts(h, \lambda 5) + F(0, \lambda 5)\, Tf(h, \lambda 5)$$

$$L(h, \lambda 6) = \rho(\lambda 6)\, I(0, \lambda 6)\, Ts(h, \lambda 6) + F(0, \lambda 5)\, A(\lambda 6)\, Tf(h, \lambda 6)$$

$$\rho(\lambda 4) = a\, \lambda 4 + b$$

$$\rho(\lambda 5) = a\, \lambda 5 + b$$

$$\rho(\lambda 6) = a\, \lambda 6 + b$$

By eliminating $\rho(\lambda i)$ $\lambda i \in \{\lambda 4, \lambda 5, \lambda 6\}$, a, and b coefficients, the system of equations (4. 6) has a unique solution for $F(0,\lambda 5)$. The solution can be easily found using Mathematica™ software:

$$F(0,\lambda 5) = N(\lambda 5) / D(\lambda 5)$$

Where:

$$N(\lambda 5) = I(0,\lambda 5)\, I(0,\lambda 6)\, L(h,\lambda 4)(\lambda 5 - \lambda 6) Ts(h,\lambda 5)\, Ts(h,\lambda 6) +$$
$$I(0,\lambda 4) Ts(h,\lambda 4) \left[I(0,\lambda 5)\, L(h, \lambda 6)\, (\lambda 4 - \lambda 5) Ts(h,\lambda 5) + I(0,\lambda 6) L(h,\lambda 5)\, (\lambda 6 - \lambda 4) Ts(h,\lambda 6) \right]$$

And:

$$D(\lambda 5) = A(\lambda 4)\, I(0,\lambda 5)\, I(0,\lambda 6)(\lambda 5 - \lambda 6)\, Ts(h,\lambda 5)\, Ts(h,\lambda 6)\, Tf(h,\lambda 4) +$$
$$I(0,\lambda 4)\, Ts(0,\lambda 4) \left[I(0,\lambda 6) \left[(\lambda 6 - \lambda 4)\, Ts(h,\lambda 6)\, Tf(h,\lambda 5) + \right.\right.$$
$$\left.\left. A(\lambda 6)\, I(0,\lambda 5)\, (\lambda 4 - \lambda 5) Ts(h,\lambda 5) Tf(h,\lambda 6) \right] \right].$$

CHAPTER 5

5.1 General Conclusions and Perspectives

This thesis work presents non-commercial laboratory-designed instruments dedicated to remote sensing measurements of chlorophyll fluorescence (ChlF). The diurnal changes of ChlF yields gotten from LIF and SIF methods at canopy level and under outdoor conditions were compared and used to detect water stress in vegetation. These research were presented in three papers recently published in Photosynthesis Research journal (Loayza et al., 2022; Moya et al., 2019, 2023). The main contributions of this work are described following:

5.1.1 Chlorophyll florescence yields at canopy level

5.1.1.1 Active measurements

We presented Ledflex, a new micro-LIDAR dedicated to measure directly the chlorophyll fluorescence yield of vegetation under natural conditions. It is able to measure continuously and at canopy level the diurnal changes of stationary chlorophyll fluorescence (Fs) emission of vegetation up to distances of 8 meters with a footprint of 100 cm in diameter.

Ledflex was tested under different weather conditions and monitored crops planted both in pots (menthe, pea, sweet potato) and in open field (potato and fescue). In all cases, the Fs diurnal cycles showed under full sunlight a M shape pattern, with a minimum at noon and two maxima about at 9 and 17 hours. Similar results were presented by Cerovic et al., (1996) on maize crop at leaf level and Rosema et al., (1998) on poplar trees under indoor conditions. However, the M shape is not symmetrical since the second maximum is lower than the first one. We suggested that part of NPQ formed before noon does not fully reverse during the afternoon and needs the entire night to dissipate (see Fig. 5. 1 and Fig. 3. 7 a).

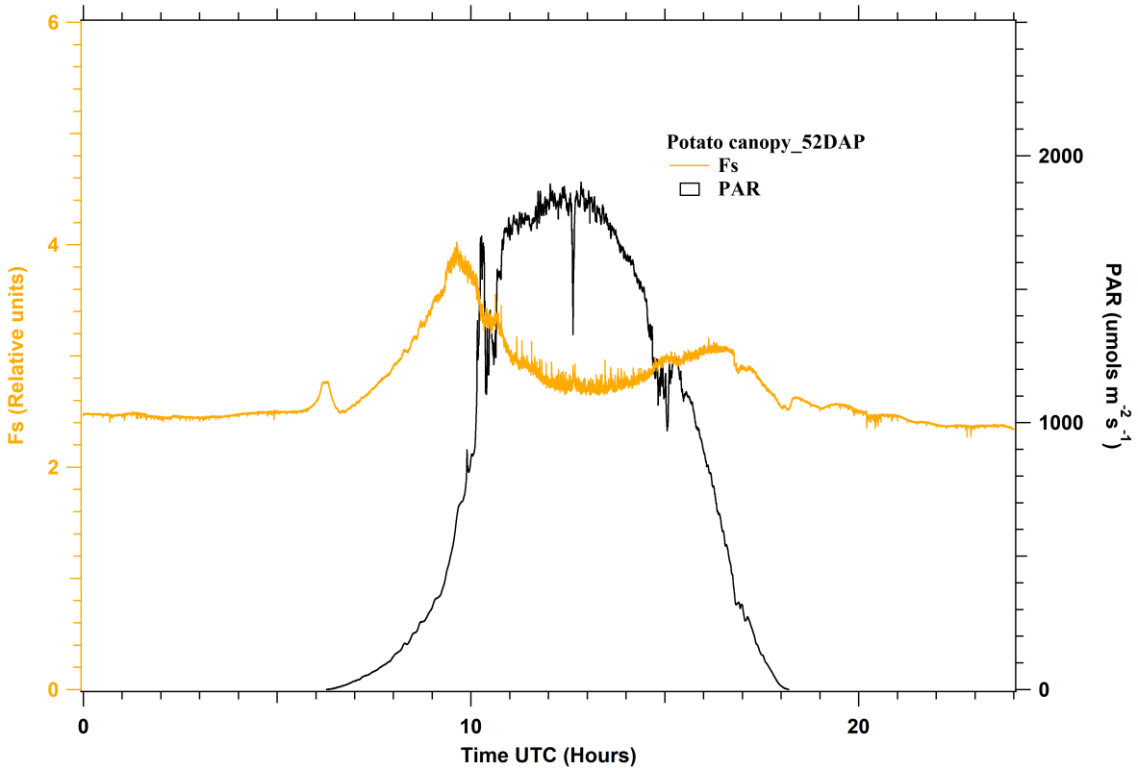

Fig. 5. 1 In orange a diurnal cycle of Fs from potato experiment conducted in Lima – Peru.

Perspectives of Ledflex

To measure at long distances. Ledflex design is flexible and adaptable. For instance, the Ledflex working distance can increase to tens of meters using light sources of higher power. A laboratory test allowed to simulate the Ledflex performance using a laser FDSS 532-1000 Q-switched, single pulse, centered at 532 nm, and 1000 uJ power according to the manufacturer. Using - mainly - a neutral filter of 10% transmittance to avoid saturating the Ledflex's fluorescence detection system, 12 volts of signal were obtained at 4 meters away. According Moya et al., (2019), a Fs signal of 1 volt in amplitude at about 3.5 meters away was sufficient to obtain a good SNR (>100). Therefore, removing the neutral filter we could get 1.2 volts at 40 meters away, a voltage similar to the Fs amplitude recovered by Ledflex in present.

To study the variable fluorescence. Because the ChlF yield varies inversely with the fraction of open reaction centers, it provides a useful tool for investigation of photosynthetic processes. However, the PS I fluorescence seems to be independent of the state of its reaction center and the variable fluorescence arise from PS II only (Dau, 1994) The Ledflex's blue LEDs source (centered at 470 nm +/- 5 nm) excites the fluorescence emission of photosystems I (PS I) and II (PS II). Nevertheless, according to Laisk et al. (2014), these wavelengths are strongly absorbed by PS II and carotenoids and with minimal absorption of PS I. Therefore, to study only the variable ChlF we can keep the blue excitation source but should restrict the spectral range of Fs measurements to red

fluorescence, from about 600 to 700 nm, reducing drastically the PS I's contribution to the Ledflex's Fs measures.

Fs diurnal cycles to detect water stress

During a diurnal cycle, a simple comparison between Fs values measured at noon (Fmin) and pre-dawn (Fo) allow to infer the water status of the vegetation: if Fmin > Fo it is well watered, and if Fmin < Fo it is a hydric deficit. This methodology was undergone to controlled water stress experiments. For pea, menthe, and sweet potato crops, the stomatal conductance measurements allowed defining the onset of water stress. While in the case of fescue (*Festuca arundinacea Schreb.*), a crop with very thin leaves, the difference in surface temperature between the plot with water deficit and the plot with normal irrigation (control) was used to know the onset of water stress. In all these experiments, the methodology proposed was successfully validated. It has shown to be an efficient remote index to detect water stress in vegetation.
The Ledflex performance during these experiments showed that it is a robust fluorometer for outdoor applications.

5.1.1.2 Passive measurements

A new version of Spectroflex, previously presented by Fournier et al., (2012), was implemented in this project. It is an instrument based on a small spectrometer with an FWHM of 0.63 nm, and it uses the Daumard et al., (2010) model to recover ChlF. This model is an approach based on the Fraunhofer Line Depth (FLD) principle in atmospheric oxygen (O_2) bands at A and B, with three channels to recover ChlF in A band and four channels for B band. Although the chosen spectrometer has a low spectral resolution and the Daumard et al., (2010) model uses few bands to recover fluorescence, the SIF diurnal cycles presented similar SNR in both O_2 bands. This new Spectroflex version measured over 26 days diurnal cycles of solar-induced fluorescence fluxes in the O_2-A and O_2-B from potato crops canopy. During this measurement campaign, it showed to be a robust instrument for SIF measurements in outdoor conditions.

On sunny days, the diurnal cycles of fluorescence fluxes in the O_2-A and O_2-B bands showed qualitative and quantitative differences. The fluorescence fluxes recovered from the O_2-A and O_2-B bands, although they presented similar patterns were not identical. This fact was interpreted as a significant contribution of the PS I fluorescence to the overall fluorescence recovered in the O_2-A band. The O_2-B band depth is less than that O_2-A band. However, it is compensated by a less vegetation radiance in O_2-B compared to O_2-A. Thus, the intensity of the fluorescence signal recovered from O_2-B is sufficient to measure it with an acceptable SNR, as shown by the O_2-B fluorescence fluxes measured from potato canopy. In short, SIF measurements in the O_2-B band are the more appropriate to study PS II fluorescence.

5.1.2 Comparing diurnal cycles of ChlF yields measured with active and passive canopy-scale methods

In this work we presented for the first time simultaneous measurements of diurnal cycles of LIF and SIF on a same potato crop canopy under full daylight conditions. The LIF measurements were conducted by Ledflex, whilst SIF measurements were done by Spectroflex2. An apparent fluorescence yield for SIF measurements was proposed taking advantage of the LIF and SIF measurements over the same spot on potato canopy. It combined the SIF measurements in A and B O_2 bands normalized by vegetation radiance. However, although the sum of squares of residuals (SSR) showed that such approach showed the best agreement with fluorescence yield deduced from active measurements, we have to keep in mind that:

1) Ledflex spans a wide spectral range of Fs emission, whilst Spectroflex2 recover fluorescence only at two narrow spectral bands.

2) Ledflex uses a fix geometry both to excite and to measure ChlF. It is an advantage with regard to SIF methods since natural light changes in direction and intensity throughout the day.

3) The SIF measurements are excited by the whole sun emission spectrum. It adds, among other things, an extra excitation of PS I fluorescence to Fs for wavelengths greater than 690 nm (Laisk et al., 2014).

4) Additionally, SIF may show variations linked to the angular distribution of incident light, depending on canopy architecture (Fournier et al., 2012; Goulas et al., 2017).

SIF remote sensing is commonly focus on the A band of O_2. However, in my experience the fluorescence in the O_2-B band was recovered with a similar SNR. These results seem to contradict the demands of current SIF methods suggesting very high spectral resolution spectrometers and models with hyperspectral radiance data - such as the Spectral fitting method (SFM) - for ChlF recovery. Lowering costs and the complexity of evaluations are a challenge in research. An experiment that considers replacing the Spectroflex2 spectrometer by other with a very high FMHM, would allow us to apply both the SFM and the Daumard et al., (2010) model to recover SIF. These evaluations, accompanied by Ledflex measurements on the same target, would allow evaluating the benefit-cost ratio of considering SIF retrieval methods that require hyperspectral radiance data versus multispectral models.

5.1.3 Airborne passive measurement to water stress detection

A second passive fluorescence instrument was used in this work. Airflex, presented by Moya et al., (2006), is a 6-channel photo-radiometer that measures the filling-in of the A band of O_2. It was modified to fit inside an ultralight plane. To get information about the context, a video camera was installed to record an image for each Airflex´s radiance measurement. This new Airflex version flown at an altitude of about 100 m over a fescue meadowland experiment in Barrax (Spain) composed by well-watered and water stress treatments. The Airflex´s data from fescue crop were identified through the aerial images.

LIF in-situ vs SIF airborne measurements

Ledflex was installed in the water stress treatment. The airborne SIF measurements were conducted only at noon on water stress treatment in three hydric status of fescue crop: control, water stress and recovery (after watering). The surface temperature difference between well-watered and water stress treatments - ΔT(Control – Stressed) - defined the onset of hydric deficit in fescue crop. The LIF measurements were more accurate and sensitive to detect the water status in the fescue crop (see Fig. 4. 10). Qualitatively, the ASFY recovered by Airflex followed the variations of Fs measured by Ledflex at noon (Fmin). However, quantitatively the SIF and LIF variations were different.

To understand these quantitative differences, it was argued:

1) Ledflex, measured Fmin values close to Fo due to water stress and high air temperature throughout experiment. Several works have pointed out contributions of 35% from PS I at Fo to the far-red fluorescence. Thus, it could mean an important contribution of PS I fluorescence at O_2-A, which limits the sensitivity of ChlF to water stress in this band.
2) We highlight the differences in fluorescence excitation between the LIF (470 nm +/- 5 nm) and SIF (whole wavelength solar range) measurements. Additionally, wavelengths greater than 690 nm are strongly absorbed by PS I compared to PS II. It favors the PS I fluorescence emission on far red (O_2-A).

An easier comparison between SIF and LIF measurements should only consider the red fluorescence (mainly PS II fluorescence).

Perspectives to detect water stress using SIF measurements

At field level, to detect water stress in vegetation, Ledflex compares Fmin with Fo. Since in passive methods it is not possible to measure Fo, a hypothesis to detect the onset of water stress could be to compare Fmin with the first maximum of Fs (Fmax), see Fig. 4. 6.The purpose is to highlight the effects of water stress exhibited by the value reached by Fmin due to the NPQ.

In Fig. 5. 2, we show an example using the data from Chap. 4 on the water stress experiment conducted in Barrax (Spain). We observe a close relationship between Fmin/Fmax and the surface temperature ΔT(Control – Stressed) (R^2 = 0.94).

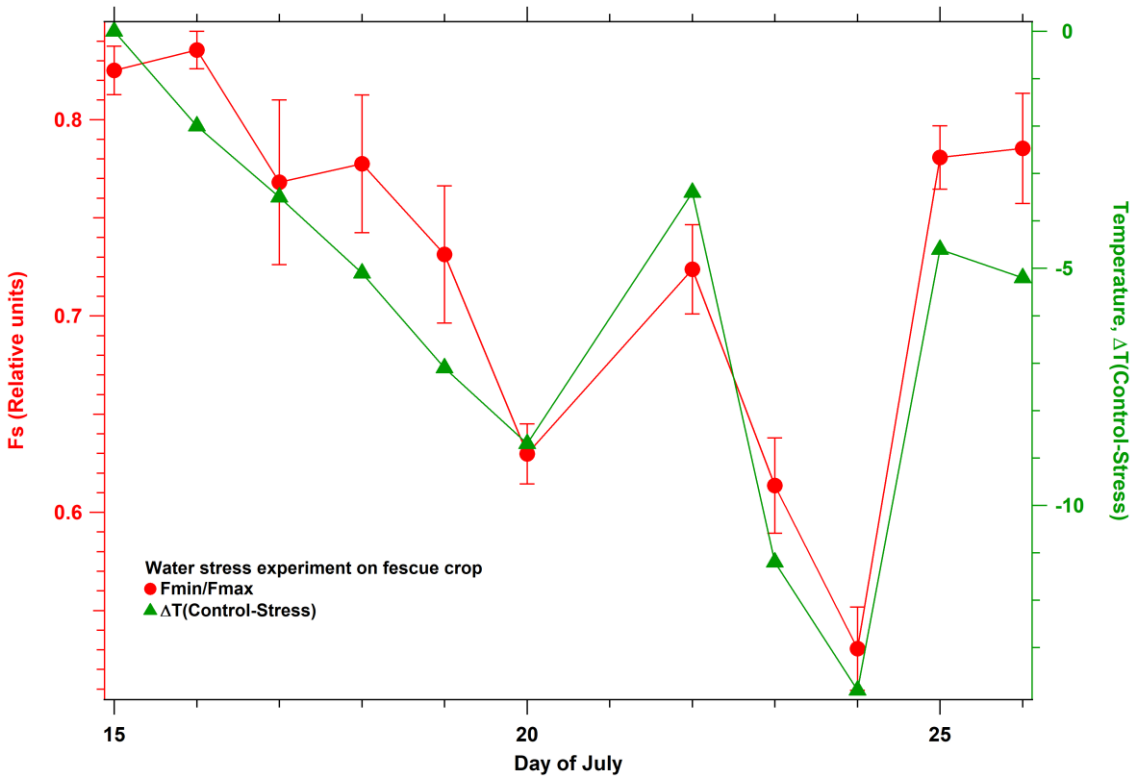

Fig. 5. 2 Ledflex data (Fim/Fmax, red) and surface temperature difference (green) corresponding to fescue crops subjected to different water stress status

Spectroflex2 recovers SIF's diurnal cycles over the same target using a fix geometry. However, to upscale from ground to airborne level, an on-board fluorescence instrument is needed. Airflex, an interference-filters-based airborne sensor allows performing passive fluorescence measurements at different heights. However, due to its weight it requires at least an ultralight to be transported.

A more economical option to perform airborne SIF measurements would be to use a small spectrometer, such as the one used by Spectroflex2. To this regard, Wang et al., (2021) presented a system based in a sub-nanometer spectrometer to acquire SIF measurement from a UAV-based payload. This work gives us important insights on this topic. Thanks to the experience with Spectroflex2's implementation, I would suggest:

- To include SIF measurements at O_2-B band.
- As long as we know the integration time of radiance measurements, the dark measurement could be performed at ground level.
- To acquire RGB images of the context. A global image of the fluorescence over the crop field would be obtained by tiling the SIF measurements and images.

Finally, this thesis presents a sum of efforts to measure, recover and interpret chlorophyll fluorescence yields of different crops at canopy level and outdoor conditions. A micro-LIDAR fluorescence was used as reference to interpret chlorophyll fluorescence fluxes recovered from both field-level and airborne passive instruments. The results of this work add to the efforts of the remote sensing of solar-induced chlorophyll fluorescence community, aligned to the FLuorescence EXplorer (FLEX) mission of European Space

Agency (ESA) that will provide global maps of the fluorescence of vegetation from space and that will be launched in 2025.

BIBLIOGRAPHY

Agati, G., Cerovic, Z. G., & Moya, I. (2000). The Effect of Decreasing Temperature up to Chilling Values on the in vivo F685/F735 Chlorophyll Fluorescence Ratio in Phaseolus vulgaris and Pisum sativum: The Role of the Photosystem I Contribution to the 735 nm Fluorescence Band ¶. *Photochemistry and Photobiology*, *72*(1), 75–84. https://doi.org/10.1562/0031-8655(2000)0720075TEODTU2.0.CO2

Allen, J. F. (1992). How does protein phosphorylation regulate photosynthesis? *Trends in Biochemical Sciences*, *17*(1), 12–17. https://doi.org/10.1016/0968-0004(92)90418-9

Ananyev, G., Kolber, Z. S., Klimov, D., Falkowski, P. G., Berry, J. A., Rascher, U., Martin, R., & Osmond, B. (2005). Remote sensing of heterogeneity in photosynthetic efficiency, electron transport and dissipation of excess light in Populus deltoides stands under ambient and elevated CO2 concentrations, and in a tropical forest canopy, using a new laser-induced fluorescence transient device. *Global Change Biology*, *11*(8), 1195–1206. https://doi.org/10.1111/j.1365-2486.2005.00988.x

Andersson, M., Edner, H., Johansson, J., Ragnarson, P., Svanberg, S., & Wallinder, E. (1994). Remote monitoring of vegetation by spectral measurements and multi-colour fluorescence imaging. *ISPRS Symposium*, 835–842.

Baker, N. R. (2008). Chlorophyll fluorescence: A probe of photosynthesis in vivo. *Annual Review of Plant Biology*, *59*, 89–113. https://doi.org/10.1146/annurev.arplant.59.032607.092759

Bannari, A., Morin, D., Bonn, F., & Huete, A. R. (1995). A review of vegetation indices. *Remote Sensing Reviews*, *13*(1–2), 95–120. https://doi.org/10.1080/02757259509532298

Bilger, W., & Björkman, O. (1990). Role of the xanthophyll cycle in photoprotection elucidated by measurements of light-induced absorbance changes, fluorescence and photosynthesis in leaves of Hedera canariensis. *Photosynthesis Research*, *25*(3), 173–185. https://doi.org/10.1007/BF00033159

Boardman, N. K., Thorne, S. W., & Anderson, J. M. (1966). Fluorescence properties of particles obtained by digitonin fragmentation of spinach chloroplasts. *Proceedings of the National Academy of Sciences*, *56*(2), 586–593. https://doi.org/10.1073/pnas.56.2.586

Brugnoli, E., & Björkman, O. (1992). Chloroplast movements in leaves: Influence on chlorophyll fluorescence and measurements of light-induced absorbance changes related to ΔpH and zeaxanthin formation. *Photosynthesis Research*, *32*(1), 23–35. https://doi.org/10.1007/BF00028795

Cecchi, G., Mazzinghi, P., Pantani, L., Valentini, R., Tirelli, D., & De Angelis, P. (1994). Remote sensing of chlorophyll a fluorescence of vegetation canopies: 1. Near and far field measurement techniques. *Remote Sensing of Environment*, *47*(1), 18–28. https://doi.org/10.1016/0034-4257(94)90123-6

Cerovic, Z. G., Goulas, Y., Gorbunov, M., Briantais, J.-M., Camenen, L., & Moya, I. (1996). Fluorosensing of water stress in plants: Diurnal changes of the mean lifetime and yield of chlorophyll fluorescence, measured simultaneously and at distance with a τ-LIDAR and a modified PAM-fluorimeter, in maize, sugar beet, and kalanchoë. *Remote Sensing of Environment*, *58*(3), 311–321. https://doi.org/10.1016/S0034-4257(96)00076-4

Cerovic, Z. G., Samson, G., Morales, F., Tremblay, N., & Moya, I. (1999). Ultraviolet-induced fluorescence for plant monitoring: Present state and prospects. *Agronomie*, *19*(7), 543–578. https://doi.org/10.1051/agro:19990701

Chekalyuk, A. M., & Gorbunov, M. Y. (1994). Development of lidar pump-and-probe technique for remote assessment of photosyrrthetic activity of vegetation. *Conference on Lasers and Electro-Optics (1994), Paper CWH1*, CWH1. https://opg.optica.org/abstract.cfm?uri=CLEO-1994-CWH1

Cheng, Y., Gamon, J. A., Fuentes, D. A., Mao, Z., Sims, D. A., Qiu, H., Claudio, H., Huete, A., & Rahman, A. F. (2006). A multi-scale analysis of dynamic optical signals in a Southern California chaparral ecosystem: A comparison of field, AVIRIS and MODIS data. *Remote Sensing of Environment*, *103*(3), 369–378. https://doi.org/10.1016/j.rse.2005.06.013

Cheng, Y.-B., Middleton, E. M., Zhang, Q., Huemmrich, K. F., Campbell, P. K. E., Corp, L. A., Cook, B. D., Kustas, W. P., & Daughtry, C. S. (2013). Integrating Solar Induced Fluorescence and the Photochemical Reflectance Index for Estimating Gross Primary Production in a Cornfield. *Remote Sensing*, *5*(12), Article 12. https://doi.org/10.3390/rs5126857

Cogliati, S., Celesti, M., Cesana, I., Miglietta, F., Genesio, L., Julitta, T., Schuettemeyer, D., Drusch, M., Rascher, U., Jurado, P., & Colombo, R. (2019). A Spectral Fitting Algorithm to Retrieve the Fluorescence Spectrum from Canopy Radiance. *Remote Sensing*, *11*(16), Article 16. https://doi.org/10.3390/rs11161840

Cogliati, S., Rossini, M., Julitta, T., Meroni, M., Schickling, A., Burkart, A., Pinto, F., Rascher, U., & Colombo, R. (2015). Continuous and long-term measurements of reflectance and sun-induced chlorophyll fluorescence by using novel automated

field spectroscopy systems. *Remote Sensing of Environment*, *164*, 270–281. https://doi.org/10.1016/j.rse.2015.03.027

Damm, A., Elbers, J., Erler, A., Gioli, B., Hamdi, K., Hutjes, R., Kosvancova, M., Meroni, M., Miglietta, F., Moersch, A., Moreno, J., Schickling, A., Sonnenschein, R., Udelhoven, T., Van Der LINDEN, S., Hostert, P., & Rascher, U. (2010). Remote sensing of sun-induced fluorescence to improve modeling of diurnal courses of gross primary production (GPP). *Global Change Biology*, *16*(1), 171–186. https://doi.org/10.1111/j.1365-2486.2009.01908.x

Damm, A., Guanter, L., Paul-Limoges, E., van der Tol, C., Hueni, A., Buchmann, N., Eugster, W., Ammann, C., & Schaepman, M. E. (2015). Far-red sun-induced chlorophyll fluorescence shows ecosystem-specific relationships to gross primary production: An assessment based on observational and modeling approaches. *Remote Sensing of Environment*, *166*, 91–105. https://doi.org/10.1016/j.rse.2015.06.004

Dau, H. (1994). Molecular Mechanisms and Quantitative Models of Variable Photosystem Ii Fluorescence. *Photochemistry and Photobiology*, *60*(1), 1–23. https://doi.org/10.1111/j.1751-1097.1994.tb03937.x

Daumard, F., Champagne, S., Fournier, A., Goulas, Y., Ounis, A., Hanocq, J.-F., & Moya, I. (2010). A Field Platform for Continuous Measurement of Canopy Fluorescence. *IEEE Transactions on Geoscience and Remote Sensing*, *48*(9), 3358–3368. https://doi.org/10.1109/TGRS.2010.2046420

Daumard, F., Goulas, Y., Champagne, S., Fournier, A., Ounis, A., Olioso, A., & Moya, I. (2012). Continuous Monitoring of Canopy Level Sun-Induced Chlorophyll Fluorescence During the Growth of a Sorghum Field. *IEEE Transactions on*

Geoscience and Remote Sensing, *50*(11), 4292–4300. https://doi.org/10.1109/TGRS.2012.2193131

Daumard, F., Goulas, Y., Ounis, A., Pedros, R., & Moya, I. (2007). *ATMOSPHERIC CORRECTION OF AIRBORNE PASSIVE MEASUREMENTS OF FLUORESCENCE*. https://www.semanticscholar.org/paper/ATMOSPHERIC-CORRECTION-OF-AIRBORNE-PASSIVE-OF-Daumarda-Goulasa/d88a4a8f796609ad10e0d3a310a78ac9a0f70edc

Daumard, F., Goulas, Y., Ounis, A., Pedrós, R., & Moya, I. (2015). Measurement and Correction of Atmospheric Effects at Different Altitudes for Remote Sensing of Sun-Induced Fluorescence in Oxygen Absorption Bands. *IEEE Transactions on Geoscience and Remote Sensing*, *53*(9), 5180–5196. https://doi.org/10.1109/TGRS.2015.2418992

Dechant, B., Ryu, Y., Badgley, G., Zeng, Y., Berry, J. A., Zhang, Y., Goulas, Y., Li, Z., Zhang, Q., Kang, M., Li, J., & Moya, I. (2020). Canopy structure explains the relationship between photosynthesis and sun-induced chlorophyll fluorescence in crops. *Remote Sensing of Environment*, *241*, 111733. https://doi.org/10.1016/j.rse.2020.111733

Devaux, A., Kromann, P., & Ortiz, O. (2014). Potatoes for Sustainable Global Food Security. *Potato Research*, *57*(3), 185–199. https://doi.org/10.1007/s11540-014-9265-1

Drolet, G. G., Middleton, E. M., Huemmrich, K. F., Hall, F. G., Amiro, B. D., Barr, A. G., Black, T. A., McCaughey, J. H., & Margolis, H. A. (2008). Regional mapping of gross light-use efficiency using MODIS spectral indices. *Remote Sensing of Environment*, *112*(6), 3064–3078. https://doi.org/10.1016/j.rse.2008.03.002

Drusch, M., Moreno, J., Del Bello, U., Franco, R., Goulas, Y., Huth, A., Kraft, S., Middleton, E. M., Miglietta, F., Mohammed, G., Nedbal, L., Rascher, U., Schüttemeyer, D., & Verhoef, W. (2017). The FLuorescence EXplorer Mission Concept—ESA's Earth Explorer 8. *IEEE Transactions on Geoscience and Remote Sensing*, *55*(3), 1273–1284. https://doi.org/10.1109/TGRS.2016.2621820

Du, S., Liu, L., Liu, X., Guo, J., Hu, J., Wang, S., & Zhang, Y. (2019). SIFSpec: Measuring Solar-Induced Chlorophyll Fluorescence Observations for Remote Sensing of Photosynthesis. *Sensors*, *19*(13), Article 13. https://doi.org/10.3390/s19133009

Evain, S., Camenen, L., & Moya, I. (2001). Three-channel detector for remote sensing of chlorophyll fluorescence and reflectance from vegetation. *CNES*, 395–400.

Evain, S., Flexas, J., & Moya, I. (2004). A new instrument for passive remote sensing: 2. Measurement of leaf and canopy reflectance changes at 531 nm and their relationship with photosynthesis and chlorophyll fluorescence. *Remote Sensing of Environment*, *91*(2), 175–185. https://doi.org/10.1016/j.rse.2004.03.012

Flexas, J., Briantais, J.-M., Cerovic, Z., Medrano, H., & Moya, I. (2000). Steady-State and Maximum Chlorophyll Fluorescence Responses to Water Stress in Grapevine Leaves: A New Remote Sensing System. *Remote Sensing of Environment*, *73*(3), 283–297. https://doi.org/10.1016/S0034-4257(00)00104-8

Fournier, A., Daumard, F., Champagne, S., Ounis, A., Goulas, Y., & Moya, I. (2012). Effect of canopy structure on sun-induced chlorophyll fluorescence. *ISPRS Journal of Photogrammetry and Remote Sensing*, *68*, 112–120. https://doi.org/10.1016/j.isprsjprs.2012.01.003

Franck, F., Juneau, P., & Popovic, R. (2002). Resolution of the Photosystem I and Photosystem II contributions to chlorophyll fluorescence of intact leaves at room temperature. *Biochimica et Biophysica Acta (BBA) - Bioenergetics*, *1556*(2), 239–246. https://doi.org/10.1016/S0005-2728(02)00366-3

Gamon, J. A., Huemmrich, K. F., Peddle, D. R., Chen, J., Fuentes, D., Hall, F. G., Kimball, J. S., Goetz, S., Gu, J., McDonald, K. C., Miller, J. R., Moghaddam, M., Rahman, A. F., Roujean, J.-L., Smith, E. A., Walthall, C. L., Zarco-Tejada, P., Hu, B., Fernandes, R., & Cihlar, J. (2004). Remote sensing in BOREAS: Lessons learned. *Remote Sensing of Environment*, *89*(2), 139–162. https://doi.org/10.1016/j.rse.2003.08.017

Gamon, J. A., Peñuelas, J., & Field, C. B. (1992). A narrow-waveband spectral index that tracks diurnal changes in photosynthetic efficiency. *Remote Sensing of Environment*, *41*(1), 35–44. https://doi.org/10.1016/0034-4257(92)90059-S

Genty, B., Briantais, J.-M., & Baker, N. R. (1989). The relationship between the quantum yield of photosynthetic electron transport and quenching of chlorophyll fluorescence. *Biochimica et Biophysica Acta (BBA) - General Subjects*, *990*(1), 87–92. https://doi.org/10.1016/S0304-4165(89)80016-9

Genty, B., Harbinson, J., Briantais, J.-M., & Baker, N. R. (1990). The relationship between non-photochemical quenching of chlorophyll fluorescence and the rate of photosystem 2 photochemistry in leaves. *Photosynthesis Research*, *25*(3), 249–257. https://doi.org/10.1007/BF00033166

Goerner, A., Reichstein, M., & Rambal, S. (2009). Tracking seasonal drought effects on ecosystem light use efficiency with satellite-based PRI in a Mediterranean forest. *Remote Sensing of Environment*, *113*(5), 1101–1111. https://doi.org/10.1016/j.rse.2009.02.001

Goulas, Y., Camenen, L., Guyot, G., Cerovic, Z., Briantais, J. -M., Schmuck, G., & Moya, I. (1997). Measurement of laser-induced fluorescence decay and reflectance of plant canopies. *Remote Sensing Reviews*, *15*(1–4), 305–322. https://doi.org/10.1080/02757259709532344

Goulas, Y., Fournier, A., Daumard, F., Champagne, S., Ounis, A., Marloie, O., & Moya, I. (2017). Gross Primary Production of a Wheat Canopy Relates Stronger to Far Red Than to Red Solar-Induced Chlorophyll Fluorescence. *Remote Sensing*, *9*(1), Article 1. https://doi.org/10.3390/rs9010097

Govindje, E. (1995). Sixty-Three Years Since Kautsky: Chlorophyll a Fluorescence. *Functional Plant Biology*, *22*(2), 131. https://doi.org/10.1071/PP9950131

Guenther K. P., Luedeker W., & Dahn H.-G. (1991). Design and testing of a spectral-resolving fluorescence lidar system for remote sensing of vegetation. *ESA SP (European Space Agency)*, *319 Vol 2*, 723–726.

Gutiérrez-Rosales, R. O., Espinoza-Trelles, J. A., & Bonierbale, M. (2007). UNICA: Variedad Peruana para mercado fresco y papa frita con tolerancia y resistencia para condiciones climáticas adversas. *Revista Latinoamericana de la Papa*, *14*(1), Article 1. https://doi.org/10.37066/ralap.v14i1.143

Hemphill, W. R., Watson, R. D., Bigelow, R. C., & Hessen, T. D. (1975). Measurement of luminescence of geochemically stressed trees and other materials. *Geological Survey Professional*, 93–112. https://pascal-francis.inist.fr/vibad/index.php?action=getRecordDetail&idt=PASCALGEODEBRGM7820097519

Hoge, F. E., Swift, R. N., & Yungel, J. K. (1983). Feasibility of airborne detection of laser-induced fluorescence emissions from green terrestrial plants. *Applied Optics*, *22*(19), 2991–3000. https://doi.org/10.1364/AO.22.002991

Horton, P., & Ruban, A. (2005). Molecular design of the photosystem II light-harvesting antenna: Photosynthesis and photoprotection. *Journal of Experimental Botany*, *56*(411), 365–373. https://doi.org/10.1093/jxb/eri023

Horton, P., Ruban, A. V., & Walters, R. G. (1994). Regulation of Light Harvesting in Green Plants (Indication by Nonphotochemical Quenching of Chlorophyll Fluorescence). *Plant Physiology*, *106*(2), 415–420. https://doi.org/10.1104/pp.106.2.415

Jordan, C. F. (1969). Derivation of Leaf-Area Index from Quality of Light on the Forest Floor. *Ecology*, *50*(4), 663–666. https://doi.org/10.2307/1936256

Kautsky, H., & Hirsch, A. (1931). Neue Versuche zur Kohlensäureassimilation. *Naturwissenschaften*, *19*(48), 964–964. https://doi.org/10.1007/BF01516164

Krause, G. H., & Jahns, P. (2004). Non-photochemical Energy Dissipation Determined by Chlorophyll Fluorescence Quenching: Characterization and Function. In G. C. Papageorgiou & Govindjee (Eds.), *Chlorophyll a Fluorescence: A Signature of Photosynthesis* (pp. 463–495). Springer Netherlands. https://doi.org/10.1007/978-1-4020-3218-9_18

Krause, G. H., & Weis, E. (1991). Chlorophyll Fluorescence and Photosynthesis: The Basics. *Annual Review of Plant Physiology and Plant Molecular Biology*, *42*(1), 313–349. https://doi.org/10.1146/annurev.pp.42.060191.001525

Laisk, A., Oja, V., Eichelmann, H., & Dall'Osto, L. (2014). Action spectra of photosystems II and I and quantum yield of photosynthesis in leaves in State 1. *Biochimica et Biophysica Acta (BBA) - Bioenergetics*, *1837*(2), 315–325. https://doi.org/10.1016/j.bbabio.2013.12.001

Loayza, H., Moya, I., Quiroz, R., Ounis, A., & Goulas, Y. (2022). Active and passive chlorophyll fluorescence measurements at canopy level on potato crops.

Evidence of similitude of diurnal cycles of apparent fluorescence yields. *Photosynthesis Research*. https://doi.org/10.1007/s11120-022-00995-8

López González, M. de los L. (2015). *Seguimiento del estrés hídrico en la vid mediante técnicas de fluorescencia de la clorofila y otros métodos ópticos* [Http://purl.org/dc/dcmitype/Text, Universidad de Castilla-La Mancha]. https://dialnet.unirioja.es/servlet/tesis?codigo=97441

Louis, J. (2004). *Télédétection et modélisation des signaux de fluorescence et de réflectance (PRI) des couverts végétaux* [Thèse de doctorat]. Université Paris Diderot - Paris 7.

Louis, J., Cerovic, Z. G., & Moya, I. (2006). Quantitative study of fluorescence excitation and emission spectra of bean leaves. *Journal of Photochemistry and Photobiology B: Biology*, *85*(1), 65–71. https://doi.org/10.1016/j.jphotobiol.2006.03.009

Louis, J., Ounis, A., Ducruet, J.-M., Evain, S., Laurila, T., Thum, T., Aurela, M., Wingsle, G., Alonso, L., Pedros, R., & Moya, I. (2005). Remote sensing of sunlight-induced chlorophyll fluorescence and reflectance of Scots pine in the boreal forest during spring recovery. *Remote Sensing of Environment*, *96*(1), 37–48. https://doi.org/10.1016/j.rse.2005.01.013

Maxwell, K., & Johnson, G. N. (2000). Chlorophyll fluorescence—A practical guide. *Journal of Experimental Botany*, *51*(345), 659–668. https://doi.org/10.1093/jexbot/51.345.659

Meroni, M., & Colombo, R. (2006). Leaf level detection of solar induced chlorophyll fluorescence by means of a subnanometer resolution spectroradiometer. *Remote Sensing of Environment*, *103*(4), 438–448. https://doi.org/10.1016/j.rse.2006.03.016

Meroni, M., Rossini, M., Guanter, L., Alonso, L., Rascher, U., Colombo, R., & Moreno, J. (2009). Remote sensing of solar-induced chlorophyll fluorescence: Review of methods and applications. *Remote Sensing of Environment*, *113*(10), 2037–2051. https://doi.org/10.1016/j.rse.2009.05.003

Mohammed, G. H., Colombo, R., Middleton, E. M., Rascher, U., van der Tol, C., Nedbal, L., Goulas, Y., Pérez-Priego, O., Damm, A., Meroni, M., Joiner, J., Cogliati, S., Verhoef, W., Malenovský, Z., Gastellu-Etchegorry, J.-P., Miller, J. R., Guanter, L., Moreno, J., Moya, I., … Zarco-Tejada, P. J. (2019). Remote sensing of solar-induced chlorophyll fluorescence (SIF) in vegetation: 50 years of progress. *Remote Sensing of Environment*, *231*, 111177. https://doi.org/10.1016/j.rse.2019.04.030

Moya, I. (1979). *Application de la fluorime´trie de phase a l'e´tude de la dure´e de vie et du rendement de la fluorescence de la chlorophylle in vivo* [PhD Thesis]. Universite´ de Paris XI, Orsay.

Moya, I., Camenen, L., Evain, S., Goulas, Y., Cerovic, Z. G., Latouche, G., Flexas, J., & Ounis, A. (2004). A new instrument for passive remote sensing: 1. Measurements of sunlight-induced chlorophyll fluorescence. *Remote Sensing of Environment*, *91*(2), 186–197. https://doi.org/10.1016/j.rse.2004.02.012

Moya, I., Camenen, L., Latouche, G., Mauxion, C., Evain, S., & Cerovic, Z. G. (1998). An Instrument for the Measurement of Sunlight Excited Plant Fluorescence. In G. Garab (Ed.), *Photosynthesis: Mechanisms and Effects: Volume I–V: Proceedings of the XIth International Congress on Photosynthesis, Budapest, Hungary, August 17–22, 1998* (pp. 4265–4270). Springer Netherlands. https://doi.org/10.1007/978-94-011-3953-3_986

Moya, I., & Cerovic, Z. G. (2004). Remote Sensing of Chlorophyll Fluorescence: Instrumentation and Analysis. In G. C. Papageorgiou & Govindjee (Eds.), *Chlorophyll a Fluorescence: A Signature of Photosynthesis* (pp. 429–445). Springer Netherlands. https://doi.org/10.1007/978-1-4020-3218-9_16

Moya, I., & Flexas, J. (2012). Remote sensing of photosynthesis. In F. Loreto, H. Medrano, & J. Flexas (Eds.), *Terrestrial Photosynthesis in a Changing Environment: A Molecular, Physiological, and Ecological Approach* (pp. 219–236). Cambridge University Press. https://doi.org/10.1017/CBO9781139051477.018

Moya, I., Loayza, H., López, M. L., Quiroz, R., Ounis, A., & Goulas, Y. (2019). Canopy chlorophyll fluorescence applied to stress detection using an easy-to-build micro-lidar. *Photosynthesis Research*, *142*(1), 1–15. https://doi.org/10.1007/s11120-019-00642-9

Moya, I., Loayza, H., López, M.-L., Sánchez, J. M., Goulas, Y., Ounis, A., Quiroz, R., & Calera, A. (2023). Active in situ and passive airborne fluorescence measurements for water stress detection on a fescue field. *Photosynthesis Research*, *155*(2), 159–175. https://doi.org/10.1007/s11120-022-00983-y

Moya, I., Ounis, A., Moise, N., & Goulas, Y. (2006). *First airborne multiwavelength passive chlorophyll fluorescence measurements over La Mancha (Spain) fields*. http://www.researchgate.net/publication/285980239_First_airborne_multiwavelength_passive_chlorophyll_fluorescence_measurements_over_La_Mancha_Spain_fields

Müller, J., Aeschbacher, R. A., Wingler, A., Boller, T., & Wiemken, A. (2001). Trehalose and Trehalase in Arabidopsis1. *Plant Physiology*, *125*(2), 1086–1093. https://doi.org/10.1104/pp.125.2.1086

Niclòs, R., Valiente, J. A., Barberà, M. J., & Coll, C. (2015). An Autonomous System to Take Angular Thermal-Infrared Measurements for Validating Satellite Products. *Remote Sensing*, *7*(11), Article 11. https://doi.org/10.3390/rs71115269

Osmond, C. (1994). What is photoinhibition? Some insights from comparisons of shade and sun plants. *Molecular Mechanisms to the Field*, 1–24. https://www.semanticscholar.org/paper/What-is-photoinhibition-Some-insights-from-of-shade-Osmond/211682b35071523d7d4d2d0b39a25f945f600ec5

Ounis, A., Evain, S., Flexas, J., Tosti, S., & Moya, I. (2001). Adaptation of a PAM-fluorometer for remote sensing of chlorophyll fluorescence. *Photosynthesis Research*, *68*(2), 113–120. https://doi.org/10.1023/A:1011843131298

Peguero-Pina, J. J., Morales, F., Flexas, J., Gil-Pelegrín, E., & Moya, I. (2008). Photochemistry, remotely sensed physiological reflectance index and de-epoxidation state of the xanthophyll cycle in Quercus coccifera under intense drought. *Oecologia*, *156*(1), 1–11. https://doi.org/10.1007/s00442-007-0957-y

Pfündel, E. (1998). Estimating the contribution of Photosystem I to total leaf chlorophyll fluorescence. *Photosynthesis Research*, *56*(2), 185–195. https://doi.org/10.1023/A:1006032804606

Pieruschka, R., Klimov, D., Kolber, Z. S., Berry, J. A., Pieruschka, R., Klimov, D., Kolber, Z. S., & Berry, J. A. (2010). Monitoring of cold and light stress impact on photosynthesis by using the laser induced fluorescence transient (LIFT) approach. *Functional Plant Biology*, *37*(5), 395–402. https://doi.org/10.1071/FP09266

Plascyk, J. A. (1975). The MK II Fraunhofer Line Discriminator (FLD-II) for Airborne and Orbital Remote Sensing of Solar-Stimulated Luminescence. *Optical Engineering*, *14*(4), 339–0. https://doi.org/10.1117/12.7971842

Plascyk, J. A., & Gabriel, F. C. (1975). The Fraunhofer Line Discriminator MKII-An Airborne Instrument for Precise and Standardized Ecological Luminescence Measurement. *IEEE Transactions on Instrumentation and Measurement*, *24*(4), 306–313. https://doi.org/10.1109/TIM.1975.4314448

Porcar-Castell, A., Tyystjärvi, E., Atherton, J., van der Tol, C., Flexas, J., Pfündel, E. E., Moreno, J., Frankenberg, C., & Berry, J. A. (2014). Linking chlorophyll a fluorescence to photosynthesis for remote sensing applications: Mechanisms and challenges. *Journal of Experimental Botany*, *65*(15), 4065–4095. https://doi.org/10.1093/jxb/eru191

Quick, W. P., & Horton, P. (1984). Studies on the induction of chlorophyll fluorescence in barley protoplasts. I. Factors affecting the observation of oscillations in the yield of chlorophyll fluorescence and the rate of oxygen evolution. *Proceedings of the Royal Society of London. Series B. Biological Sciences*, *220*(1220), 361–370. https://doi.org/10.1098/rspb.1984.0006

Rascher, U., Agati, G., Alonso, L., Cecchi, G., Champagne, S., Colombo, R., Damm, A., Daumard, F., de Miguel, E., Fernandez, G., Franch, B., Franke, J., Gerbig, C., Gioli, B., Gómez, J. A., Goulas, Y., Guanter, L., Gutiérrez-de-la-Cámara, Ó., Hamdi, K., … Zaldei, A. (2009). CEFLES2: The remote sensing component to quantify photosynthetic efficiency from the leaf to the region by measuring sun-induced fluorescence in the oxygen absorption bands. *Biogeosciences*, *6*(7), 1181–1198. https://doi.org/10.5194/bg-6-1181-2009

Rascher, U., Alonso, L., Burkart, A., Cilia, C., Cogliati, S., Colombo, R., Damm, A., Drusch, M., Guanter, L., Hanus, J., Hyvärinen, T., Julitta, T., Jussila, J., Kataja, K., Kokkalis, P., Kraft, S., Kraska, T., Matveeva, M., Moreno, J., … Zemek, F. (2015). Sun-induced fluorescence – a new probe of photosynthesis: First maps

from the imaging spectrometer HyPlant. *Global Change Biology*, *21*(12), 4673–4684. https://doi.org/10.1111/gcb.13017

Rosema, A., Snel, J. F. H., Zahn, H., Buurmeijer, W. F., & Van Hove, L. W. A. (1998). The Relation between Laser-Induced Chlorophyll Fluorescence and Photosynthesis. *Remote Sensing of Environment*, *65*(2), 143–154. https://doi.org/10.1016/S0034-4257(98)00020-0

Rossini, M., Meroni, M., Migliavacca, M., Manca, G., Cogliati, S., Busetto, L., Picchi, V., Cescatti, A., Seufert, G., & Colombo, R. (2010). High resolution field spectroscopy measurements for estimating gross ecosystem production in a rice field. *Agricultural and Forest Meteorology*, *150*(9), 1283–1296. https://doi.org/10.1016/j.agrformet.2010.05.011

Running, S. W., & Nemani, R. R. (1988). Relating seasonal patterns of the AVHRR vegetation index to simulated photosynthesis and transpiration of forests in different climates. *Remote Sensing of Environment*, *24*(2), 347–367. https://doi.org/10.1016/0034-4257(88)90034-X

Sánchez, J. M., Galve, J. M., González-Piqueras, J., López-Urrea, R., Niclòs, R., & Calera, A. (2020). Monitoring 10-m LST from the Combination MODIS/Sentinel-2, Validation in a High Contrast Semi-Arid Agroecosystem. *Remote Sensing*, *12*(9), Article 9. https://doi.org/10.3390/rs12091453

Sánchez, J. M., Kustas, W. P., Caselles, V., & Anderson, M. C. (2008). Modelling surface energy fluxes over maize using a two-source patch model and radiometric soil and canopy temperature observations. *Remote Sensing of Environment*, *112*(3), 1130–1143. https://doi.org/10.1016/j.rse.2007.07.018

Sánchez, J. M., López-Urrea, R., Doña, C., Caselles, V., González-Piqueras, J., & Niclòs, R. (2015). Modeling evapotranspiration in a spring wheat from thermal

radiometry: Crop coefficients and E/T partitioning. *Irrigation Science*, *33*(6), 399–410. https://doi.org/10.1007/s00271-015-0476-2

Sánchez, J. M., López-Urrea, R., Rubio, E., & Caselles, V. (2011). Determining water use of sorghum from two-source energy balance and radiometric temperatures. *Hydrology and Earth System Sciences*, *15*(10), 3061–3070. https://doi.org/10.5194/hess-15-3061-2011

Sánchez, J. M., López-Urrea, R., Rubio, E., González-Piqueras, J., & Caselles, V. (2014). Assessing crop coefficients of sunflower and canola using two-source energy balance and thermal radiometry. *Agricultural Water Management*, *137*, 23–29. https://doi.org/10.1016/j.agwat.2014.02.002

Sánchez, J. M., López-Urrea, R., Valentín, F., Caselles, V., & Galve, J. M. (2019). Lysimeter assessment of the Simplified Two-Source Energy Balance model and eddy covariance system to estimate vineyard evapotranspiration. *Agricultural and Forest Meteorology*, *274*, 172–183. https://doi.org/10.1016/j.agrformet.2019.05.006

Sarvikas, P. (2010). *Photoinhibition of Photosystem II. Kinetics, Photoprotection and Mechanism*. https://www.utupub.fi/handle/10024/62910

Schreiber, U. (1986). Detection of rapid induction kinetics with a new type of high-frequency modulated chlorophyll fluorometer. *Photosynthesis Research*, *9*(1–2), 261–272. https://doi.org/10.1007/BF00029749

Schreiber, U. (1998). Chlorophyll fluorescence: New Instruments for Special Applications. In G. Garab (Ed.), *Photosynthesis: Mechanisms and Effects: Volume I–V: Proceedings of the XIth International Congress on Photosynthesis, Budapest, Hungary, August 17–22, 1998* (pp. 4253–4258). Springer Netherlands. https://doi.org/10.1007/978-94-011-3953-3_984

Schreiber, U., & Klughammer, C. (2021). Evidence for variable chlorophyll fluorescence of photosystem I in vivo. *Photosynthesis Research*, *149*(1), 213–231. https://doi.org/10.1007/s11120-020-00814-y

Schreiber, U., Schliwa, U., & Bilger, W. (1986). Continuous recording of photochemical and non-photochemical chlorophyll fluorescence quenching with a new type of modulation fluorometer. *Photosynthesis Research*, *10*(1), 51–62. https://doi.org/10.1007/BF00024185

Sellers, P. J. (1987). Canopy reflectance, photosynthesis, and transpiration, II. The role of biophysics in the linearity of their interdependence. *Remote Sensing of Environment*, *21*(2), 143–183. https://doi.org/10.1016/0034-4257(87)90051-4

Sobrino, J. A., & Skoković, D. (2016). Permanent Stations for Calibration/Validation of Thermal Sensors over Spain. *Data*, *1*(2), Article 2. https://doi.org/10.3390/data1020010

Suárez, L., Zarco-Tejada, P. J., Berni, J. A. J., González-Dugo, V., & Fereres, E. (2009). Modelling PRI for water stress detection using radiative transfer models. *Remote Sensing of Environment*, *113*(4), 730–744. https://doi.org/10.1016/j.rse.2008.12.001

Suárez, L., Zarco-Tejada, P. J., Sepulcre-Cantó, G., Pérez-Priego, O., Miller, J. R., Jiménez-Muñoz, J. C., & Sobrino, J. (2008). Assessing canopy PRI for water stress detection with diurnal airborne imagery. *Remote Sensing of Environment*, *112*(2), 560–575. https://doi.org/10.1016/j.rse.2007.05.009

Tremblay, N., Wang, Z., & Cerovic, Z. G. (2012). Sensing crop nitrogen status with fluorescence indicators. A review. *Agronomy for Sustainable Development*, *32*(2), 451–464. https://doi.org/10.1007/s13593-011-0041-1

Trissl, H.-W. (1997). Determination of the quenching efficiency of the oxidized primary donor of Photosystem I, P700+: Implications for the trapping mechanism. *Photosynthesis Research*, *54*(3), 237–240. https://doi.org/10.1023/A:1005981016835

Tyystjärvi, E., & Aro, E. M. (1996). The rate constant of photoinhibition, measured in lincomycin-treated leaves, is directly proportional to light intensity. *Proceedings of the National Academy of Sciences of the United States of America*, *93*(5), 2213–2218. https://doi.org/10.1073/pnas.93.5.2213

van Kooten, O., & Snel, J. F. H. (1990). The use of chlorophyll fluorescence nomenclature in plant stress physiology. *Photosynthesis Research*, *25*(3), 147–150. https://doi.org/10.1007/BF00033156

Wada, M. (2013). Chloroplast movement. *Plant Science*, *210*, 177–182. https://doi.org/10.1016/j.plantsci.2013.05.016

Wang, N., Suomalainen, J., Bartholomeus, H., Kooistra, L., Masiliūnas, D., & Clevers, J. G. P. W. (2021). Diurnal variation of sun-induced chlorophyll fluorescence of agricultural crops observed from a point-based spectrometer on a UAV. *International Journal of Applied Earth Observation and Geoinformation*, *96*, 102276. https://doi.org/10.1016/j.jag.2020.102276

Wollman, F. A. (2001). State transitions reveal the dynamics and flexibility of the photosynthetic apparatus. *The EMBO Journal*, *20*(14), 3623–3630. https://doi.org/10.1093/emboj/20.14.3623

Xu, S., Atherton, J., Riikonen, A., Zhang, C., Oivukkamäki, J., MacArthur, A., Honkavaara, E., Hakala, T., Koivumäki, N., Liu, Z., & Porcar-Castell, A. (2021). Structural and photosynthetic dynamics mediate the response of SIF to

water stress in a potato crop. *Remote Sensing of Environment*, *263*, 112555. https://doi.org/10.1016/j.rse.2021.112555

Zarco-Tejada, P. J., Berni, J. A. J., Suárez, L., Sepulcre-Cantó, G., Morales, F., & Miller, J. R. (2009). Imaging chlorophyll fluorescence with an airborne narrow-band multispectral camera for vegetation stress detection. *Remote Sensing of Environment*, *113*(6), 1262–1275. https://doi.org/10.1016/j.rse.2009.02.016

Zhen, S., & Bugbee, B. (2020). Far-red photons have equivalent efficiency to traditional photosynthetic photons: Implications for redefining photosynthetically active radiation. *Plant, Cell & Environment*, *43*(5), 1259–1272. https://doi.org/10.1111/pce.13730

TABLE OF FIGURES

TABLE OF TABLES